BEHAVIOR OF BRIDGE PIERS DURING VEHICULAR IMPACTS

By

GUANGYONG LIU

A dissertation submitted to the Graduate Faculty in Engineering in partial fulfillment of the requirements for the degree of Doctor of Philosophy, The City University of New York

2012

This manuscript has been read and accepted for the
Graduate Faculty in Engineering in satisfaction of the
dissertation requirement for the degree of Doctor of Philosophy.

Professor Anil K. Agrawal

Date | Chair of Examining Committee

Professor Mumtaz K. Kassir

Date | Executive Officer

Dr. Screenivas Alampalli, NYS Department of Transportation

Dr. Mohammed Ettouney, Weidlinger Associates

Professor Michel Ghosn, The City College of New York

Professor Feng-bao Lin, The City College of New York

Professor Huabei Liu, The City College of New York

Supervisory Committee

THE CITY UNIVERSITY OF NEW YORK

Abstracts

BEHAVIOR OF BRIDGE PIERS DURING VEHICULAR IMPACTS

by

Guangyong Liu

Supervisor: Prof. Anil Kumar Agrawal

Accidental collision of vehicle with highway bridges is the third leading cause of bridge failures in USA. Recent studies show that the dynamic forces because of truck impacts may be significantly higher than the 400kips force recommended by the AASHTO. Because of the highly cost of the vehicular impact tests on bridge piers, this dissertation extensively investigated the behavior of a three-span bridge with reinforced concrete piers impacted by trucks using finite element models in LS-DYNA.

An appropriate material model to describe the high nonlinear deformation of concrete elements under impact loads is crucial for numerical simulation. For simulation of vehicular impact on bridge structures, the CSCM model demonstrates a more reasonable damage mode than the JHC model. Various numerical parameters have been verified through comparisons between simulations and impact tests on reinforced concrete beams. A high fidelity numerical model of highway bridge has been developed. With low, medium and high velocities of truck impacts on the bridge piers, the failure modes are indentified. The profiles of impact force and the mid-height displacement are captured during the simulation.

In order to study the correlation between seismic detailing and vehicle impact effects, four seismic bridge models have been developed. With twelve numerical cases of vehicle collision, the framework of seismic-impact correlations has been built for the further safety assessment. The ductility and shear strength can be taken as key parameters to evaluate impact-resistance capacities of bridge piers.

Numerical simulation using the whole bridge models requires significant capability. A simplified Pier-bent model is proposed based on the simulations of whole bridge model. Under the condition of 95% impulse from the vehicle impact, simulation results show that the simplified Pier-Bent model can be a reliable replacement of whole bridge model for future research.

Traditional seismic steel/FRP jacketing can be used to strengthen bridge piers vulnerable to vehicular impacts. Numerical simulations have been carried out to evaluate the efficiency of this rehabilitation approach. It is observed that both steel jacket and FRP wrapping can be effective in reducing damages to bridge piers during vehicular impacts.

Acknowledgements

I would like to express my sincere gratitude and appreciation to my advisor, Professor Anil K. Agrawal for his continuous academic support, mentorship and moral support during my graduate studies at City College of New York.

My sincere appreciation also goes to the faculty members of Department of Civil Engineering at the City College of New York for their help and encouragement. In particular, I would like to thank Professor Mumtaz Kassir, Professor Kolluru Subramaniam, Professor Fengbao Lin, Professor Michel Ghosn, Professor Huabei Liu and Professor Camille Kamga.

I sincerely acknowledge the support of Dr. Mohammed Ettouney of Weidlinger Associates, Dr. Sreenivas Almpalli of the New York State Department of Transportation and Mr. Waider Wong of the Federal Highway Administration. Their continuous feedback played a very important role in helping my research for this dissertation.

Finally, I would like to express my gratitude and love to my family for their endless love and support.

Content

List of Figures

List of Tables

Chapter 1 Introduction

1.1 Background

Figure 1.1 Bridge damaged by a relatively small amount of explosives during a terrorist attack.

Thousands of highway bridges throughout the United States have been constructed and put into public service during the past several decades. Because of the long service duration of these bridges compared to the design life-span, the safety concerns of existing bridges has become crucial in recent years. A recent study has reported that 503 bridges of various types failed during 1989 to 2000 in the United States. The age of these failed bridges ranged from one year to 157 years, with an average of 52.5 years. Moreover, domestic and international terrorist activities have heightened the concerns about the safety of various infrastructure systems, and highway bridges could be among the most vulnerable targets of potential terrorist attacks. On the other hand, some catastrophic collapses of bridge systems have occurred because of accidental collisions of heavy vehicles with bridge piers in the past, resulting in

loss of life and the complete deconstruction of the impacted bridges. Two example events could be documented here as examples of bridge failures under explosive terrorist attack (Figure 1.1) and under vehicular collision (Figure1.2).

Figure 1.2 Semi Tractor-Trailer Crash on FM 3041 Bridge over I-45, Corsicana TX on May 30, 2007

The principal factors affecting bridge failures can be categorized as deficiencies in design, detailing, construction, maintenance, use of materials and inadequate capacity to resist effects of an external event. First five deficiencies can be included in the category of internal enabling reasons for bridge failures, whereas the external events are responsible for triggering causes of these failures. In past decades, bridge structures were generally designed to resist gravity, wind and earthquake loads. Relevant bridge design specifications achieved significant success in ensuring the safety of the public highway bridge structures during these loads. However, a highway bridge is always expected to experience various extreme events during its lifetime. For most of the bridges designed 30 years ago, extreme events in general and even the seismic loads were not included in the design considerations. It has been observed that approximately

83% (420 occurrences) of all bridges failures (503 occurrences) from 1989 to 2000 are caused by the external events [Wardhana and Hadipriono, 2003]. Based on the analysis of recent bridge failures, the following external events have been identified to cause the most significant failures of highway bridges:

- Hydraulic
- Overload
- Collision
- Earthquake

These external events can be divided in two categories. Both hydraulic and earthquake loads are nature-induced events, whereas overload, vehicular collision and terrorist attack are human-induced events. The most frequent causes of bridge failures have been attributed to floods and collisions. The National Highway Traffic Safety Administration (NHTSA) estimates that annually 1000 buses or trucks (10,000 pounds gross weight or greater) collide with bridge structures. Recent data show that the bridge overloads and lateral impact forces from trucks, barges/ships, and train are responsible for approximately 20% of all bridge failures[Wardhana and Hadipriono, 2003].

Figure 1.3 shows that more than 40 states in United States believe that hits to bridge by overheight vehicles is a major problem for the safety of the highway bridge system [Agrawal (2011)]. Furthermore, 42 states have reported that bridge systems suffered serious damage because of impacts by trucks as shown in Figure1.4; 40 states observed minor damages

because of vehicle impacts and 30 states observed minor scrapes due to vehicle impact, however, these accidents cause serious traffic congestion problems [Agrawal (2011)].

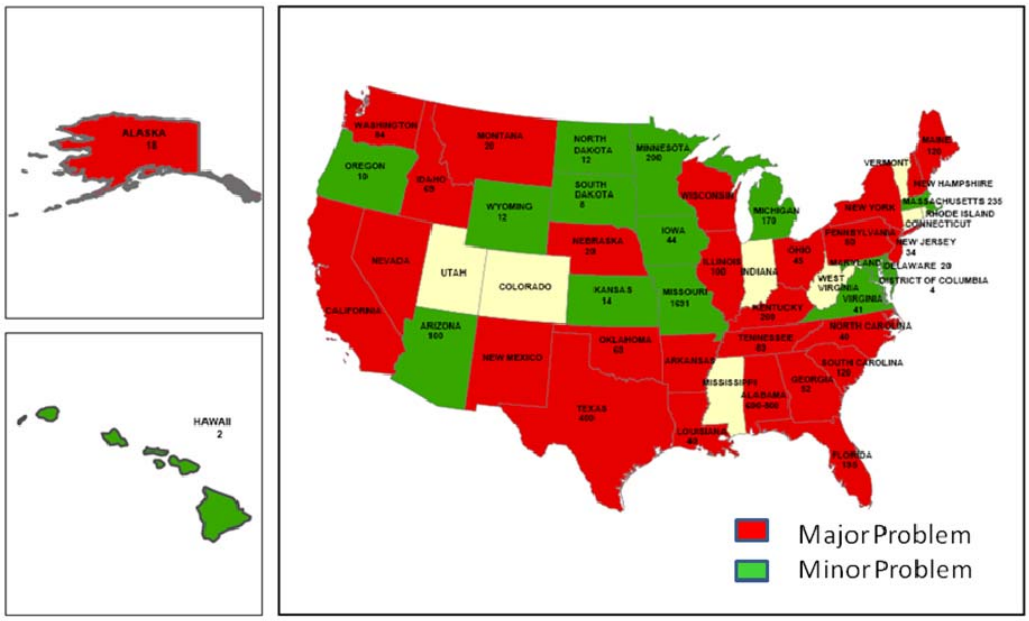

Figure 1.3 Seriousness of the Bridge Hits Problem across the Country.

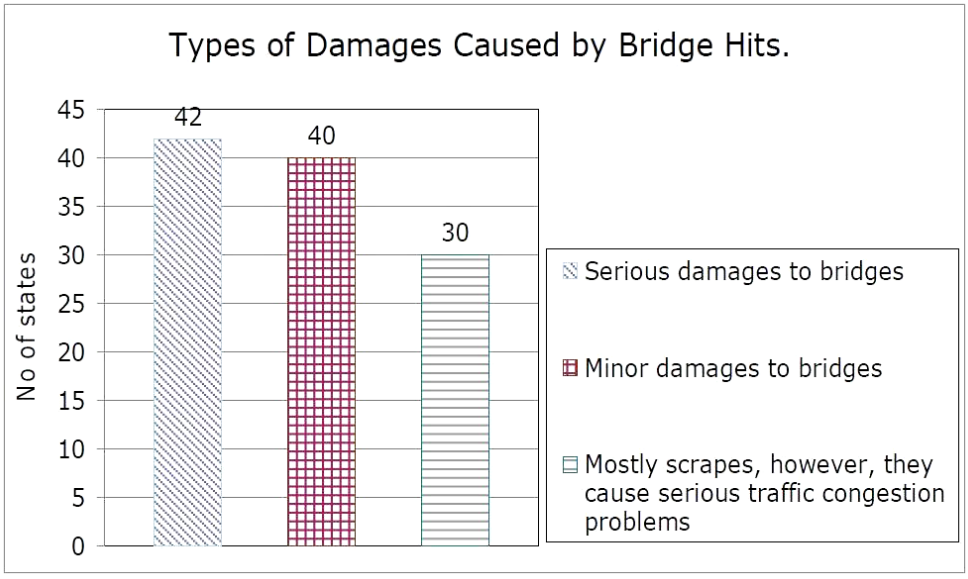

Figure 1.4 Types of Bridge Damage Because of Vehicle Impacts

Hence, it is important to investigate unavoidable extreme loads that may almost suddenly lead to the collapse of bridge structures. Newly designed bridge structures crossing highway or railroad must be capable of resisting vehicular collision loads. Likewise, existing vulnerable bridge structures should be evaluated and retrofitted to improve their resistance against vehicular impacts.

1.2 Research objectives

The objectives of the research work in this dissertation are to (i) extensively investigate the suitability of finite element tools for simulation of impact loads on bridge components, (ii) develop high-fidelity finite element models of a typical highway bridge in USA, (iii) investigate the performance of the critical highway bridge components during vehicle collisions, (iv) identify factors causing damage/failure of typical components, (v) investigate the correlation between seismic capacity and vehicular impact resistance capacity of highway bridges, (vi) develop a simplified structural response model for the impact resistant design of highway bridge structures and (vii) evaluate effective retrofit methods to improve the performance of highway bridges subject to vehicular impact loads.

Develop and Validate a Reliable and High Resolution Finite Element Numerical Model: In order to simulate the highly nonlinear bridge-vehicle impact problem, a reliable and high resolution full-scale finite element model of a 3-D bridge and a reliable finite element model of moving vehicles should be developed and validated. The element size, time step, material

model and simulation time should be determined correctly to eliminate numerical errors and numerical instability. In this research, our focus is on a traditional concrete bridge substructure. Hence a reasonable concrete material model should represent realistic stress-strain relationship and damage modes of concrete under the specific strain rate according to the real physical mechanism. In this dissertation, LS-DYNA, which is used extensively for the simulation of impact load effects on highway bridges.

Behavior of Bridge Components during a Vehicular Impact: There is very limited information on the behavior of bridge components and prominent failure modes during vehicular impacts. Using the 3-D finite element model of the bridge and the truck in LS-DYNA, extensive simulation will be carried out to investigate various aspect of vehicular impact on bridge piers, such as: (i) various failure modes of bridge components subject to vehicular impacts; (ii) peak dynamic and equivalent impact forces acting on bridge piers as functions of truck weight and velocity; (iii) efficiency of rebar detailing considering current AASHTO specifications; and (iv) comparison between the static load prescribed in the current AASHTO specifications and dynamic impact forces based on bridge-vehicle dynamic impact.

Bridge-Vehicle Collision using Different Seismic Resistant Pier Designs under Various Impact Velocities: Based on current seismic design provisions, four highway bridge numerical models with different sizes of piers and rebar detailing are developed. Under various impact velocities of the moving trucks, the impact forces and displacements of the pier should be captured and compared. Since the same bridge is likely to be subjected to both earthquake

and vehicular loads during its service life, a detailed understanding of correlations between seismic resistance and impact demands of a bridge designed to sustain earthquake loads as per current AASHTO specifications is necessary. Through the results of extensive numerical simulations, we propose to develop a performance-based framework for seismic-impact correlations for highway structures.

Simplified Pier-bent Model for the Assessment of Bridges Subject to Vehicular Impacts: Simulations of vehicular impacts using a full 3-D model of a bridge is very time consuming and expensive. It has been observed that the failure modes of bridge structures under vehicle collision are almost localized and most of the damage occurs on piers and bents directly impacted by a truck. In order to decrease the degrees of freedom and simulation time, a simplified Pier-bent model is proposed. Preliminary simulation results show that the behavior of the simplified Pier-bent model is almost identical to that obtained by the full bridge model subjected to vehicular impacts. The simplified pier-bent model still utilizes the detailed modeling of concrete and rebars in the pier of the bridge, hence the simplified Pier-bent model with equivalent axial gravity load can capture essential behavior of the full 3D bridge model during vehicular impacts.

Effective Measures to Protect Existing Bridge Piers: For existing bridges that are vulnerable to failure during impact with heavy vehicles, numerical simulation provides an applicable and convenient way to evaluate the effectiveness of retrofit approaches such as wrapping vulnerable components of a bridge by fiber reinforced plastics (FRP) or steel jackets.

Research on this aspect will include modeling of FRP or steel jackets in LS-DYNA and extensive simulations of vehicle impacts on piers wrapped by FRP and steel jackets. Based on simulation results, guidelines to apply these protective measures on bridges will be developed.

1.3 Outline of the dissertation

This dissertation presents our research to achieve the objectives mentioned above. The outline of the dissertation is presented in the following. Each of the chapters deals with separate but integrated tasks to meet the objectives described above.

Chapter 2 presents a detailed review of literature relevant to vehicular impact loads. The state-of-art and state-of-practice on impact analysis, design and application in civil engineering are reviewed critically. The development and validation of vehicle numerical model is also explained in this chapter.

Chapter 3 describes a hypothetical bridge and the development of its finite element model. A comprehensive discussion of the concrete material model available in LS-DYNA is presented in this chapter, including the literature review on constitutive concrete models and a comparison of the different material damage models based on simulation results. The concrete Cap Model has been selected to carry out the simulation of vehicle impact in this research. The last part of this chapter discusses numerical modeling issues, such as simulation time step, element mesh size, application of gravity load and hourglass numerical stability that must be addressed. The simulation of RC beams under impact load has been carried out to validate the material model and numerical issues for the simulation in this dissertation.

Chapter 4 presents twelve numerical analysis cases of four bridge models under three approach impact velocities. The related impact forces and displacements have been recorded and compared, and failure modes of the bridge structures are identified. The four bridge models have been developed based on the seismic load requirements of AASHTO 2007. Hence, a comprehensive framework on seismic-impact correlations has been developed.

Chapter 5 recommends a simplified Pier-bent model for bridge vehicle collision simulation based on the deformation profiles and failure modes of the whole bridge model obtained in the previous chapter. The validation of the Pier-bent model is discussed by comparing the results with those of whole bridge numerical model.

Chapter 6 recommends retrofit methods for highway bridges to improve their impact resistance. Following procedures used for seismic retrofits, numerical simulations of the most vulnerable bridge pier retrofitted with steel jackets and FRP jackets have been carried out. The numerical results demonstrate that seismic retrofit methods could be effective means to improve the performance of highway bridges under vehicular impact loads.

Chapter 7 presents the conclusions of this dissertation and recommends future research in the subject area.

Chapter 2 Literature Review

2.1 Introduction

The primary purpose of this research is to develop a comprehensive numerical framework for vehicle-bridge collision simulation. The work outlined in this dissertation deals with a high fidelity investigation of the failure modes of highway bridge structures under the vehicular impact loads. To achieve this objective, a comprehensive understanding of past research work on this subject is necessary, including available design provisions related impact loads on highway bridge structures, recent experimental tests, numerical simulations on vehicle-bridge collisions, and advantage and validation of simulation software. In order to prevent a vulnerable highway bridge from severe damage because of vehicular impact loads, seismic retrofit methods can be applied to strengthen a bridge pier. This chapter present state-of-the-art on important aspects of vehicular impact loads on highway bridges.

2.2 State of Practice in Design Provisions for Vehicle Collision

In most design manuals, vehicular collision loads are included in the category of extreme event loads. The probability of two or more extreme event loads occurring simultaneously is extremely small and therefore is not to be applied. In most cases of vehicular impact loads, bridge designers should consider protecting bridge structures by external safety features (e.g., barriers). However, if a bridge is unprotected or isn't protected sufficiently, vehicular collision forces will govern the design of bridge piers. In order to protect bridges during accidental

collisions by heavy vehicles, the AASHTO LRFD (1998&2007) code provides design criteria to incorporate vehicle collision-loads in the design of piers. The design provision requires that unprotected structural elements that may be impacted bluntly by a vehicle or train should be designed to resist an equivalent static collision force of 400 kips, which is assumed to act in any direction in a horizontal plane, at a distance of 4.0 ft above ground level. In the commentary of this provision, it is explained that the 400 kips force is based on information on full-scale barriers for redirecting 80.0 kips tractor-trailers and the analysis of other truck collisions. For an individual column shaft, the equivalent static load should be considered as a point load. According to the description above, the statement of the provision about the vehicle collision in AASHTO LRFD code is rather vague and it does not indicate that the design force of 400 kips was derived directly from head-on collision tests between moving vehicle and bridge piers. It has been pointed out that the specifications of the AASHTO code have a number of significant limitations, including: (1) the design collision force is not specified as a function of the design velocity of the adjacent roadway or the vehicle characteristics, (2) dynamic interaction between the colliding vehicle and the bridge structure is not recognized, and (3) there are no guidelines on how to design a vulnerable member to ensure that it will survive a severe impact.

With concerns about the vague statement of the AASHTO code, some State DOT have tried to define their own policies for the design of bridge substructures vulnerable to potential

vehicular collisions. For instance, the Bridge Office Substructure Protection Policy of the Minnesota State Department of Transportation comments that the vehicle collision article of AASHTO is overly restrictive because it does not include any variation in requirement due to probability of vehicle collision. For example, bridges spanning over roadways with low design speeds (i.e., roadways with design speed less than 40 mph) or minimal traffic volume are at low risk of impact by vehicles. On the other hand, bridges spanning over roadways with high design speeds or significant traffic volume are at higher risk of impact. The Minnesota DOT guideline recommends specific design requirements based on redundancy since the redundancy of bridge piers increases with an increase in the number of piers. New York State DOT has developed a Collision Vulnerability Manual in 1996. In this manual, a detailed procedure has been presented to quantitatively evaluate collision vulnerability of superstructures and substructures of highway bridges under the hazard of vehicular impact. The procedure of classifying and rating for bridge collision vulnerability is quiet clear and applicable. It is applicable to new bridges, existing bridges and bridges programmed for rehabilitation. However, the guideline is based on qualitative factors, rather than mechanics based simulations.

In U.K., the Highways Agency (HA) is responsible for specifying the loading criteria for highway bridges. The requirement to design bridge piers to resist heavy weight collision loads was first introduced in the UK in 1978. The static load was derived from the assumption of a

90 degree impact for a 40 ton vehicle at 50 MPH. A slowing down of 10 MPH can be reasonably expected as the effect of the driver braking, if the giving maximum design travelling speed is 60 MPH. The Highways Agency also presented possible criteria to evaluate the risk for each specific site, including the following issues:

i) Risk assessment: risk assessment provides an approach to identify the hazards and the relation between the hazards and the consequences after the accident.

ii) Risk methodology: risk is expressed as the product of the probability and the consequence, and is expressed as:

$$Risk = P_v \times P_c \times P_f \quad (2.1)$$

Where P_v stands for the probability that the vehicle leaves the traffic lane and impacts piers; P_c stands for the probability that the impact load is greater than the pier's load capacity; and P_f stands for the consequence of pier failure.

iii) Probability of pier impact and probability of impact load being greater than pier load capacity.

It is possible to calculate the probability of pier impact and the impact load. However, it is difficult to estimate the impact load capacity of bridge piers. The probability of a moving vehicle impact on a bridge pier is quite low, however the consequence could be very severe if the impact leads to the collapse of the bridge. P_f and P_v can be determined based on parameters

such as: lateral clearance from the traffic lane, likely speed of impact; vehicle mass and type, and highway characteristics. For applications, it should consider more important factors and allow appropriate weights. A typical risk acceptance curve can be illustrated in Figure 2.1.

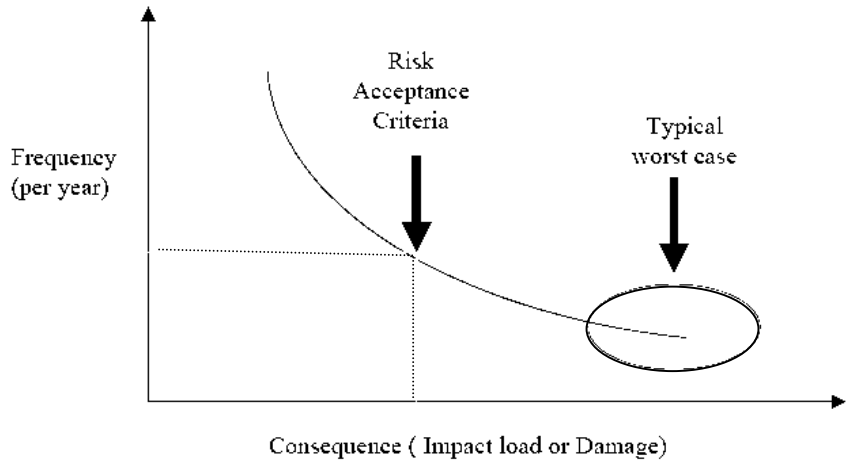

Figure 2.1 Typical Risk Acceptance Curve Described by U.K. Highway Agency

The development of design criteria based on risk assessment requires addressing the following issues:

- Definition of risk acceptance criteria.
- Definition of the type of consequence or outcome.
- Assessment of factors influencing the probability of vehicular impact.
- Modeling of severity of the collision for consequence analysis.

Risk criteria have often been defined in term of casualty. Risk acceptance criteria have been recommended based on so called target reliability in some design provisions such as AASHTO LRFD. For example, AASHTO suggests an individual risk of death of 10^{-3} to 10^{-4}

per annum. The consequence of collapse of the pier could also be assessed by evaluating the robustness of the bridge and the type of road that could be affected. The consequence outcomes could be affected by various factors, such as, injury to passengers, cost of repair or replacement of a bridge and the effects on the highway network due to closure or restriction. In the design book of HA, typical groups of event consequences from a heavy goods vehicle (HGV) collision event are illustrated in Table 2.1

Table 2.1 Event Sequence of the Vehicle Collision

Event	Consequence outcome	Impact
HGV leaves carriageway and strikes bridge support	Damage to pier Possible bridge collapse Potential for collateral damage Injury to road collision vehicle occupant Secondary effects, injury to other road users	Injury and fatality to road users Cost of repair or replacement Effects on road network due to closure or restriction

Some public agencies have published a detailed procedure, e.g., collision vulnerability manual published by the New York State Department of Transportation, for evaluating influencing factors and probability of the vehicle impact on bride structures. However, the

modeling of severity of vehicular collision on a bridge for the consequence analysis remains the crucial step in the design and safety assessment of vehicle-bridge collision.

2.3 Experimental and Numerical Investigation of Impact Loads on Bridge Structures

Research work on the influence of moving vehicles on bridge structures has been ongoing for a long period. Before the middle of the nineteenth century, the load of vehicle was only considered as a static live load in the design and evaluation of bridges. Significant research focusing on the dynamic interaction between moving vehicles and bridge structures has been carried out during the last few decades. However, most of the studies involve bridge response under dynamic forces on a bridge structure, as a vehicle moves across a bridge with different speeds. Because of computational resource limitation, these studies modeled vehicle-bridge interactions by semi-analytical dynamic equations for the bridge and vehicle coupled through contact conditions. The moving vehicle is coarsely modeled as a moving load without considering the effect of inertia force [Timoshenko and Young (1974)]. Feng and Ayre (1979) resolved the inertia force effect by proposing a moving mass model. Yang and Lin (1995) presented a new approach for bridge-vehicle interaction by introducing damping effects between a truck and a bridge by considering a more complicated vehicle model.

Even though the dynamic model of the vehicle-bridge interaction has been improved gradually, it has been noted that the previous work is based on a relatively simplified dynamic

model with small number of degrees of freedom. For a instance, Tan (1995) simply modeled the bridge as a grillage model where the continua of the deck was idealized into a series of discrete elements connected at joints where it is possible to apply loads and restraints, as shown in Figure 2.2(a).

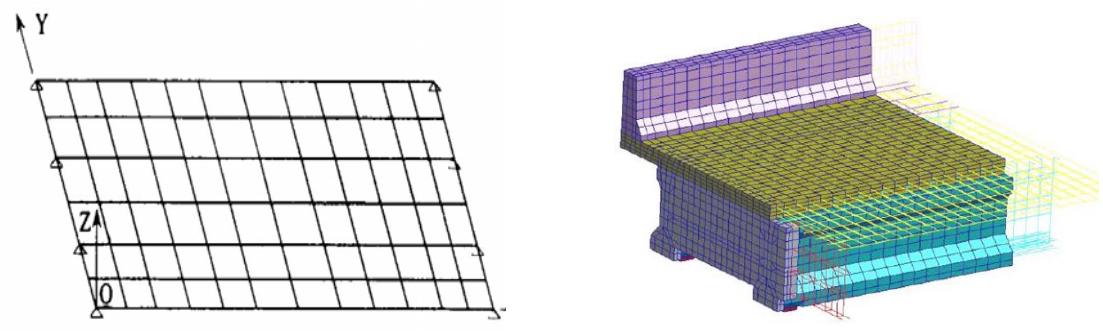

(a) Grillage of bridge structure (b) Three dimension model of bridge deck

Figure 2.2 Comparison of Numerical Model for Bridge Deck

During the last decade, advances in computer technology and high resolution finite element software have made it possible to improve the modeling of bridge structures. More sophisticated and rational 3-D finite element models with detailed modeling of various components can be used to simulate the interaction between moving vehicles and bridge structures. Concrete members can be modeled by fully integrated solid elements with eight or more nodes. Rebars and strands can be modeled as one dimensional beam elements with nodes coinciding with nodes of concrete solid elements. Figure 2.2(b) shows a cut-away segment of a FE model for a span of a bridge for bridge-vehicle interaction simulation [Kwasniewski and Li (2006)]. The numerical concrete structure in Figure 2.2(b) was used to model a common

multi-girder concrete bridge with short span located in North-West Florida. The simulation captured the deformation of the bridge deck when heavy truck is moving on top. Compared with the simple grillage model shown in Figure 2.2(a), more realistic and detailed numerical results can be expected using the three dimensional model in Figure 2.2 (b). Furthermore, a more complicated vehicle model was built with 3-D solid elements instead of the equivalent moving block of mass, and the coupling of the bridge and vehicle was replaced with a real contact and impact simulation between the tires of the truck and the top surface of the bridge deck, simulating the real physical procedure while the vehicle was moving on the top of the bridge deck.

Although bridge-vehicle interaction, when the vehicle is moving on the bridge, has been investigated extensively, the magnitude of the load in such studies is much less than that of the impact load during vehicle-bridge collisions. Material models used during bridge-vehicle interaction studies are also not appropriate for simulations involving vehicular impacts on bridges. Impact loads on bridge structures during vehicle-bridge collisions are extremely high with a very short time history, usually less than one second. Such impacts cause geometric large deformation and nonlinearity in both the bridge and the vehicle. Components of both the bridge and the vehicle undergo significant damage, stiffness redistribution and plastic hinge formation. This behavior cannot be modeled by semi-analytical methods. A detailed modeling of the entire phenomenon using LS-DYNA is one of the most efficient approaches to understand its different aspects.

Ships or vessels moving in water ways are much heavier than moving vehicles on highways. Collision safety of bridges crossing waterways is considered much more crucial because of significant economic, societal and life-safety concerns. Hence, collision of ships with bridges has been investigated more extensively than vehicle collisions. Current AASHTO code prescribes a much more detailed and operable design provisions for vessel/ship- bridge impact loads. The calculations conducted according to the AASHTO provisions involve the use of both an empirical load prediction model and a risk assessment procedure. Unfortunately, as a consequence of the fact that very little ship collision data has been published in the literature, the ship impact provisions derive primarily from experimental studies conducted by Woisin (1976) that focused on protecting reactors in nuclear powered ships against accidental impact by other ships. In April, 2004, the Florida Department of Transportation conducted a series of full-scale experiments with barge impact on an old (now demolished and replaced) St. George Island Casuseway Bridge as shown in Figure2.3 [Consolazio,2005]. The impact load and resulting structure, soil and barge responses were measured directly by an array of sensors and high-speed data acquisition systems.

Figure 2.3 Full scale test of the barge bridge collision in Florida

One of the most interesting findings from the analysis of the test results shows a tremendous influence from inertial restraints by the superstructures on the column design forces. It was found that the inertial restraint from superstructure mass can produce column design forces that are more than 200% larger than those calculated by the static procedure prescribed in AASHTO. Hence, if the equivalent static design procedure is used for bridge column design, a reasonable pier-column and dynamic amplification factor should be adopted to revise the design force of the pier to resist the high speed impact loading.

Unfortunately, because of significant costs, logistics of conducting full-scale tests and size effects involved with small scale tests on concrete structures, information available on full scale impact tests on real bridge piers under the impact of moving ships or moving vehicles is very limited. Recently, two experimental tests on vehicular collision with infrastructure have been reported in the literature. An experimental study of anti-ram bollards (Concrete filled steel columns acting as barrier to vehicles) based on truck collision testing was conducted in Hunan University, China [Xiao and Liu (2009)]. The Test bollards were concrete-filled steel tube columns with outer diameter of 219 mm and height of 1300 mm. The thickness of steel pipe was 20 mm, and C40 concrete was filled in the steel tube. There were 5 columns in these testing bollards with the interval distance of 1500mm as shown in Figure 2.4(a).

(a) Front view of anti-bollards

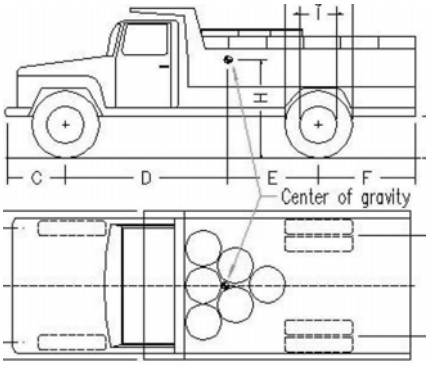

(b) Truck Geometry diagram

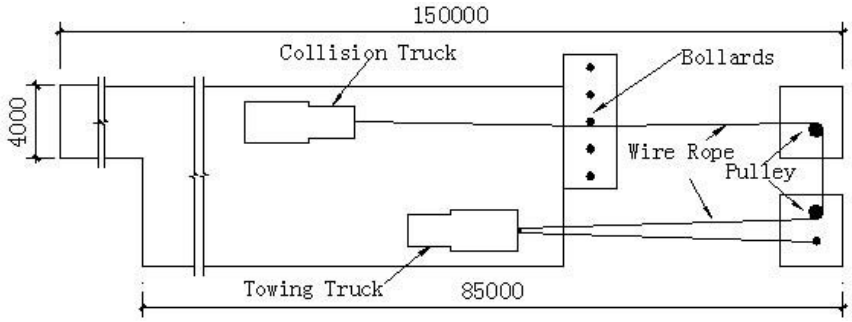

(c) Diagram of test site and facilities

(d) Truck and bollards after the collision

Figure 2.4 Truck collision Testing of Anti-ram Bollards

A Dongfeng EQ140 was selected as collision vehicle in the test shown in Figure 2.4 (b). The weight of the truck was 5.17 tons and six petrol barrels filled with soil were loaded on the truck to reach the total weight of 6.8 tons. The collision test truck was driven by a wire system with a pulley wheel connecting the towing truck, as shown in Figure 2.4(c). The collision truck impacted the mid column with 40 km/h (25.9MPH) speed. Figure 2.4(d) shows the truck and bollards after the collision. The acceleration time history of the moving truck was recorded during the impact test. The maximum acceleration was 52g and the associated maximum impact force was measured as 3465KN (779kips). Considering 0.07 seconds of deceleration time, the average impact force of 1660 KN(373kips) has been calculated during the collision. Static load capacity of the bollard has been estimated as 350KN, which is about one fifth of the average impact force calculated based on the collision test. Because of the high capacity of the steel tube column filled with concrete, the column under impact didn't undergo large deformation and a residual displacement of only 33 mm was measured(a drift ratio of 2.54%).

Texas Transport Institute carried out experimental tests, sponsored by Federal Highway Administration, to study collision loads on bridge piers. The objective of these tests was to measure impact forces on the bridge piers. A 36-in diameter simulated steel bridge pier, 14 feet in height, was fabricated with 1 in thick A53 Grade B pipe material. The inner surface of the 36 in pipe was welded with a 120^{o} arch of A53 Grade B pipe (34-in in diameter and 1inch in thick). The steel pier was supported by braced column load frame and foundation system. The capacity of the test pier was extremely high and the pier could be considered as rigid body in

the analysis. In addition to comprehensive accident survey and risk analysis of vehicle/bridge column and abutment collisions, two full-scale collision test involving 80,000lb heavy truck (2001 Freightliner FLD tractor and 1979 Bud van Trailer) were performed at TTI. The approach speed of the truck was set at 50 MPH in both cases. The difference in the two collision tests was the alignment of the truck with the pier. In the first test, right quarter point of the vehicle was aligned with the centerline of the pier, whereas the centerline of the vehicle was aligned with the centerline of the pier in the second test. The final images of first test are shown in Figure 2.5. In both these tests, there was no apparent structural damage in the rigid pier. Test results show that there is no apparent structural damage in the instrumented bridge pier. Only cosmetic damage on the pier surface was observed. However, the vehicles suffered catastrophic damage.

(a) Test No.1 (b) Test No.2

Figure 2.5 Tractor-trailer and Rigid Steel Pier Collision Test by TTI.

The impact force was recorded by load cells installed at the top and bottom of the instrumented pier. Figure 2.6 shows impact force time histories for the two tests. It is observed from the time-history of the measurement that the peak impact force was 600 kips when the

ballast hit the bridge in the first test. The peak impact force reached 900 kips in the second impact test because of the collision between the engine of the truck and the bridge pier. Based on the 900 kips impact forces, after several filtering processes, a value of 600 kips was taken as a more appropriate equivalent static force and was recommended to replace current 400 kips force in the AASHTO guideline.

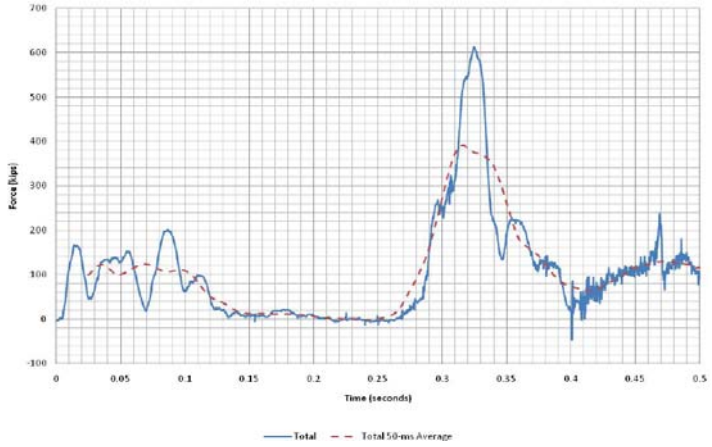

(a) Test No.1

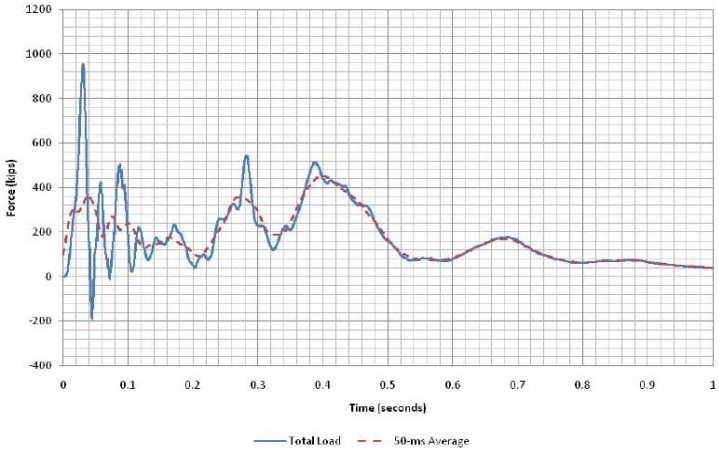

(b) Test No.2

Figure 2.6 Impact Force Time history recorded by TTI Test

The research conducted by TTI was the first direct measurement of the impact force between a bridge pier and a moving heavy vehicle. Because the experimental investigation is

very expensive, there were only two tests using one collision speed. However, for the general purpose of design, there still exist several limitations on the results of this study i) effect of the collision speed cannot be investigated from the available information since the approach speed of the truck was set at 50 MPH only; ii) only one rigid steel tube bridge pier was impacted. There was almost no structural deformation and damage to the pier. Hence, the failure mechanisms after vehicle collision were not obtained through the tests; iii) it was not appropriate to directly take the filtered peak impact force during the vehicle collision as the magnitude of the equivalent static force, because the structural response of bridge pier under the high speed impact load is totally different from the response under static load, even if the magnitudes of the two loads may be the same, iv) It is observed from Figure 2.6the peak force occurred at 0.32 second when front on the truck hit the pier. It has been observed from the video of the test that trailer containing majority of the weight hit the pier after the front of the tractor hits. Hence, impact for time history should have a second larger peak. More discussion and comprehensive research should be carried out to resolve above limitations of the experimental tests conducted by TTI.

Recent advances in the finite element method and computer hardware allow researchers to investigate such extreme events as high speed vehicle bridge collision through high-fidelity computer models. For example, Consolazio (2003) presented the results of the nonlinear analysis of barge-bridge crush behavior to investigate impact resistant bridge designs. The finite element model of the barge was constructed with sufficient mesh resolution so that local

buckling, yielding and internal contact could be adequately represented. Since the rear portion of the barge did not experience large deformation, the barge model was divided into three separate zones, each represented by a different degree of mesh resolution, as shown in Figure 2.7. The entire barge FEM model contains 25,000 shell elements, 2000 beam elements and 250 solid elements. Two most commonly used bridge pier shapes (circular and square) were developed to study the crush behavior when the barge collided with concrete bridge piers. However, the concrete was assigned an elastic material model. Three circular piers with diameters: 4, 6 and 8 ft and three square piers with width: 4, 6 and 8 ft were used for a parametric study of impact forces during collisions.

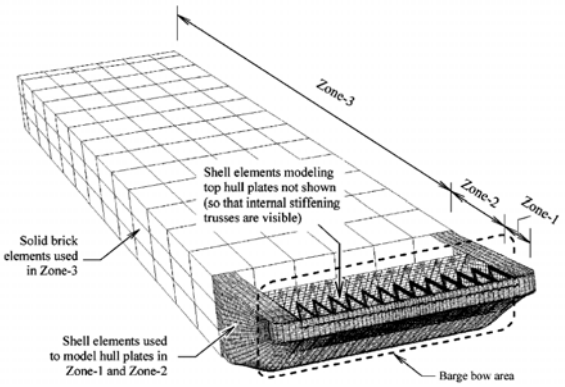

Figure 2.7 FEM model of the barge using in the bridge impact simulation

Crush forces in the case of square piers were observed to increase rapidly with an increase in pier size. Contact forces for square piers increased rapidly to peak value for a certain crush depth and then decreased gradually to certain values for higher crush depths as shown in Figure 2.8(b). The difference between impact forces for piers of different sizes for

circular piers has been found to be very small, as shown Figure 2.8(a). Crush forces, in this case, increase monotonically with increase in the crush depth.

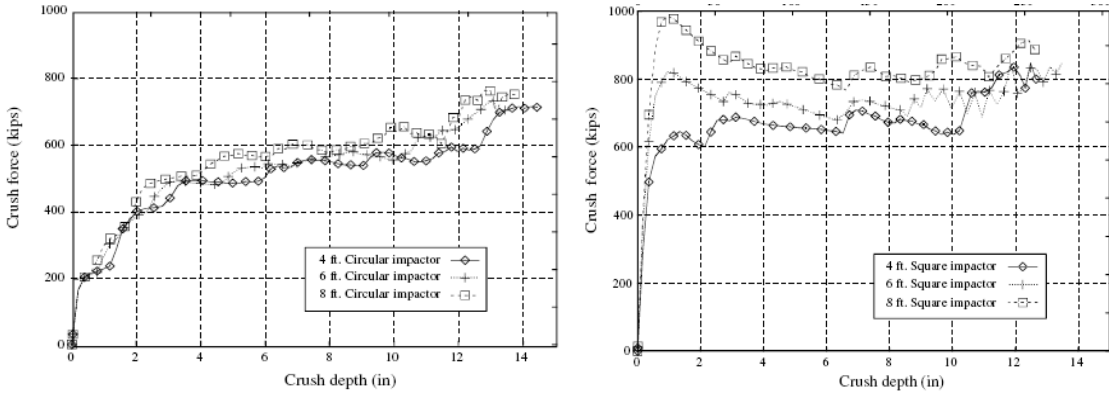

(a) Circular Pier Case (b) Square Pier Case

Figure 2.8 Crush force time history of the barge and the piers

The influence of pier geometry on crush behavior is related to the internal structure of the vessel. In the bow of a barge, numerous internal trusses run parallel to one another resulting in significant stiffness in the contact direction. Contact zone of the square pier is surface to surface where it is point to surface in the case of circular piers. During impact on a square pier, more internal trusses come in contact with the pier when the width of the pier increases. However, fewer internal trusses near the contact point contribute to the contact between the barge and the pier in the case of circular piers.

Similar numerical results were obtained by Abu-Odeh and Brackin (2007) as a part of Texas Department of Transportation sponsored study. Resultant forces similar to those in Figure 2.9 were observed through the simulation of vehicular impact on round piers with

diameters of 24 in, 36 in and 48 in. However, the simulated round piers were modeled as rigid body. Hence, the failure mechanisms of the piers were not obtained during the simulation.

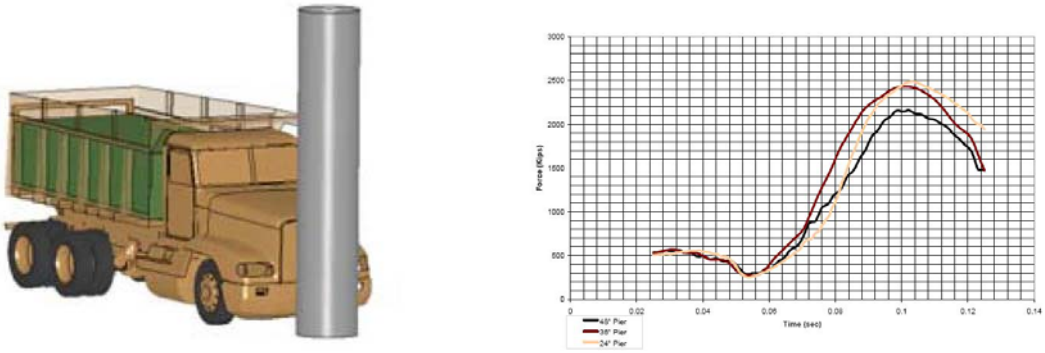

(a) FEM model (b) Resultant impact force

Figure 2.9 Truck Pier Impact Simulation by Texas DOT

The most recent published literature on vehicle collision simulation with bridge piers presents various data of interest which were extracted from the finite element results [Sherif EI-Tawil and Edward Severino (2005)]. Two publicly available truck models were introduced in the simulation: a light weight truck with a weight of 14 KN and a medium weight truck with a weight of 66 KN. Two different bridge piers were studied and peak dynamic forces and equivalent static forces were calculated. Some valuable results from this study will be compared with the research work in this dissertation in Chapter 4. Their results imply that the AASHTO-LRFD design provisions are not sufficient to protect bridge piers during reasonable crash scenarios. More research work on the simulation of vehicle bridge collision should be carried out to develop adequate design specifications. The peak impact force from the case of

66 KN (15,000 lb) truck with 90 KMH (56 MPH) speed reached the magnitude of 7600KN (1708kips), and even the related so-called ESF (equivalent static force) has been found to be 850 kips. Compared with 600 kips that the test result in the TTI study (80,000 lb truck with speed of 50 MPH), the 850 kips is extremely high, considering the fact that the weight of the truck is only one-fifth of that in the TTI test. Another major concern is the material models in the two studies cited above. The bridge pier in the research by Sherif (2005) was modeled with perfectly elastic material, whereas the pier tested in the TTI study was very rigid without any deformation. It has been observed that the stiffness of bridge piers may dramatically influence the impact force between the pier and the truck.

Although the finite element model of the vehicles were built with nonlinear material properties and the validation of the vehicle models has been discussed, it should be emphasized that all the previous simulations modeled the concrete pier as rigid or elastic material because of computational limitations. In fact, the inelastic behavior of concrete influences the impact forces and the damage modes of the bridge piers dramatically after the high speed impact from the vehicle. The study in this dissertation applies recently developed nonlinear concrete material models for a detailed investigation of vehicular impacts on bridges.

2.4 Computer Program and Code Validation of Impact Numerical Simulation

The theoretical background for the numerical simulation of high speed impact problem is

addressed in the field of computation mechanics. Because of recent advances in computer technology, the finite element method has become one of the most efficient and popular approaches to investigate complicated problems such as vehicle-bridge collisions. Several general finite element software packages, such as ABAQUS, MSC/DYTRAN, LS-DYNA and ADINA, can be used for such problems. Since blast and impact loads cause large deformation in a very short time, LS-DYNA has the following significant advantages for investigating such problems:

- LS-DYNA has been originally developed to simulate the impact of a nuclear bomb for low altitude release with impact velocity of 40 meters/second. In LS-DYNA, inertial forces are considered as an important term in the transient analysis of high speed, short duration events. Any of the LS-DYNA's features can be combined to model a wide variety of physical events. A good example of a simulation that involves a unique combination of features is the NASA JPL Mars Pathfinder landing which simulated the space probe's use of airbags to aid in its landing.

- The program can treat the following strong applications of nonlinearity: changing boundary conditions (such as contact problems changing over time); large deformations like the crumpling of sheet metal parts; nonlinear material properties (for example thermoplastic polymers and damage concrete model). The contact algorithms of LS-DYNA range from the rigid body contact and include almost all

kinds of contact types, such as flexible body contact, edge to edge contact and eroding contact.

- LS-DYNA has a comprehensive and continuously improved material model library. Almost all kinds of engineering materials are included in the material library of LS-DYNA, such as metals, plastics, foams, viscous fluids, concrete and soils. In the numerical modeling of bridge structures, two major material models are steel and concrete. As a commonly used structural material, steel has been studied for long time, and the material properties and mathematical description of steel have proven to be correct and reliable. Concrete is a special brittle-cracking structural material. In the material library of LS-DYNA, there are five material models for concrete: soil and foam model(Material model 5), smooth cap model for the underground technology (Material model 37), soil/concrete model (Material model 78), Johnson-Cook Holmquist Concrete Model (Material model 111) and Continuous Surface Cap Model (Material 159). Particularly, recently developed JHC model 111 and Cap Model 159 have been developed to simulate the penetration and impact problems with relatively high strain rates. For the numerical simulation of bridge vehicle collision presented in this dissertation, the JHC concrete and Concrete Cap Model will be introduced and discussed in detail in the following chapter. The numerical bridge model will be constructed and validated with the most appropriate material model.

- LS-DYNA has been successfully used in many applications involving crash simulation in the automobile industry. Comprehensive automobile numerical models have been developed using LS-DYNA. These models were had all detailed structures using appropriate material models. The mesh size for auto crash model started from 3439 elements in 1986 and has reached to approximately 10 milions, as shown in Figure 2.10 [Benson (2009)]. All the numerical models have been revised according to real impact experimental tests by the mobile company research centers, and parameters such as mesh size, material parameters and contact algorithms have been validated for future simulations of vehicular impacts. Plenty of publicly available truck models have made research on vehicular impacts on bridges feasible and convenient.

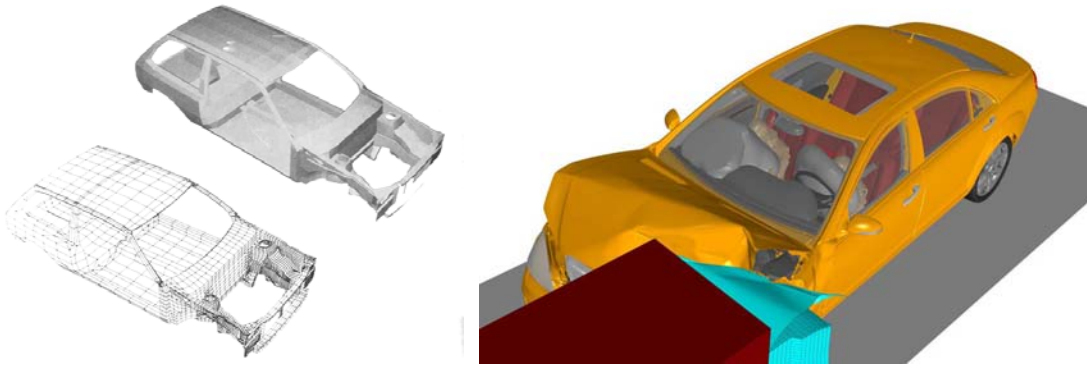

(a) Early model with 3439 elements (b) Current model with millions of elements

Figure 2.10 Numerical Model of the Crush Automobiles

Because of the significant advantages described above, LS-DYNA will be used in this study to simulate vehicle-bridge collisions. Furthermore, since a comprehensive and reliable

vehicle model is available, we will focus on the modeling of concrete bridge in the following chapter. The selected vehicle model will be combined with the numerical bridge model in LS-DYNA.

Chapter 3 Validation of Concrete Material Model and Numerical Bridge Modeling

3.1 Introduction

The research carried out in this dissertation focuses on the numerical simulation of bridges impacted by trucks and investigates the structural response and failure mechanisms of highway bridges using the explicit finite element method. The first and essential step in the simulation is to build a reliable high fidelity finite element model of the bridge and the vehicle with appropriate numerical algorithms and correct material models. The FEM vehicle models have been built and tested by the research center of the automobile industry. Based on several years of extensive work, vehicle FEM models have been revised and validated on the basis of experimental crash tests. Hence, the available truck model, which has been adopted in this research, is believed to be numerically stable and reliable.

In this chapter, we present a detailed approach for the modeling of highway bridges. The procedure of modeling a bridge by finite element method is shown in the Figure 3.1. In the numerical simulation using explicit finite element method, material properties, mesh size and time step size are important factors for ensuring reliable results. Furthermore, if the contact and erosion effects of the concrete material are considered in the simulation, the eroding contact algorithm and hourglass energy should still be carefully analyzed to ensure numerical stability and reliability of numerical results. The following parts of this chapter present

detailed description of the modeling and validation of the concrete material model, numerical bridge model, and related numerical algorithm for the vehicle bridge collision simulation using LS-DYNA.

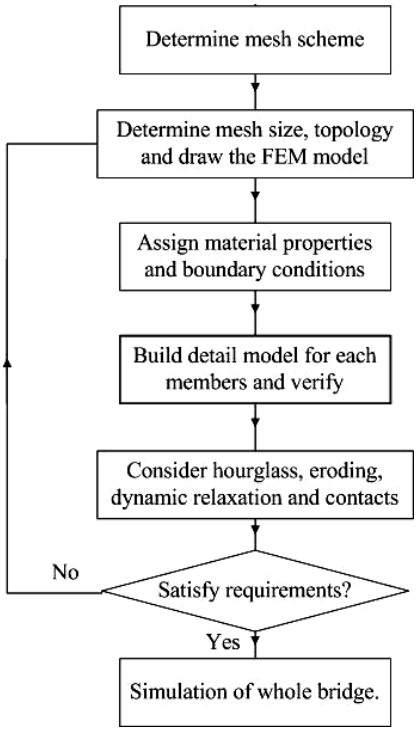

Figure 3.1 Procedure of FEM modeling of highway bridges

3.2 Concrete Material Model for Impact Loads

In the current version of LS-DYNA, there are five concrete constitutive models to simulate the behavior of concrete structures. Three concrete material models (Plastic/kinematic Model, soil/Concrete Model and Winfrith concrete model) are not suitable for solving problems with damage failure, large strains and high strain rates. The remaining two concrete material models (Johnson-Cook Holmquist Concrete Model and Continuous Surface Cap

Concrete Model) include material damage, strain rate effects and permanent damage erosion, which are highly nonlinear effects during high speed impacts. Even though these two models are mathematically complicated and require significantly higher level of computer capacity and time, they are much more reliable for identifying failure modes of concrete bridge piers subject to loads with high strain rates, such as blast and impact. In this section, we perform a comparison between these two models based on available examples.

3.2.1 Johnson Holmquist Cook Concrete Model

Holmquist and Johnson (1993) presented a computational constitutive model for concrete subjected to large strains, high strain rates and high pressure in the Fourth International Symposium on Ballistics. This constitutive model has been incorporated into LS-DYNA to simulate the concrete behavior under high speed impacts. This model is originally based on the Johnson Cook Model proposed to investigate fracture characteristics of three metals subjected to various strains, strain rates, temperature and pressures [Johnson and Cook (1983)]. It is first assumed that the difference between the "dynamic" material property and "static" material property is not only because of the strain rate effects, but also because of the large strains, high temperature and high pressure associated with high strain rates. The Johnson Cook Model for metals assesses the effects of each variable properly. A cumulative-damage fracture model has been developed and evaluated with an independent series of tests and computations.

In the JHC model, the normalized equivalent stress is defined as $\sigma^* = \sigma / f_c'$, where σ is the actual equivalent stress and $f_c^{'}$ is the quasi-static uniaxial compressive strength of

the concrete. The normalized equivalent stress σ^* is expressed as:

$$\sigma^* = [A(1-D) + BP^{*N}][1 + C\ln\dot{\varepsilon}^*] \tag{3.1}$$

where D is the damage ($0 \le D \le 1$),in the same manner similar to that used in the Johnson-Cook Fracture Model for metals, which accumulates damage from an equivalent plastic strain; $\dot{\varepsilon}^* = \dot{\varepsilon}/\dot{\varepsilon}_0$ is the dimensionless strain rate(where $\dot{\varepsilon}$ is the actual strain rate and $\dot{\varepsilon}_0$=1.0 S^{-1} is the reference strain rate); ***A*** is the normalized cohesive strength, ***B*** is the normalized pressure hardening coefficient and ***N*** is the pressure hardening coefficient. Using test data on perforation of concrete slabs having 48 MPa and 140 MPa unconfined compressive strengths [Hanchak (1991)], parameters for the JHC model in equation (3.1) can be determined using a procedure similar to that for Johson-Cook fracture model for metals. Even though there are 26 parameters for the JHC model in the material card of LS-DYNA, most of the parameters are not sensitive to variation in concrete strength and can be assumed to be the same as those provided by Holmquist and Johnson (1993). The specific description of the parameters for the JHC model can be found in the material manual of LS-DYNA for Model_111. Computational results using the JHC model show a good agreement with experimental results on penetration tests of concrete under impact of steel bullet obtained by Hanchak (1991).

3.2.2 CSCM Concrete Material Model

In order to improve roadway safety, the Federal Highway Administration (FHWA) sponsored a study by APTEK Incorporated and the Texas Transportation Institute to develop a

concrete material model for use in roadside safety simulations, implement the model into LS-DYNA finite element code, and evaluate the model against available data. The concrete model developed by APTEK is referred to as a smooth or continuous surface "cap" model (CSCM).

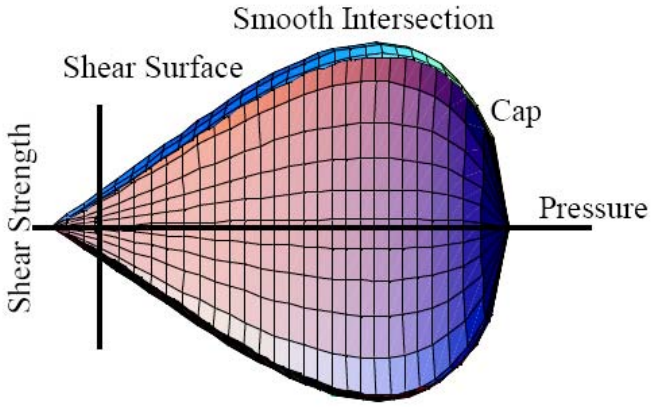

Figure 3.2 General shapes of the concrete model shear failure and cap hardening surfaces in two dimensions.

As shown in Figure 3.2, the failure surface is plotted as shear strength versus pressure, and a smooth and continuous intersection is formulated between the failure surface and hardening cap. The theoretical description of this concrete model contains constitutive equations, yield and hardening surfaces, damage-based softening with erosion and rate effects formulation for the increase of strength with strain rate. Used as a comprehensive material model for concrete, particularly for modeling strain softening in tensile and low confining pressure regimes, the model can be grouped into five formulations, which are elastic update, plastic update and yield surface definition, damage, rate effects, and kinematic hardening.

- **Elastic:** Concrete is assumed to be isotropic and Hooke's Law is applied with two constants: the bulk modulus (**K**) and the shear modulus (**G**).
- **Plastic and Yield Surface:** If a trail elastic stress σ_{ij}^{T} lies inside the yielding surface, the behavior is elastic, otherwise the behavior is elastoplastic with possible damage, hardening and rate effects, and plasticity algorithm returns stress state to the yield surface, and related elasto-plastic stress is denoted as σ_{ij}^{P}. The yielding surface uses a multiplicative formulation to combine shear (failure) surface with hardening compaction surface (cap) smoothly and continuously, which is referred to as smooth cap model, as shown in Figure 3.2. The yielding surface is formulated in terms of three invariants, J_1-the first invariant of the stress tensor, $J_2^{'}$-the second invariant of the deviatoric stress tensor, and $J_3^{'}$-the third invariant of the deviatoric stress tensor. J_1, $J_2^{'}$ and $J_3^{'}$ are defined in terms of the deviatoric stress tensor S_{ij} and pressure P. The yield function is defined as

$$f(J_1, J_2^{'}, J_3^{'}, \kappa) = J_2^{'} - \Re^2 F_f^2 F_c \tag{3.2}$$

where κ is the cap hardening parameter; F_f is the shear failure surface, F_c is the hardening cap, and $\Re$ is the Rubin three-invariant reduction factor.

- **Shear Surface and Cap Hardening Surface:** The strength of concrete is modeled by the combination of the cap and the shear surface in the low to high confining pressure regimes. The shear surface is defined along the compression meridian and the cap function has a tedious but straightforward definition which can be found in the

LS-DYNA User Manual(2007). Figure 3.3 shows the failure surface combining the shear surface and the cap surface in one dimension for typical concrete values.

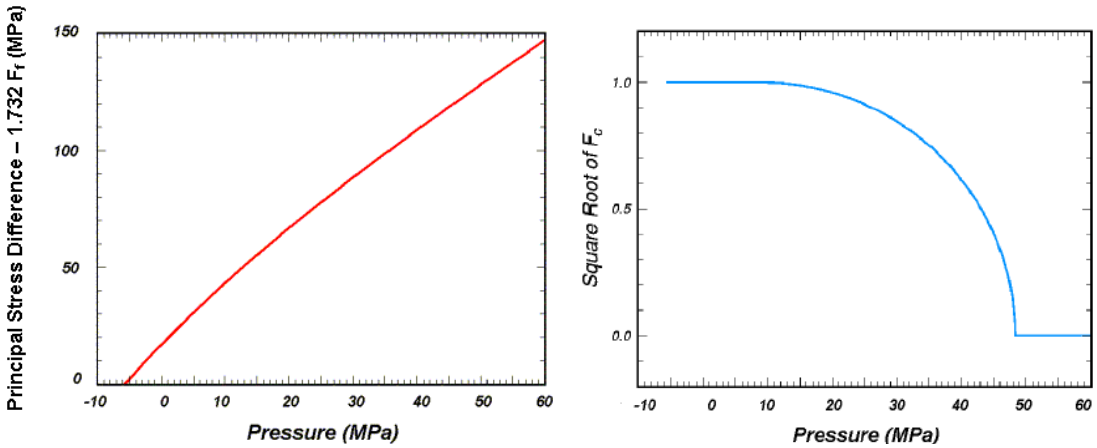

(a) Graph Schematic of Shear Surface (b) Graph Schematic of Cap Function

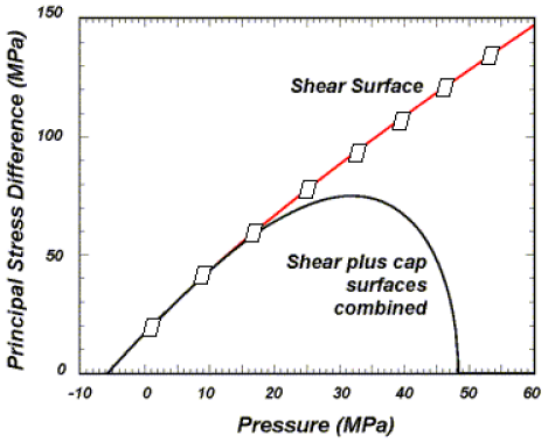

(c) Combined Failure Surface

Figure 3.3 Multiplicative Formulation of the Shear and Cap Surfaces

- **Damage:** Damage accounts for the softening of concrete in the tensile and low to moderate compressive regimes. The damage formulation models both strain softening and modulus reduction. Strain softening is a decrease in strength during progressive

straining after a peak strength value is reached; the modulus reduction is the reduction in the unloading/loading slopes in the process of cyclic unload/load tests. Damage initiates and accumulates when the strain-based energy terms exceed the threshold and is based on two distinct formulations: brittle damage and ductile damage, where brittle damage accumulates when pressure is tensile and the ductile damage accumulates when pressure is compressive. Brittle damage accumulation depends on the maximum strain, $\varepsilon_{\max}$, which is defined as

$$\tau_b = \sqrt{E\varepsilon_{\max}} \tag{3.3}$$

Brittle damage initiates when τ_b exceeds an initial threshold. Ductile damage accumulation depends on the total strain components, ε_{ij}, which is defined as

$$\tau_d = \sqrt{\frac{1}{2}\sigma_{ij}\varepsilon_{ij}} \tag{3.4}$$

The stress components σ_{ij} are the elasto-plastic stresses calculated before application of damage and rate effects. Ductile damage initiates when τ_d exceeds an initial threshold.

- **Rate Effects:** rate effects accounts for an increase in strength with increasing strain rate, and are applied to the plasticity surface, the damage surface and the fracture energy.

In order to evaluate the CSCM model, the model developer performed numerical simulations for basic material properties to reinforced concrete structures. These detailed

studies include single element simulations to check the implementation of the model via examination of the stress versus displacement behavior; plain concrete cylinder simulation to check the damage modes; drop tower impact simulation and the bogie vehicle impact simulation of reinforced concrete compared with experimental data. All the work shows that that CSCM model can accurately simulate the displacement and damage modes of reinforced concrete structures under dynamic loading.

The current version of CSCM model in LS-DYNA has 37 input parameters. 19 parameters of the 37 input parameters must be fit to the data from triaxial extension (TXE) tests, triaxial compression (TXC) tests and torsion (TXO) tests. However, the usage of the model has been made easy by implementing a set of standardized material properties for use as default material properties. The CSCM model with default input parameters for normal strength concrete (with compressive strengths between 28MPa to 58MPa), and with aggregates sizes (between 8mm and 32mm) has been provided. Hence, concrete compression strength, aggregate size and unit of these parameters are the necessary input parameters for the CSCM material model in this dissertation.

3.2.3 Single Material Cylinder Simulations

This section presents comparison between single material cylinder simulations using JHC and the CSCM models under different loading rates since the simulations of plain concrete allow us to evaluate the behavior of the concrete model without the complicated effects of steel reinforcement. The length of the concrete cylinder is 304.8mm (12 inches) and

the diameter is 152.4mm (6 inches), as shown in Figure 3.4. The bottom of the steel end cap of the cylinder is fixed. The loading condition is an unconfined compression at the top of the steel end cap.

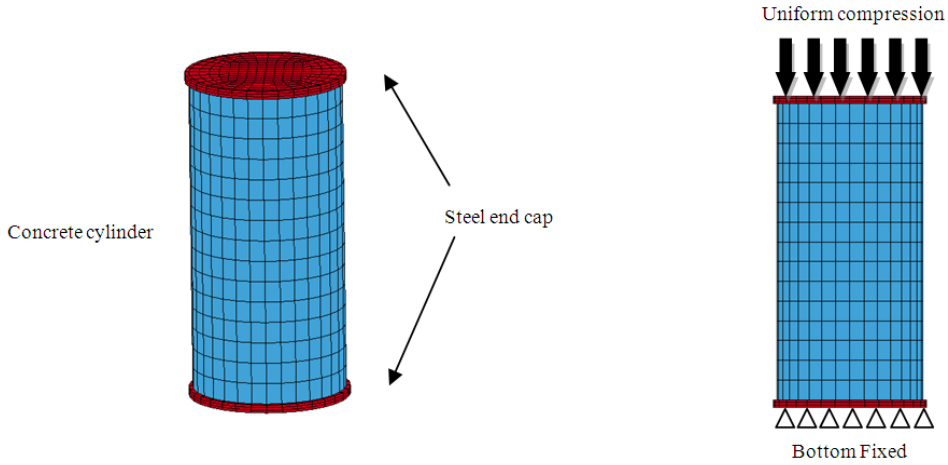

Figure 3.4 Numerical Model of Plain Concrete under Unconfined Compression

A uniform displacement was applied to the nodes at the top end cap. However, the loading time was varied, so this type of displacement control was expected to simulate the formation and failure modes of concrete cylinders with different loading strain rates. The mesh size of the concrete cylinder was taken as about 20 mm, which was recommended by the CSCM concrete model developer. The strength of the concrete was assumed as 46 MPA and the size of aggregate was set as 19 mm in the simulation. The cylinder was compressed by approximately 3.81 mm (0.15 in) during the loading durations of 1 ms, 10ms, 100ms, and 1000ms respectively. Figures 3.5-3.8 show the damage mode on a slice through the mid plane of the cylinder simulated using two concrete models under loading strain rates with durations 1000 ms, 100 ms, 10 ms and 1 ms, respectively. Fringe levels in these figures show the

damage level calculated by the concrete model. A fringe value of 0 indicates no damage, whereas a value of 1 indicates maximum damage in which the stiffness and strength of concrete are reduced to zero. When a concrete element loses all strength and stiffness or the maximum principle strain is greater than a user-supplied input value, the element is eroded from the numerical model to prevent computational difficulties.

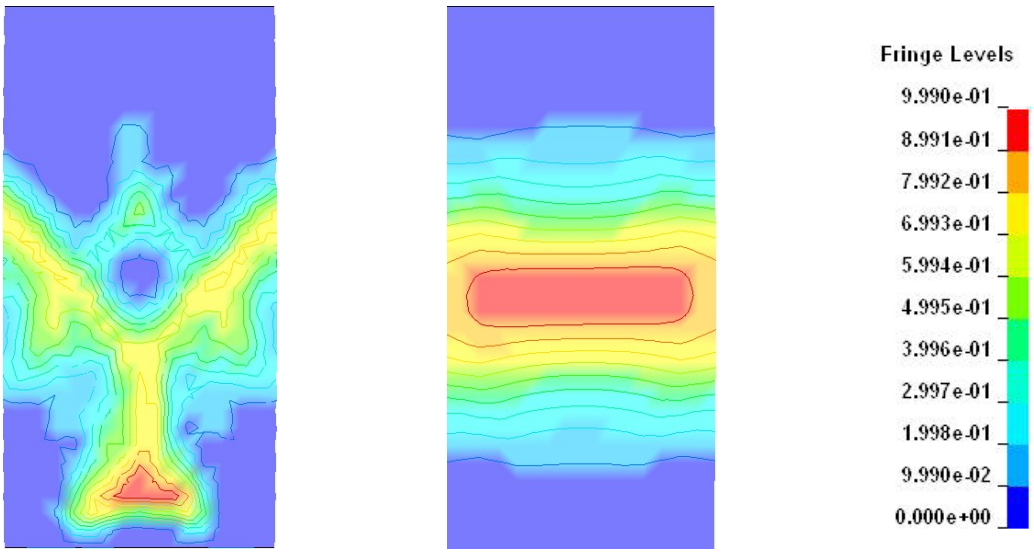

(a) CSCM Model (b) JHC Model (c) Damage Level

Figure 3.5 Damage Mode of Cylinder with Loading Time of 1000ms.

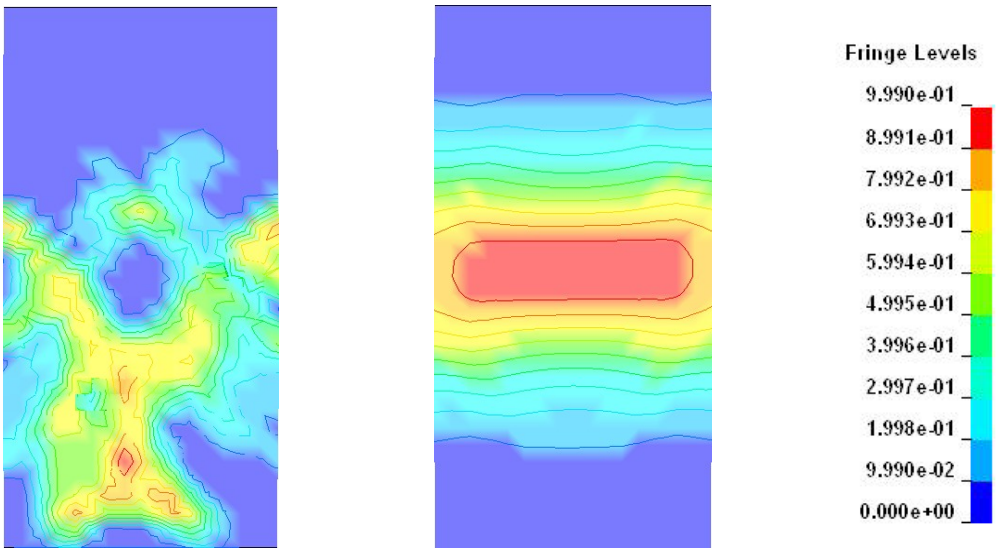

(a) CSCM Model (b) JHC Model (c) Damage Level

Figure 3.6 Damage Mode of Cylinder with Loading Time of 100 ms.

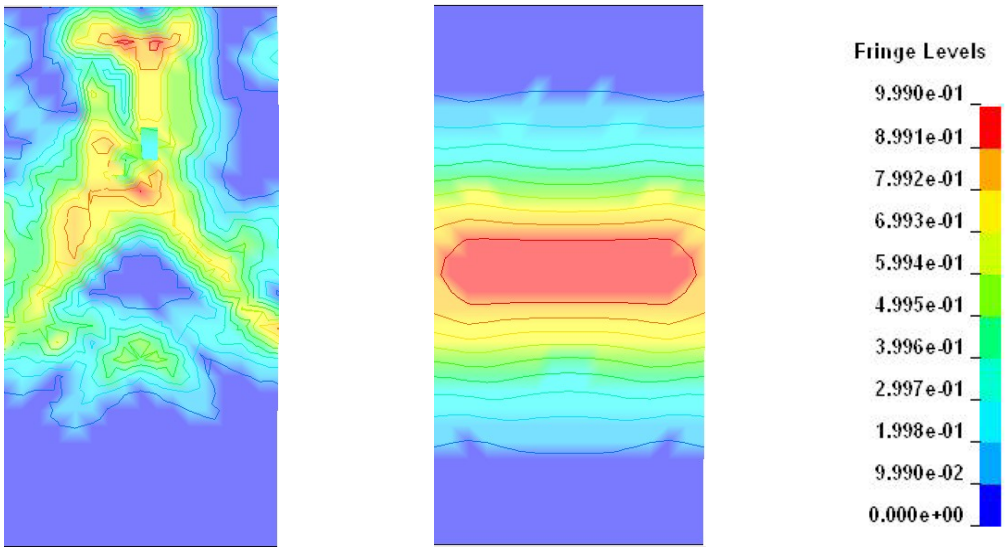

(a) CSCM Model (b) JHC Model (c) Damage Level

Figure 3.7 Damage mode of Cylinder with Loading Time of 10 ms.

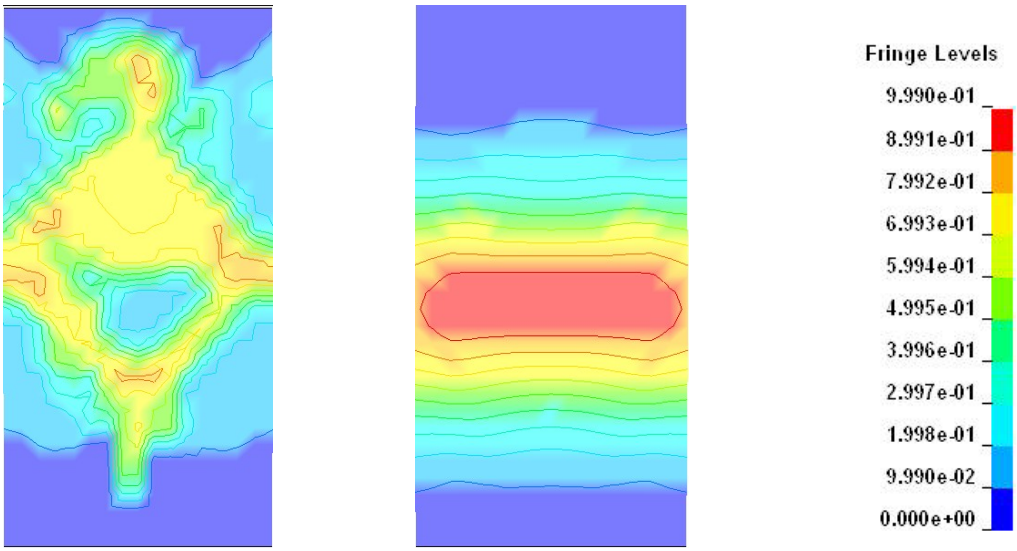

(a) CSCM Model (b) JHC Model (c) damage level

Figure 3.8 Damage mode of Cylinder with Loading Time of 1 ms.

As the loading time is decreased from 1000 ms to 1 ms, which means the loading strain rates increases 1000 times, the damage mode of the cylinder modeled with JHC model doesn't change significantly. On the other hand, the damage mode of the cylinder using the CSCM model varies with the loading strain rate. In Figure 3.6, where the loading time is 1000ms (which is almost close to quasi-static loading), the damage mode of the cylinder using CSCM model matched well with the concrete cylinder test shown in Figure 3.9 since an obvious shear failure appeared in the cylinder. In the case of 1 ms loading time, Figure 3.8 shows that the damage mode (in the middle of the cylinder) of the cylinder using CSCM model matches with that using the JHC model. This implies that the CSCM model can simulate the same damage mode as that by the JHC model when the strain rate is high.

It has been noted that the JHC model for concrete is typically based on the same

mathematical plasticity theory used to model common metals. However, the constitutive behavior of concrete differs from that of metals. Concrete displays brittle behavior in tension and its compressive strength is almost ten times its tensile strength. The yield stress depends on the mean stress (pressure). Hence, it can be concluded from these observations that the JHC model cannot appropriately simulate the concrete behavior in low to medium range of strain rates. For very high strain rate cases with high confined pressure, such as the cases of high speed penetration and explosive blast loading, JHC model is preferred. The JHC model also improves convergence and reduces computational time in such cases because of its comparably simpler mathematical expression. The impact speed of the vehicle during impact with bridges is significantly lower than those for blast and flying missile cases. Loading strain rates during vehicular impact cases are not in the applicable region of the JHC model. Hence, the CSCM model has been used in this dissertation to simulate the dynamic behavior of the concrete structures.

Figure 3.9 Concrete Cylinder Compression Test under Quasi-static Load.

3.3 Numerical Algorithm for the Finite Element Analysis

The validation of the numerical model should be discussed based on the mesh size sensitivity and integration time step because the finite element method solves partial differential equations through the discretization in space and time. Gebbekin and Ruppert (1999) state that "every finite method has methodical inherent errors of discretization in space (e.g. mesh size sensitivity) and in time (timestep)." The convergence theorem states that the numerical solution of a partial differential equation, which is discretized by finite elements method, must monotonically converge to the exact solution when element size and time step tend to zero.

3.3.1 Mesh size

Generally, a proper mesh size for a finite element problem is decided by convergence. If the difference in response using two different mesh sizes is small, the coarser mesh size is selected. For the finite element analysis of dynamic behavior of concrete structures, numerous previous studies discuss element size sensitivity. For the elastic response of a structure with homogeneous material, exact solution can be obtained by decreasing the size of the mesh to zero. However, this doesn't apply in the case of the inelastic response of structures with non-homogeneous material. In the case of concrete, cement is a porous material with low stiffness and highly compressible property, whereas the aggregate is very stiff and incompressible. If the size of the mesh is taken to be less than dimension of the aggregate, numerical results on failure modes in the structures may not be realistc since fracture

properties change dramatically. For commonly used concrete, crack always starts and moves along the cement and doesn't propagate through aggregates. Bazant(2002) has shown that there exists a characteristic length for concrete material fracture.

However, the material model of concrete has to consider it as a kind of homogeneous material to avoid unsolvable complexity. Numerical modeling of the bond-slip problem in reinforced concrete should also be considered while determining the mesh size effect, since concrete and steel are modeled separately in one component of the bridge. Research on the influence of bond slip [Chen and Baker (2003)] shows that the damage near reinforcement is distributed when bond slip isn't considered in the modeling and it is localized when bond slip is considered. The bond between concrete and steel is highly nonlinear and can be matched with element size. Yi and Agrawal(2008) investigated effects of mesh size on the response on reinforced concrete members subjected to blast loads. Using four different element sizes to mesh a beam under blast loads and calibrating their numerical results with experimental tests carried out by Magnusson and Hallgren(2004), they found that the finite element model with a mesh size of 1.08 in matched the experimental results very well. In order to evaluate the CSCM model, the developer of the model conducted reinforced concrete beam drop tower impact simulations and impact tests on the safety-shaped barrier test. During the numerical simulations of their experimental results, they used solid elements of 1 inch length and verified the validity of the results. In this dissertation, mesh size of the concrete element is taken as 1 inch for components directly affected by the impact load.

3.3.2 Time Step Size

For dynamic impact problems, a critical time step size should satisfy the following equation:

$$\Delta t_{crit} \le \min_{e} \frac{l_e}{c_e} \tag{3.3}$$

where l_e is the smallest distance between any two nodes of an element and c_e is the instantaneous wave speed. Physically, this equation implies that the stress wave should not propagate further than the shortest length of one element in each time step to guarantee numerical stability. The critical time step is deduced from linear or linearized physically stable systems. Very little is known about the stability behavior of numerical procedures during physically unstable processes. Furthermore, the deduction of time steps considers only numerical stability (i.e., material stability is not considered). Generally, the smallest distance between two nodes is 1 in (mesh size) and the instantaneous wave speed can be taken as 10,000 in/s (2.5km/s) [Popovis and Song, (1998)]. Hence, Δt_{crit} should be 10^{-4} seconds. We can assume that numerical methods which are stable for linear systems are also stable for nonlinear systems. Hence, in this research, the time step is set as 1 μs (10^{-6} second).

3.3.3 Hourglass Effects and Energy Conservation

In order to avoid a numerical problem called “hourglass” because of one-point integration [Hallquist (1998)], a small damping is usually added into the system in the simulation of high strain rate problems by the explicit method. Undesirable hourglass modes

tend to have periods that are typically shorter than the periods of structural response, and they are often observed to be oscillatory. Hourglass technique helps in avoiding all numerical stability problems caused by zero energy modes, which means the explicit method with small damping is not suitable to study buckling problems for structures under high strain rate loads. The hourglass energy could be recorded during the simulation. In the head-on collision validation exercise conducted by Zaouk (1996), hourglass energy was reported as 17 % of the total energy. In the simulation of vehicular impacts on bridges in this research, the worst case of damage (which is for a bridge designed for seismic guidelines in 'New York' and impacted by a medium weight truck with a velocity of 70 MPH, See Chapter 4) has been selected as an example to study hourglass energy and energy conservation during the numerical simulation. The total energy, kinetic energy, internal energy, energy loss due to element erosions and hourglass energy were recorded during the simulation. The evolution of various energy quantities are shown in Figure 3.10.

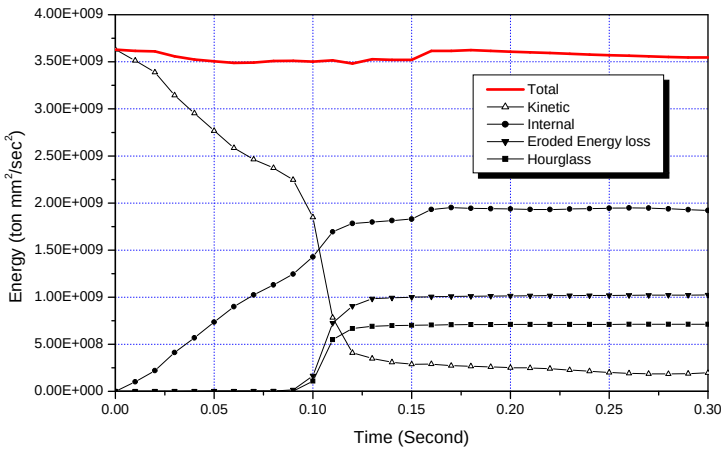

Figure 3.10 Time Histories of Various Energy Quantities for NY-70 Case

During vehicle impact to the bridge, kinetic energy of the vehicle is converted to target bridge's internal energy and internal energy of components of the vehicle itself. As the impact occurs, the kinetic energy of the vehicle gradually decreases as the internal energies of the target bridge and vehicle increase. The maximum energy exchange occurs at the time of 0.11 second, when heaviest carriage part of the truck hits the bridge pier. At this instant, 10% of energy accounting for erosion increases suddenly, since most of the eroded elements are deleted from the system. Finally, the hourglass energy takes 17% of the total energy whereas 25% energy is lost due to failure and erosion of elements during the vehicular impact. The final internal energy of the damaged bridge and the vehicle is almost 60% of the total energy of the whole system. However, the total energy keeps constant during the simulation, and conservation of the energy during the numerical simulation demonstrates numerical stability of the simulation.

3.3.4 Simulation of Reinforced Beams under Impact Loads

Because of the involvement of highly nonlinear damage mode in the simulation of vehicular impact loads on highway bridge piers, calibration of finite element model parameters, such as simulation time step, mesh size and material parameters with observed or experimental data is required. However, direct impact test data on reinforced concrete piers are not available in the literature. The calibration of the numerical model can only be carried out by using test data on reinforced concrete components made of similar material types. We try to employ this process to validate the parameters of material model, finite element mesh size, simulation time

step and contact algorithm. We couldn't find any data on experimental tests on reinforced concrete columns (including reduced scale models) under impact load in the literature. On the other hand, numerous references are available on experimental tests on reinforced concrete beams. For example, Krishis and Nakano (2001) conducted an experimental study on the ultimate strength of flexural-failure-type RC beams under impact loading. Eight 2-meters-clear-span RC beams of various cross sections and reinforcement ratios have been impacted by a 200 kg steel weight for various falling height. The impact force and the mid-span displacement have been recorded during the falling weight impact. Interesting findings in this research [Krishis and Nkano (2001)] include: (i) the maximum reaction force for all RC beams exceeds 2.0 times the corresponding reaction force during static bending, and (ii) the ratio of absorbed energy (estimated using the area of reaction force-displacement curve) to input kinetic energy are distributed in the region from 0.5 to 0.9 for all the tested RC beams (the mean value is 0.7). Based on these results, they assume the dynamic response ratio as 2.0 and the ratio of absorbed energy to input energy as 0.7 for all the cases of flexural-failure-type RC beams under impact loads. Although these results may not be applicable to the present research directly, they do serve as a meaningful basis to discuss the numerical results.

Most recent experimental tests to study the impact response of reinforced concrete beams have been carried out by Fujikake and Li (2009). They used a drop hammer with a mass of 400 kg to impact reinforced concrete beams. The influence of drop height and the effect of the

longitudinal reinforcement ratio have been investigated. The RC beams specimens in their tests have cross-sectional dimensions of 250 mm in depth, 150 mm in width and 1700 in length, as shown in Figure 3.11.

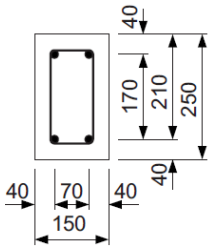

(a) Cross section View

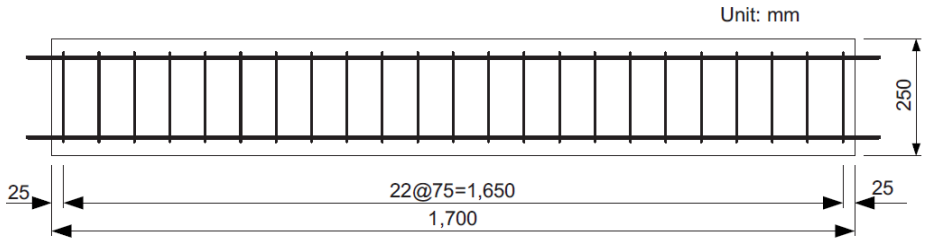

(b) Side view

Figure 3.11 Geometry and Rebar Detailing of the RC Beam Specimens

The RC beams specimens have been constructed using three longitudinal reinforcement ratios using D13, D16 and D22 deformed bars. The yield strength of D13, D16 and D22 bars are 397 MPa, 426 MPa and 418 MPa respectively. D10 bars with yield strength of 295 MPa have been used for stirrups. For each arrangement of longitudinal reinforcement, four impact tests have been carried out by freely dropping a hammer of 400kg on the top surface of a RC beam (at mid-span) from four different heights. A total of 12 RC beams were tested under hammer impact loading. Table 3.1 presents the reinforcement arrangement for the RC beam specimens.

Table 3.1 Longitudinal Reinforcement Arrangement

	Compression side		Tension side	
Designation	Number and size (mm)	Area A_s (mm^2)	Number and size (mm)	Area A_s (mm^2)
S1616	2-D16	397	2-D16	397
S1322	2-D13	126.7	2-D22	774
S2222	2-D22	774	2-D22	774

The drop hammer impact test setup is shown in Figure 3.12. For beam series S1616, the hammer was dropped freely from four different heights of 0.15m, 0.3m, 0.6m and 1.2m. For beam series S1322 and S2222, the hammer was dropped from four different heights of 0.3m, 0.6m, 1.2m and 2.4m. The hammer had the hemispherical striking head with a radius of 90mm. The RC beam was supported by a device designed to allow it to freely rotate while preventing it from moving up or down. The span between the supports was set at 1400mm. The contact force between the hammer and the RC beam was recorded by the load cell attached with the hammer. The mid-span displacement was tested by a laser sensor. The strength of the concrete was 42 MPa and the maximum size of the aggregate was 10mm.

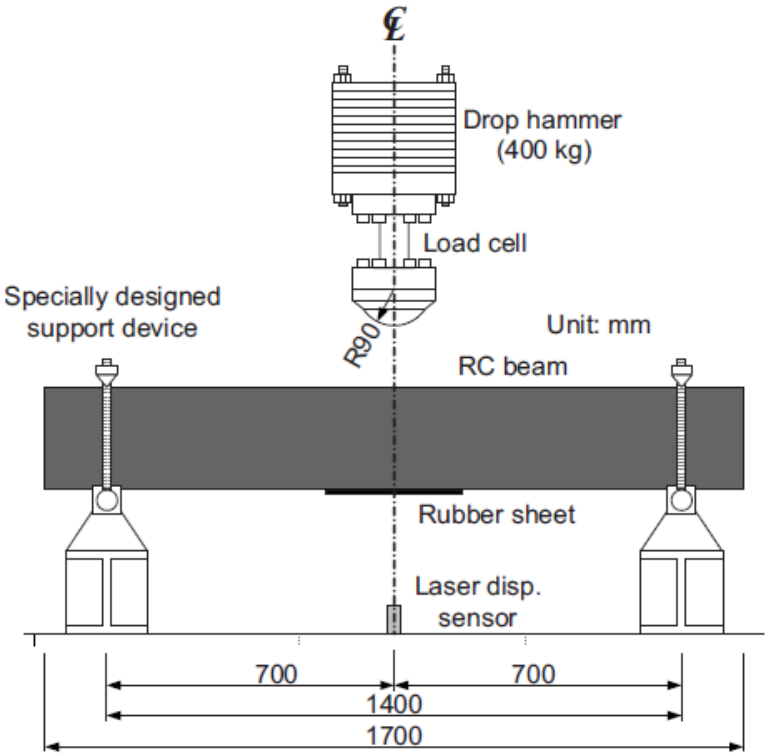

Figure 3.12 RC Beam Hammer Impact Test Setup

It is observed from Table 3.1 that specimens in series S1616 and 2222 have the same longitudinal rebars on both tension and compression sides, which is similar to rebar detailing in columns. Hence, these two specimens have been selected for simulation in LS-DYNA. For series S1616 beams, tests with drop heights of 0.6m and 1.2m have been simulated. For series S2222, tests with drop heights of 1.2 m and 2.4m have been simulated. Table 3.2 summarizes bending and shear resistances for simulated beams.

Table 3.2 Numerical Simulation Cases for Beam Impact

	Drop Height (m)	Bending resistance *RM*=4Mu/L (KN)	Shear resistance *RS*=2Vu (KN)	Shear to Bending ratio (*RS*/*RM*)
S1616	0.6	91.1	232.0	2.55
S1616	1.2	91.1	232.0	2.55
S2222	12.	162.6	245.4	1.51
S2222	2.4	162.6	245.4	1.51

Numerical models of impacts on RC beams have been built in LS-DYNA, as shown in Figure 3.13. Concrete components of the RC beam are modeled with eight-node solid elements with a characteristic size of 20mm. Steel Reinforcements are modeled by beam elements. Both solid and beam elements are meshed with the same size, so that the nodes of the concrete solid element could be attached to the nodes of beam elements to simulate the confinement of reinforcements. CSCM model is used to model material behavior of concrete. Main parameters of concrete in this model are the compressive strength of 42 MPa and aggregate size of 10 mm. Plastic-kinematic material model is used to the model beam elements with the same yield strength and plastic characteristics as the reinforcements in the impact tests. The elastic and hardening modulus of the reinforcement are taken as 200GPa and 3 GPa, respectively. The hamper is simplified into a half-sphere with a mass of 400kg, which is

achieved by increasing the density in the material property definition. The half-sphere hammer was assigned an impact velocity calculated from different dropping heights. The hammer hit contacts and interacts with the top surface of the mid-span of the RC beam to simulate the impact loading. The time step is set as 10^{-6} second for each of the four cases.

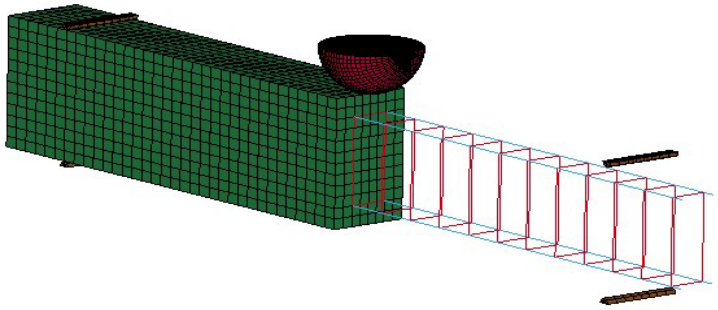

Figure 3.13 Numerical Model of the Beam Impact Test

Contact forces during the impact of the hammer on RC beams and displacements at the bottom surface of RC beams have been recorded in the simulation. The impact force time history and mid-span displacement time history plots are shown in Figures 3.14 and 3.15 for series S1616 beams. Figures 3.16 and 3.17 show these plots for series S2222 beams. In these figures, impact forces and displacement profiles measured during experimental tests by Fujikake and Li (2009) are also plotted for comparison.

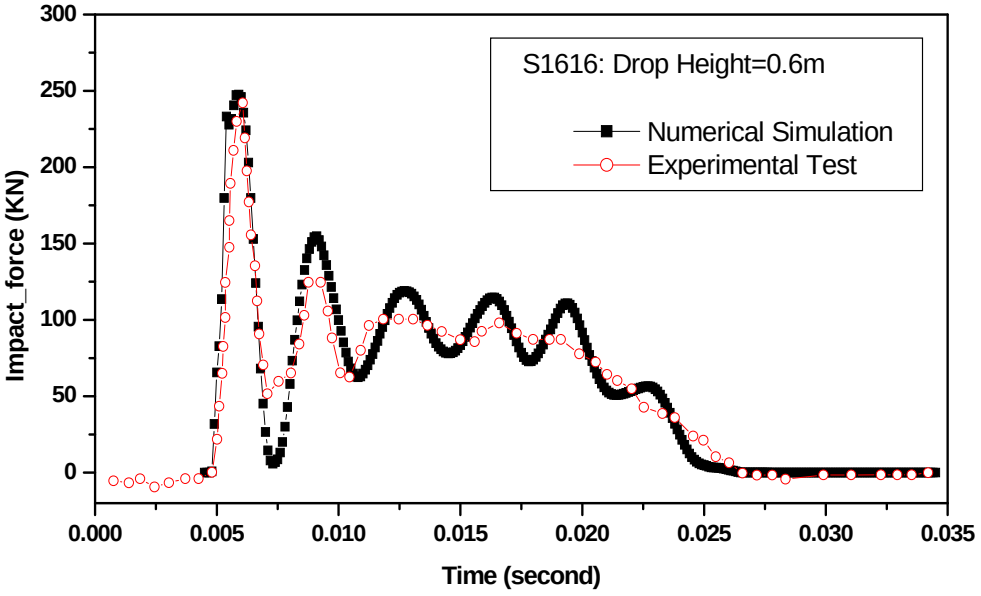

(a) Impact Forces Time History

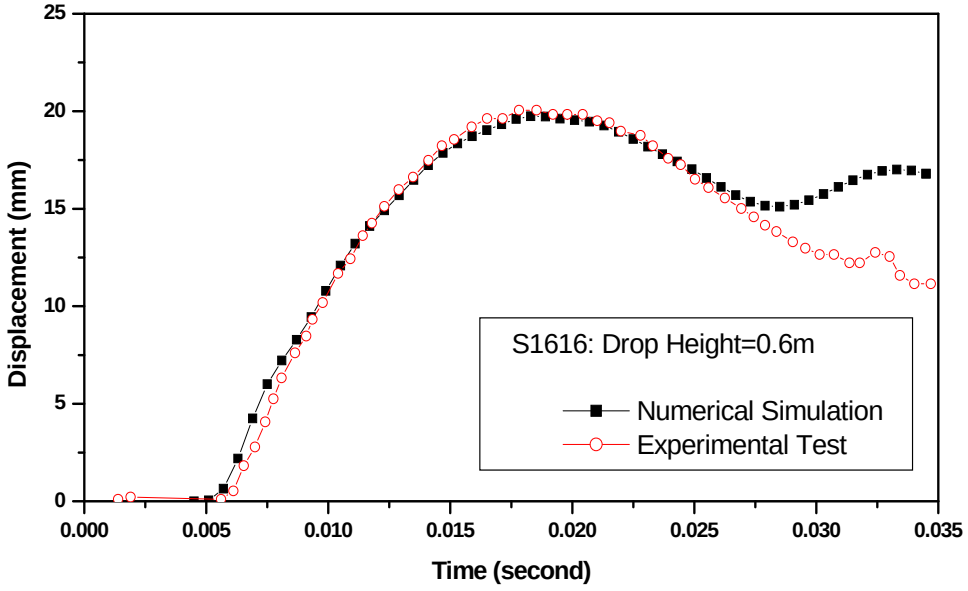

(b) Mid-span Displacement Time History

Figure 3.14 Impact Response Comparisons for S1616 with Drop Height of 0.6m

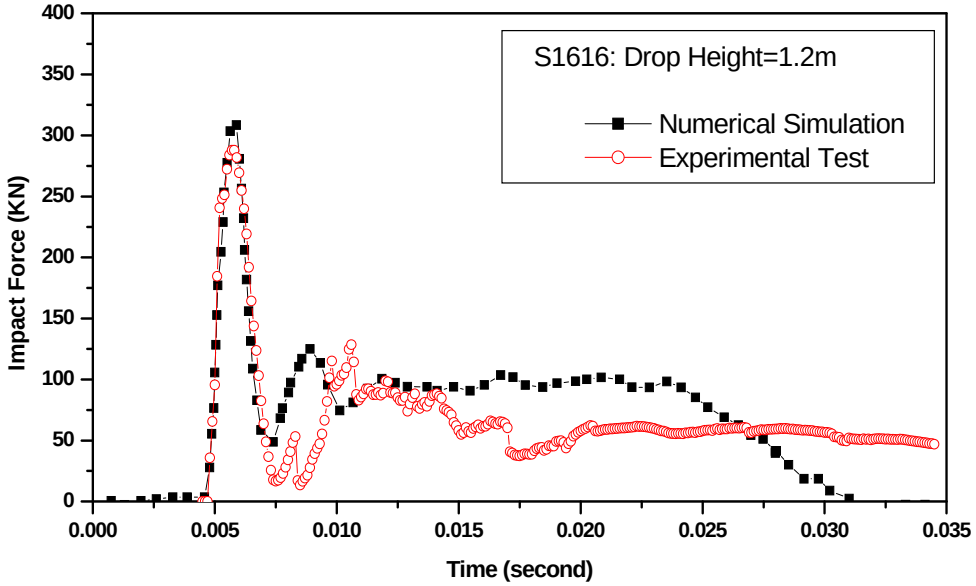

(a) Impact Forces Time History

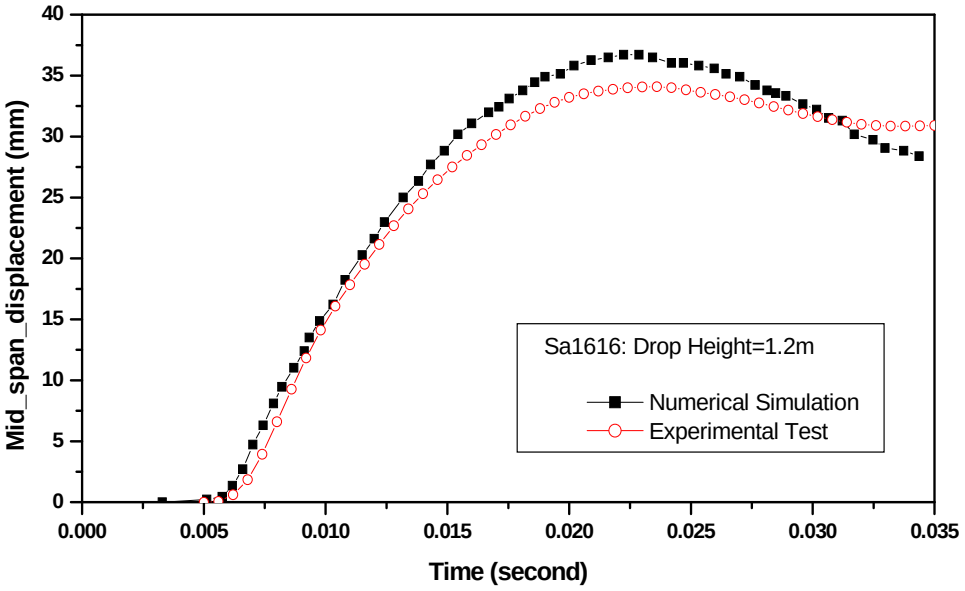

(b) Mid-span Displacement Time History

Figure 3.15 Impact Response Comparisons for S1616 with Drop Height of 1.2m

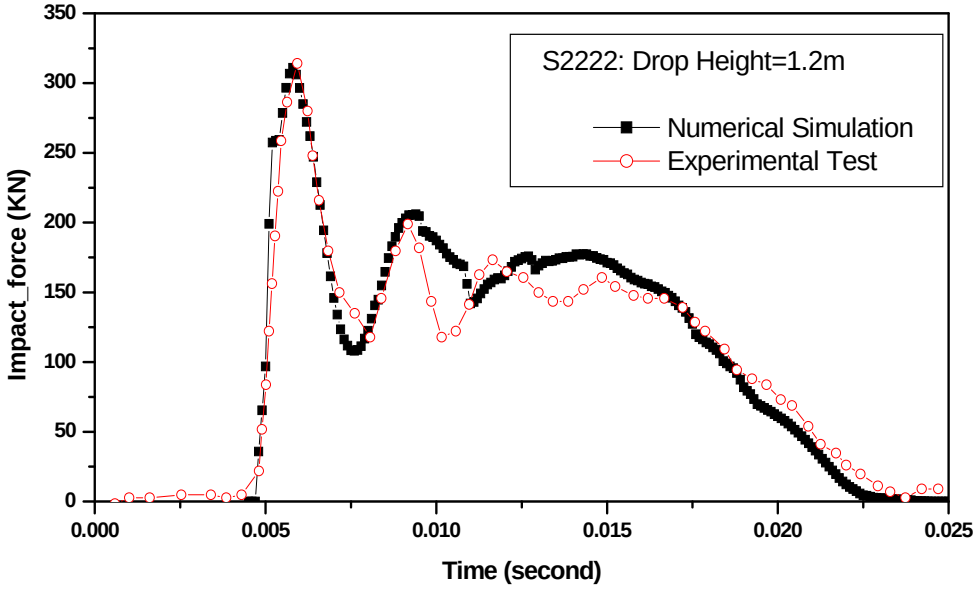

(a) Impact Forces Time History

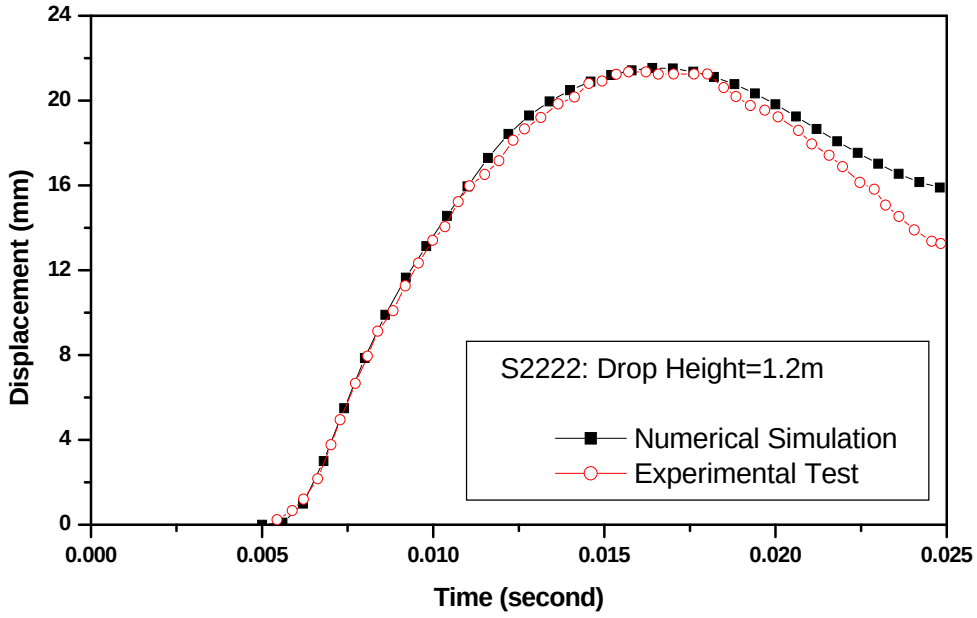

(b) Mid-span Displacement Time History

Figure 3.16 Impact Response Comparisons for S2222 with Drop Height of 1.2m

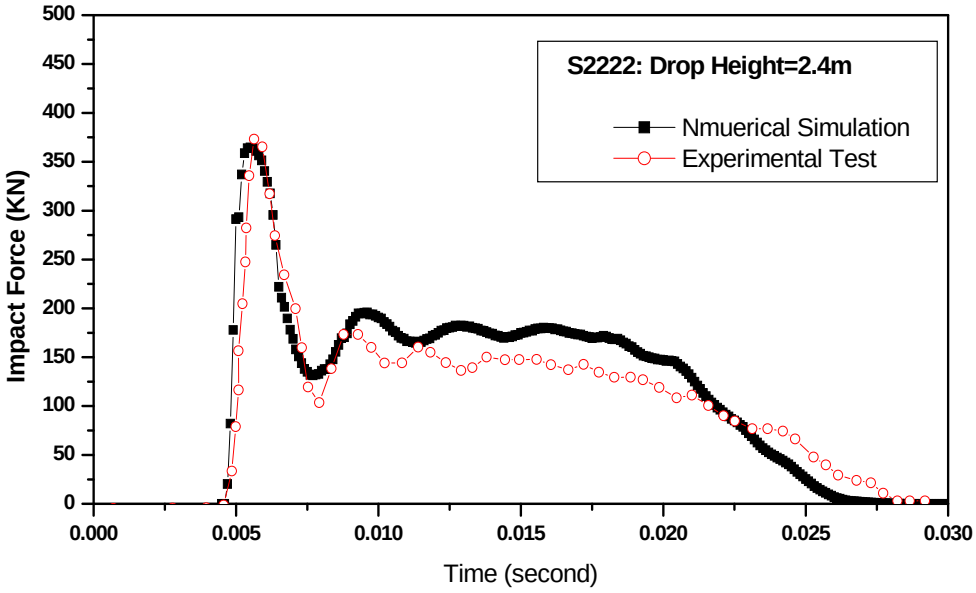

(a) Impact Forces Time History

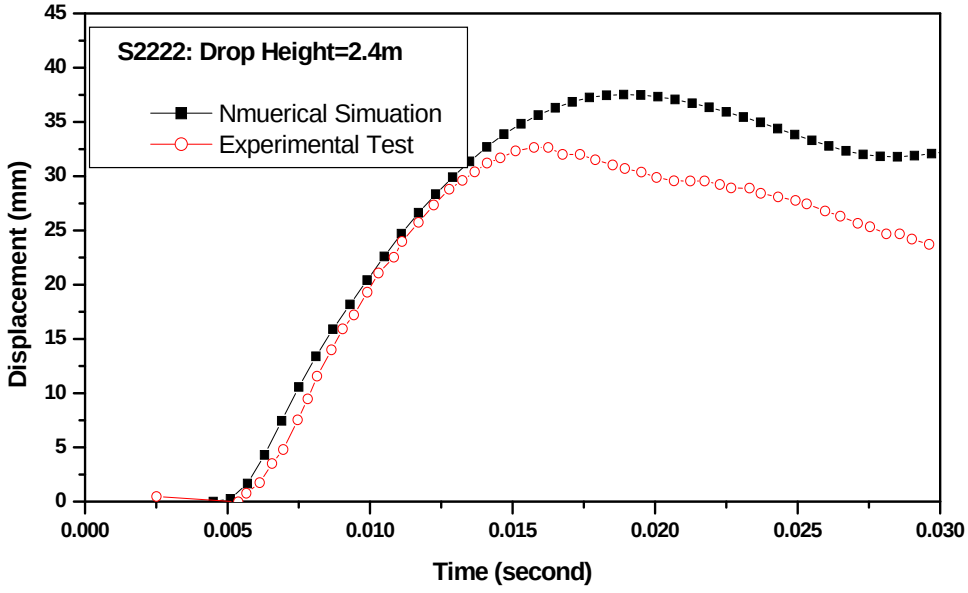

(b) Mid-span Displacement Time History

Figure 3.17 Impact Response Comparisons for S2222 with Drop Height of 2.4m

It is observed from Figures 3.14 to 3.17 that both impact force and mid-span displacement profiles from numerical simulations match those from experimental tests very well. The displacement profiles from numerical simulations match those from experimental tests better for beams with lower longitudinal reinforcements and lower impact heights (Figure 3.14 to 3.16). Reinforce concrete beams with higher longitudinal reinforcements are expected to display more local damage other than overall failure response. In cases with more local damages, numerical simulations overestimated the mid-span displacement as compared with experimental tests. However, the difference is still tolerable since the deviation of the two displacement results is within the range of 30%. The maximum impact forces from simulations match very well with those from the experimental tests. Since the geometry of beam supports and drop hammer are simplified in the simulation, the dynamic characteristics of the numerical model are different than those of experimental models. This results in lesser matching between numerical and experimental time-histories of impact forces at times after the peak impact force. This is more prominent in case of lower drop heights, e.g., Series S1616 beam with 0.6 m drop height, see Figure 3.14(a).

The simulations of RC beams impact are shown to be in good agreement with the experimental tests when RC beams exhibits a flexural failure, which could be taken as a calibration for the selection of material model, mesh size and time step to model the reinforced concrete components of highway bridges in this dissertation. In the next section of this chapter, a three span highway bridge with concrete components will be built with the same material

models and numerical algorithms as the RC beam specimens described in this section.

3.4 Numerical Bridge Modeling

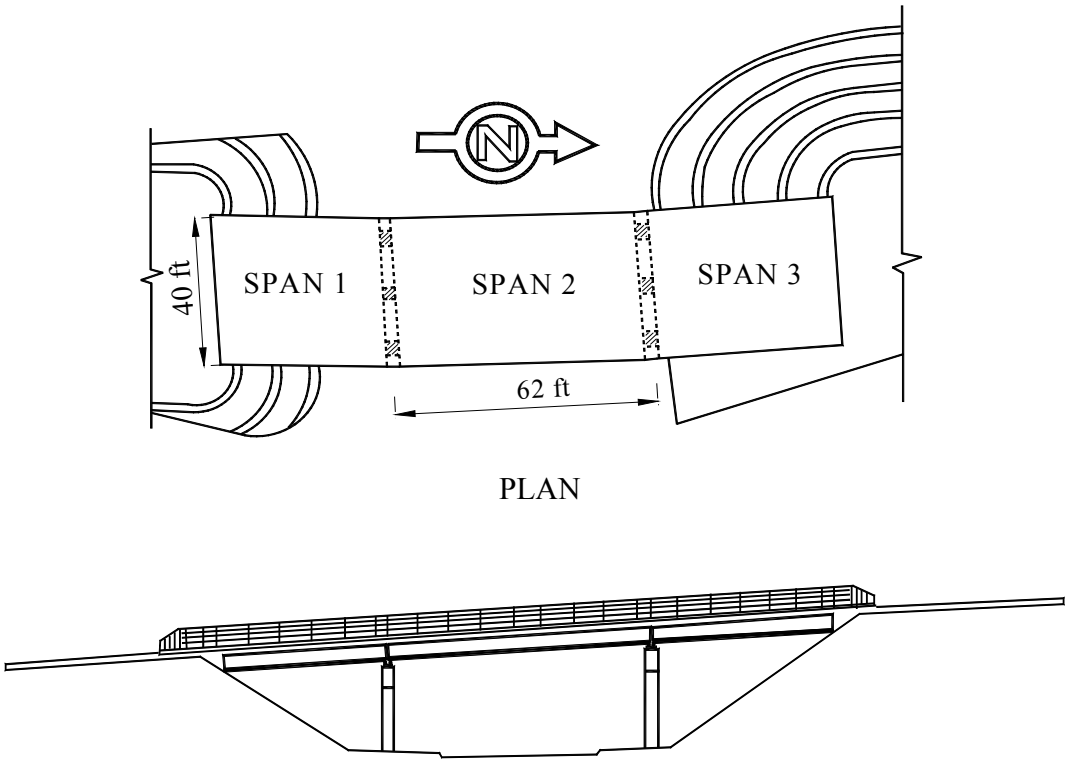

Figure 3.18 Plan View and Elevation of the typical bridge

Traditionally, the finite element analysis of bridges is carried out by software packages such as SAP2000, by modeling typical members as beams, plates and frames. However, in order to simulate localized failure modes of components of a bridge during vehicle impacts, a detailed modeling of all components representing actual bridge geometry is required so that all possible failure modes could be identified. In this dissertation, the finite element model of a three span bridge previously developed by Yi (2009) has been adopted. Following the

numerical algorithm in Section 3.3, parameters, such as finite element mesh size and time step size, have been selected to satisfy the stability requirement. Reinforced concrete material has been modeled by the CSCM model. Figure 3.18 shows a plan view and elevation of the typical bridge in this research.

Table 3.3 shows key parameters of the bridge geometry and design load. This typical highway bridge is a three span non-continuous highway bridge with reinforced concrete piers and bents. The height of the pier is 16 ft. The length of middle span is 62 ft. The distance between the center lines of adjacent piers is 18 ft. Figure 3.19 shows rebar detailing in the piers and bent of the bridge.

Table 3.3 Key Parameters of the Bridge Geometry

ITEM	VALUE
Redundancy	Non-continuous
Length of Middle Span	62 ft
Number of Spans in Main Unit	3
Design Load	MS 18 or HS20
Deck Width	40 ft
Deck Thickness	13 in
Lanes on Structure	2
Height of Pier	16 ft
Number of Piers	3×(2bents)=6
Pier section	Rectangular 3.0ft×3.0ft
Material Type	RC concrete pier, bent &deck, steel stringer

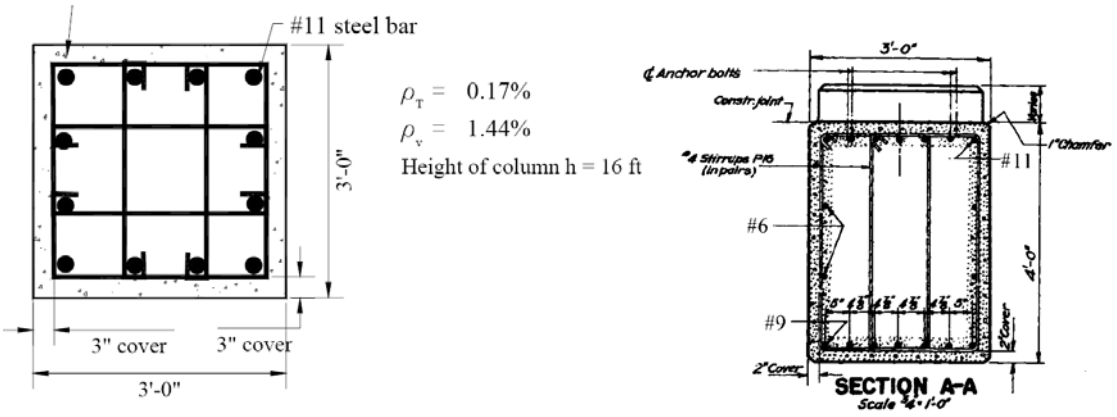

(a) Pier Section (b) Bent Section

Figure 3.19 Details of (a) Pier and (b) bent

3.4.1 Description of the bridge model

A detailed model of the bridge described previously has been built in LS-DYNA with the procedure in Figure 3.1 by Yi (2009). The explicit solver in LS-DYNA has been selected for the simulation. The finite element model of the bridge is meshed with Lagrangian mesh, since constitutive equations can be easily applied on this kind of mesh and Lagrangian mesh is suitable for simulation of structures with large deformation. The element eroding technique is used to avoid severe element distortion during the simulation of the impact loads. In a step-by-step procedure of modeling by finite element methods, in order to investigate the behavior of each component of the bridge under vehicle impact load, each component is built separately and assembled into a whole bridge in LS-DYNA preprocessor. Specifically, the footing, pier, bent bearing and deck are modeled by solid elements, stringers and diaphragms are modeled by shell elements and steel reinforcements are modeled by beam elements. Elastomeric bearings are used in this research since they are used extensively to replace old

bearings. The characteristic mesh size of the concrete element is 1 in. The components of the bridge and related modeling elements are summarized in Table 3.4. Figure 3.20 shows the whole bridge finite element model.

Table 3.4 Element Types Used in the Bridge Modeling

Solid Elements	Footing, Piers, Bent, Deck, Concrete Support, Elastomer Bearing
Shell Elements	Stringers, Diaphragms
Beam Elements	Steel Reinforcements

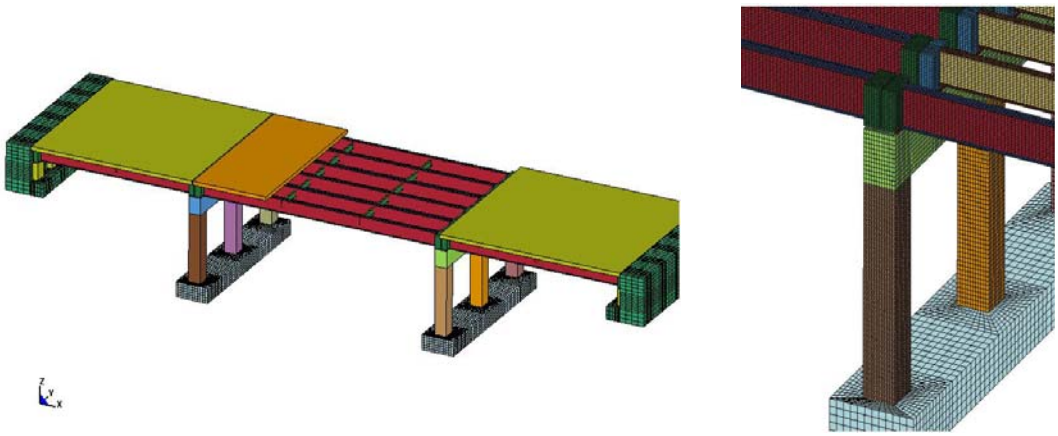

(a) Whole Bridge Model (b) Local Detailing of the Model

Figure 3.20 Finite Element Model of the Three-span Bridge

3.4.2 Concrete Piers, Pier Bents and Footing

Although superstructures of bridge are hit frequently by over height trucks, direct impact to pier by trucks usually causes serious damages, frequently leading to collapse of the entire

bridge. The FEM model of the bridge pier consists of concrete core, cover concrete and steel rebar. According to Krauthmmer and Otani (1997), a detailed modeling of the rebars is important for the simulation of extreme loads on concrete structures. Generally, reinforced concrete members are modeled by an equivalent monolithic element that can represent combined behavior of both concrete and steel rebar during ordinary hazards such as seismic load, wind load, etc. However, monolithic element is not appropriate for reinforced concrete subject to vehicular impact loads. In this research, modeling of the reinforced concrete pier and bent is done by modeling concrete by pure concrete solid element and rebars as steel beam elements, which has been validated by the reinforced beam impact simulation in the previous section. For the geometry and rebar detailing given in Figure 3.19, Figure 3.21 shows finite element model of the pier.

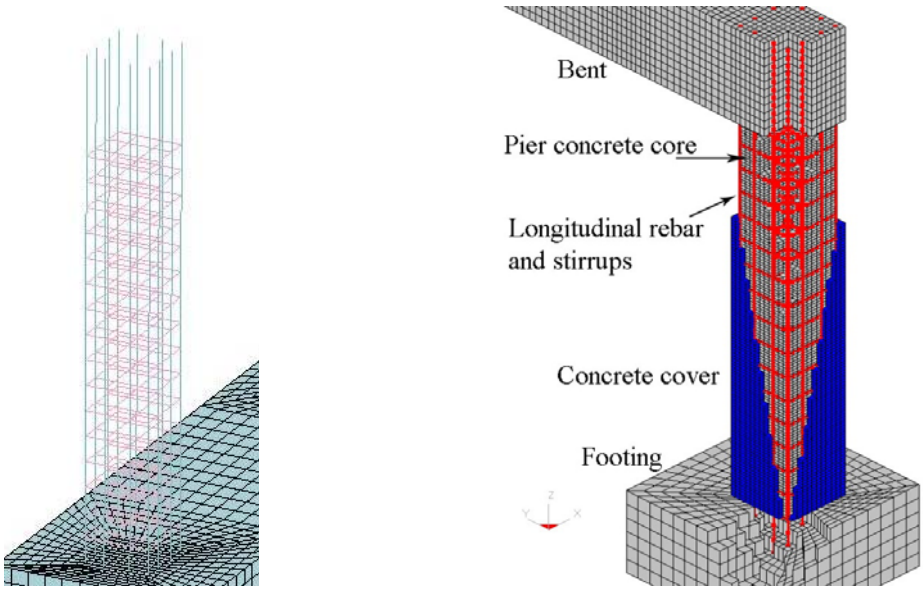

Figure 3.21 Modeling of Concrete Pier

In modeling of piers, core concrete and cover concrete are modeled as separate layers to include confining effects of steel rebars on core concrete. Rebar cage for concrete piers has been developed by modeling rebars with beam elements as shown in Figure 3.21. The longitudinal rebars have been extended into the footing and the bent as per as built bridge drawings. Core concrete is added to the rebar cage and cover concrete is added as a separate layer with different material properties on top of the core concrete. The detailed modeling of the bridge pier, pier-bent and footing, as shown in Figure 3.21, has been done so that failure mechanisms of the pier system subject to vehicle impact can be identified. It is mentioned that the footings of bridge piers are directly anchored to the bedrock.

Chapter 4 Numerical Simulations of Highway Bridges under Vehicle Impact Loads

4.1 Introduction

The development of design criteria for highway bridges, susceptible to vehicular impacts, depends on risk acceptance criteria, factors influencing the probability of vehicular impacts, failure modes of bridge components, and consequences of impacts. The risk acceptance criteria and factors influencing the probability have been discussed in various published guidelines, as stated in Chapter 2. However, there is still a severe knowledge gap on determining the dominant failure modes and severity of collision in determining consequences. Generally, failure modes of highway bridges during vehicular collision are directly influenced by two main factors: characteristics of the truck (including its weight and velocity before a collision) and the design capacity of bridge piers. Traditionally, bridge piers are designed for dead, live and seismic loads, where lateral load capacity, rebar detailing and the size of piers are influenced or governed by seismic loads. Hence, it is important to investigate the influence of various levels of seismic detailing on damage and failure modes of bridge piers during vehicular impacts. In this chapter, we present a detailed numerical simulation of truck impacts on piers of highway bridges designed for different levels of seismic resistances. A hypothetical three-span steel bridge with reinforced concrete piers has been redesigned for four different levels of seismic resistance. Each of these bridges has been

impacted by a medium weight truck with low, medium and high approach velocities to identify failure modes and damage scenarios.

4.2 Models of Bridges of Various Seismic Capacities

4.2.1 AASHTO Seismic Design Specifications

A typical three-span non-continuous bridge is considered for the finite element modeling as described in Chapter 3. The plan and elevation of the bridge are shown in Figure 3.18. Key parameters of the bridge geometry and design loads are shown in table 3.3. In order to conduct the research on the vehicle impact with correlations to seismic resistance, numerical models of the bridge with different levels of seismic resistances are developed in this section. Generally, seismic resistance of bridges can be improved using any of the four approaches (Seismic Design and Retrofit of Bridges,1996):

1. Using larger pier section size and high strength materials to increase the lateral load level such as acceleration coefficient.
2. Preventing the superstructure from sliding away from the pier cap by imposing more stringent displacement requirements.
3. Utilizing a better design detailing to guarantee ductility of bridge members and the full use of material strength.
4. Utilizing supplemental damping systems to dissipate energy.

The hypothetical bridge in Figure 3.18 is based on an existing bridge in the New York State, and was designed to satisfy AASHTO bridge service loads. Following the 2002 AASHTO Guide Specifications for Seismic Design of Highway Bridges [AASHTO (2002)], the three span hypothetical example bridge has been designed and discussed by Yi(2009) to meet the local seismic requirements in New York State. This example bridge is referred as "NY Bridge" in this dissertation. This bridge satisfied the seismic load with acceleration coefficient of 0.2g according to the AASHTO-USGS design spectrum. In order to investigate the impact resistance capacity of highway bridges with higher seismic load capacity, three more example highway bridges with higher seismic capacity need to be designed following the AASTHTO Guide Specifications for LRFD Seismic Bridge Design (2007). The typical core flow chart for bridge seismic design based on AASHTO Guide is shown in Figure 4.1. The design procedure is straight forward. More details about the design details are available in the introduction part of AASHTO Guide Specification for LRFD Seismic Bridge Design (2007).

The procedure of seismic design can be divided into three major steps according to Figure 4.1. The first step is to decide the seismic design category for the bridge using the ASHTO-USGS acceleration design spectrum. According to LRFD-GS Section 3.5, each bridge is assigned to one of four Seismic Design Categories (SDC), A through D, based on the one second period design spectral acceleration (SD_1) for the design earthquake. Figure 4.2 shows the most stringent seismic response spectrum selected for the example bridge in this Chapter,

which is the acceleration spectrum in San Francisco, California (zip code: 94720). The 1-sec spectral acceleration for this site is 2.3g. Hence, based on AASHTO LRFD Guide Specifications, this bridge should be designed as per SDC D category.

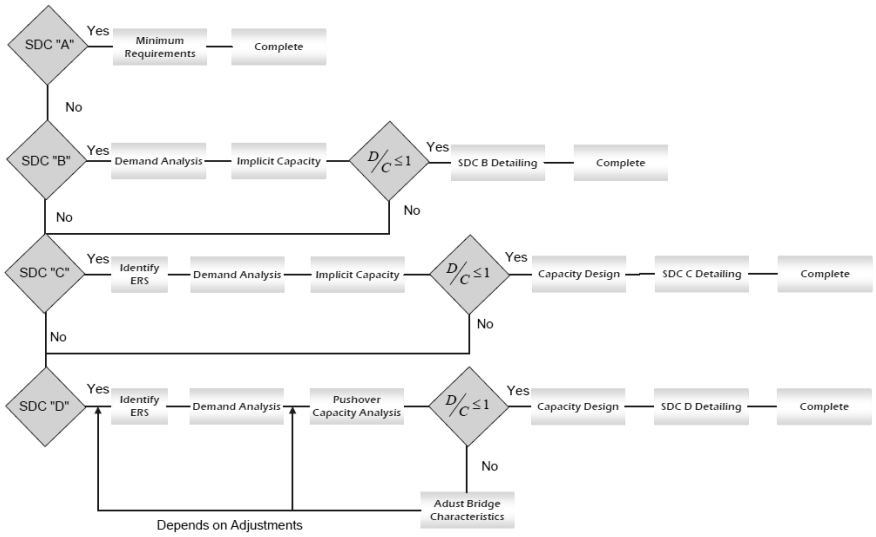

Figure 4.1 Seismic Design Category Core Flowchart

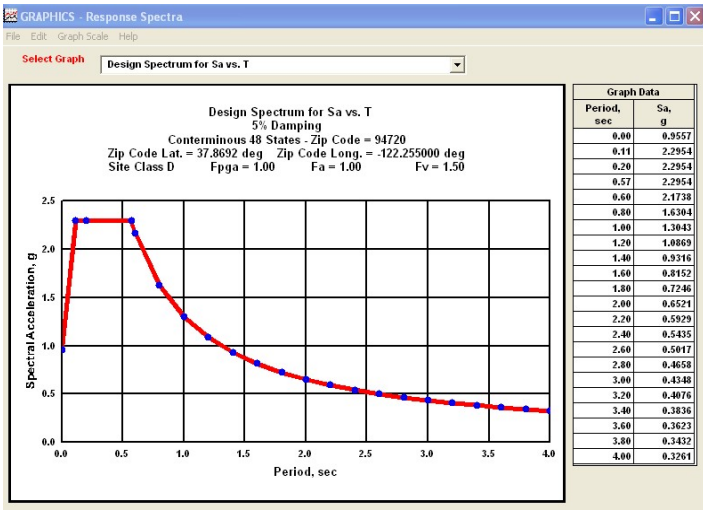

Figure 4.2 AASHTO-USGS Site Class D Unfactored Design Spectrum

The second step is to calculate the seismic demand on bridge components. The objective of the demand analysis is to estimate the force and displacement induced by the earthquake. The

equivalent static analysis and linear elastic dynamic analysis are the appropriate methods for calculating the displacement demands for normal bridges. For the normal bridge with regular configuration, a single degree of freedom model is sufficient to obtain the seismic response. Hence, the AASTO Seismic guideline recommends an equivalent static analysis method to establish the displacement demand. The procedure based on the uniform load method based on the fundamental mode of vibration can be found in Section 4.7 in the AASTO code. It is emphasized that the section property (flexural rigidity E_cI_{eff}) shall reflect the cracking that occurs before the yield limit state. The cracked flexural stiffness I_{eff} can be estimated by the initial slope of the moment –curvature curve for the designed bridge pier. Since the three span simply supported bridge has a regular configuration, and the equivalent static analysis is used to estimate the displacement demand because of seismic load.

The third step is to determine the displacement capacity of the pier and bent. If the ratio of the demand to capacity is less than 1, the design can be accepted, otherwise the bridge should be redesigned so that the demand/capacity ratio satisfies the requirement. For bridges classified in SDC B, the displacement capacity of the piers and bents can be calculated by the approximate formulas in Section 4.8.1 of the AASHTO guideline. For the bridge design assigned to SDC C and SDC D, inelastic static analysis, i.e., “Pushover Analysis”, is the appropriate analytical tool to establish the displacement capacities for normal bridges. In this research, the displacement capacities of the four bridges are obtained using the “pushover

analysis".

Once the pier bent satisfies the seismic demand requirement, the following procedure is used to determine rebar detailing, seating width of bearings and shear capacity check for the overturn moment induced by the seismic load. The shear demand for a column in SDC C or D is determined based on the force associated with the overstrength moment, which is defined in Article 8.5 and outlined in Article 4.11 of the AASHTO. Given the uncertainty in seismic hazard and consequence of column shear failure, it is very important to satisfy the capacity protection requirement for column shear. The column shear capacity within the plastic hinge region as specified in Article 4.11.7 should be calculated on the basis of nominal material strength properties. In three example bridges designed for seismic capacities higher than that of the New York bridge, shear reinforcements in the pier have been redesigned to satisfy the higher seismic load requirements.

4.2.2 Design of Bridges with Various Seismic Capacity

According to the AASHTO LRFD Design Specifications, highway bridges are essentially designed to be elastic during small to moderate earthquake. During severe earthquakes, the intent of the seismic design is to accept structural damage while avoiding total bridge collapse. It is expected that inelastic deformations (plastic hinging) occur at locations in columns (top or bottom or both) where they can be readily inspected and repaired. This objective can be achieved by a design that makes members that are not part of the primary energy-dissipating system stronger than the over-strength capacity of primary energy-dissipating members. Hence,

we assume that the bridges with higher seismic capacity have the same superstructure configuration as the NY bridge. Three bridges with higher seismic capacity than that of the NY bridge are referred to as CA bridge, LA bridge and SF bridge. The values of spectral acceleration for these three bridges are 0.8g, 1.5g and 2.3g respectively. Figure 4.3 shows cross sectional profiles of piers in NY, CA, LA and SF bridges. Table 4.1 shows the geometry and reinforcements arrangements for the four example bridges.

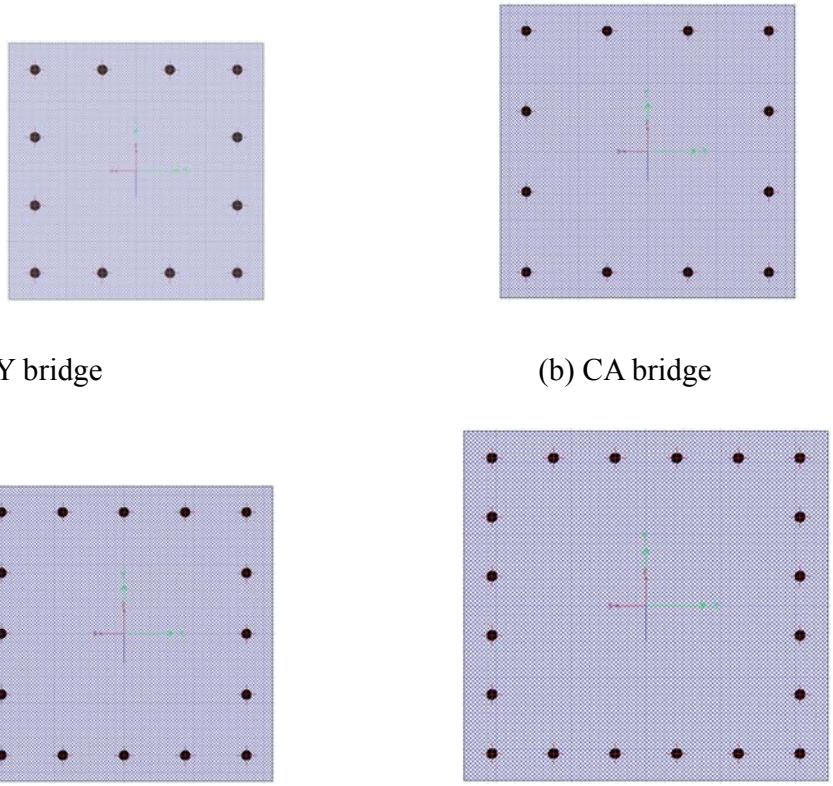

(a) NY bridge (b) CA bridge

(c) LA bridge (d) SF bridge

Figure 4.3 Crossing Section Configuration of the Four Example Bridges

In the design of these example bridges, effective (cracked) moment of inertia should be used to assess the seismic demand on ductile columns. The effective moment of inertia is calculated

from the initial slope of the Moment-curvature curve for each section. Moreover, in order to carry out the pushover analysis for the bridge piers, the plastic hinge property for each column section is imported from the Moment-curvature plot. Figure 4.4 shows the Moment-curvature plots for four seismic bridges designed in this dissertation. The Moment-curvature plot is generated by the BIAX computer program [Wallace and Ibrahim (1996)]. BIAX includes the calculation of section properties, interaction diagrams and moment-curvature relations for a bridge pier cross section. In the program BIAX, the bilinear material model for steel reinforcement and modified Kent-Park model for the stress-strain relations of confined and unconfined concrete is selected to calculate the moment-curvature curve. Table 4.2 shows the characteristic moment capacities and curvatures of piers of four example bridges. It is observed that the moment capacity increases with an increase in the seismic load, whereas the maximum curvature decreases with an increase in seismic load. The moment required to initiate plastic hinge deformation in brige piers increases from the low seismic capacity to high seismic capacity. Hence, stiffness of piers of four bridges increases in the order of NY bridge, CA bridge, LA bridge and SF bridge.

Table 4.1 Geometry and Reinforcement Arrangement of Piers in the Example Bridges.

	Acceleration (g)	Pier Height (ft)	Pier Size (ft)	Longitudinal Bars	Stirrups Bars
NY Bridge	0.15	16	3	Bar 11 4×4	Bar 3 12 in Spacing
CA Bridge	0.8	16	3.5	Bar 11 4×4	Bar 4 12 in Spacing
LA Bridge	1.5	16	3.5	Bar 11 5×5	Bar 4 6 in Spacing
SF Bridge	2.3	16	4	Bar 14 6×6	Bar 5 6 in Spacing

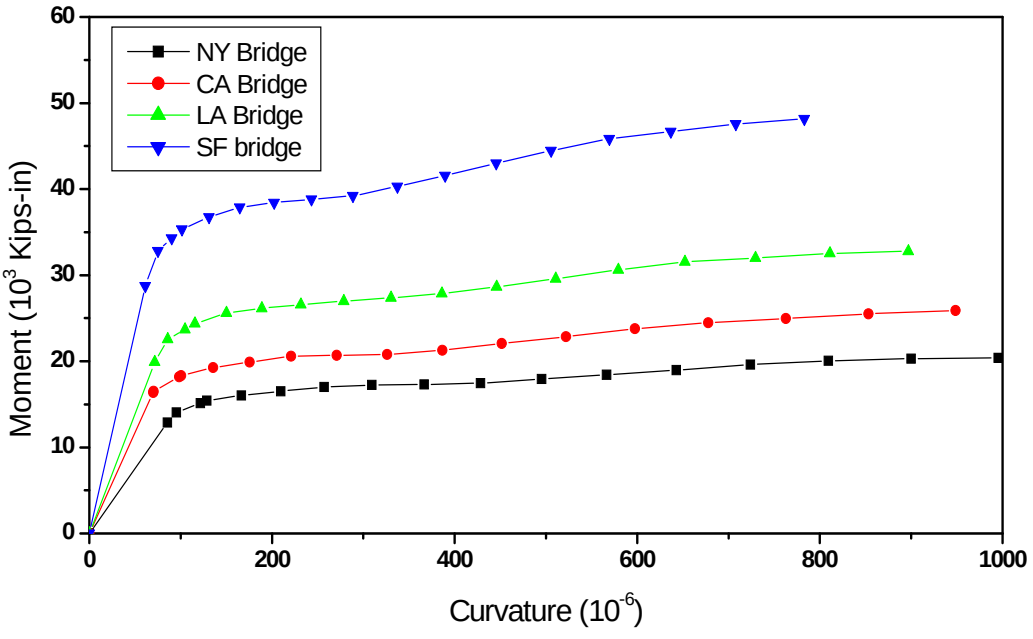

Figure 4.4 Moment Curvature Plots for the Four Example Bridges

Table 4.2 Comparisons of Moment Capacities and Curvature for Example Bridges

	Elastic Moment Capacity (10^3 Kips-in)	Elastic Curvature (10^{-6})	Maximum Moment Capacity (10^3 Kips-in)	Maximum Curvature (10^{-6})
NY Bridge	14.4	95.2	48.1	783.1
CA Bridge	17.5	91.9	32.8	896.7
LA Bridge	22.6	85.8	25.9	948.6
SF Bridge	32.9	72.9	20.4	995.1

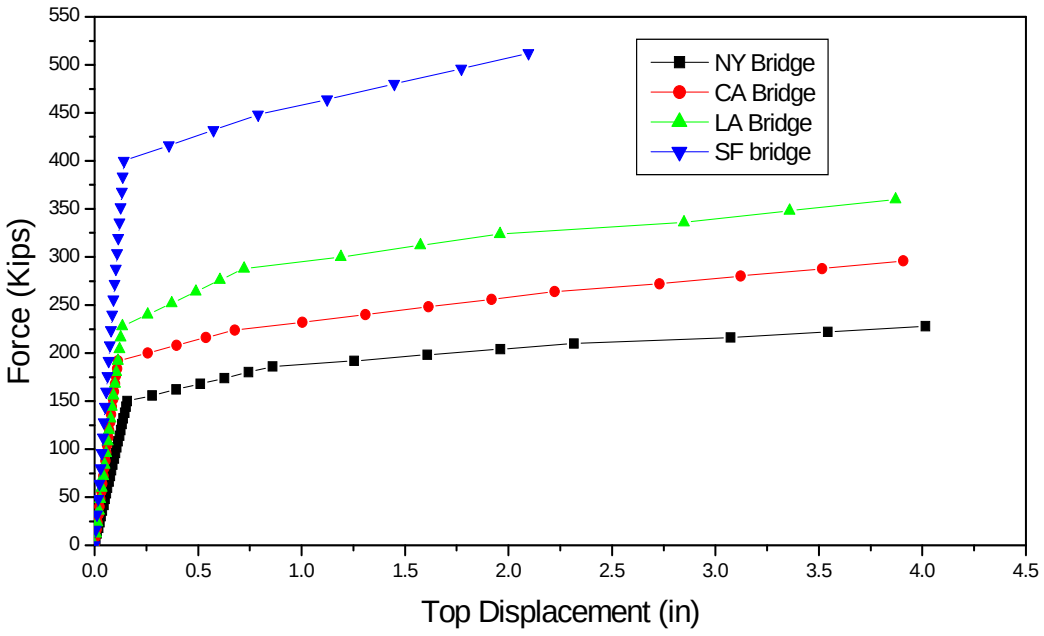

Figure 4.5 Pushover Analysis for the Four Example Bridges

Moment-curvatures plots in Figure 4.4 have been used to represent nonlinear plastic hinge properties for the Push-over analysis by SAP2000 program (CSI 2007). The lateral force vesus deflection curves have been obtained from the Pushover analysis as shown in Figure 4.5.

The ductile displacement capacities of the four example bridges can be obtained from the results of the pushover analysis.

4.2.3 Ductility Analysis of the Four Seismic Bridges

Seismic capacity of bridge piers can be quantified in terms of the ductility factor defined as [Chopra (2001)]

$$\mu = \frac{u_m}{u_y} \tag{4.1}$$

Where u_m is peak inelastic deformation and u_y is the deformation at the yield point. The yield strength reduction factor R_y can be defined as

$$R_y = \frac{f_0}{f_y} = \frac{u_0}{u_y} \tag{4.2}$$

Where f_y is the yield strength and f_0 is defined as the minimum strength required for the structure to remain linearly elastic during the ground motion. It should be emphasized that the effective (cracked) section property should be used in the "linearly elastic" range of structures. Figure 4.6 illustrates the concept of ductility factor and strength reduction factor for a typical structure possessing elastic-perfectly plastic behavior.

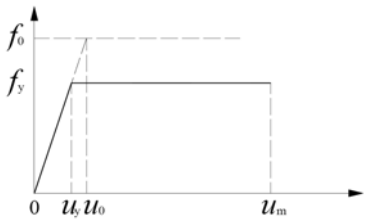

Figure 4.6 Strength Versus Ductility in Seismic Design of Structures

In order to compare the ductility factor of all example bridge piers, R_y and u are calculated for piers of NY, CA, LA and SF bridges as shown in Table 4.3. The ratio $\mu/R_y = u_m / u_0$ is defined as the ratio of maximum inelastic and elastic displacements during the seismic ground motion. This ratio can be considered as a quantitative measurement of ductile capacity for bridge piers with respect to an equivalent elastic system. The ratio μ/R_y decreases from 24.3 to 3.3 as the seismic spectral acceleration increasing from 0.2g to 2.3g. This ratio can be taken as the key parameter for the comparison of vehicle impact displacements in the forthcoming section.

Table 4.3 Ductility Factors of Four Seismic Bridges

	u_y (in)	u_m (in)	u_0 (in)	μ	R_y	μ/R_y
NY Bridge	0.15	4.01	0.16	26	1.1	24.3
CA Bridge	0.10	3.91	0.33	39	3.3	11.8
LA Bridge	0.12	3.89	0.63	32	5.3	6.1
SF Bridge	0.14	2.09	0.63	15	4.5	3.3

4.3 Numerical Simulations of the Bridge-Vehicle Collision

Four example bridges described in the previous section are combined with the truck model to simulate the bridge-vehicle collisions in LS-DYNA.

4.3.1 Heavy Vehicle Numerical Model

The truck model must provide realistic characterization of the overall dynamics of vehicle and accurate loading to the impacted structures. A Ford Truck, which represents the medium weight truck model, has been built and evaluated by the National Crash Center in the George Washington University. The weight of the truck is 15,000 pounds (66-KN), and the dimension of the truck model is 27 feet in length, 8 feet in width and 10 feet in height, as shown in Figure 4.7.

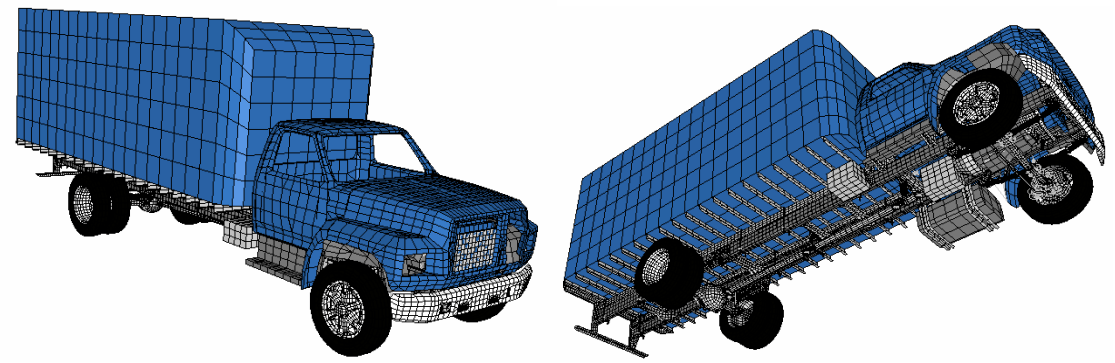

Figure 4.7 Ford 80 Truck Finite Element Model

The truck model developer states that the model should be used primarily as a “bullet” object for computational evaluation of roadside safety hardware. There are two important aspects in the “bullet” model for road safety features: accurate mass distribution and realistic stiffness properties. The truck model was created through a rigorous process by importing the geometry of various parts of the truck into the finite element software and by assigning each part of the truck a proper material model. The material models which have been used in the

Truck model are shown in table 4.4. Different parts of the truck model are represented using shell, solid or beam elements, and all components of the truck are connected and interact together in a realistic manner using various types of constraints. The numerical model of the Ford truck in Figure 4.7 has 159 parts and 32,669 elements in total.

Table 4.4 Material Model of the Truck Component

Material Model	Truck Component
Elastic Material Models	Engine, Transmission, Radiator
Rubber Material Model	Mounts between the cabin and rails, engine and rails, etc.
Rate-dependent Isotropic Elastic-plastic Material Model	Chassis components and the body shells

The accuracy of the medium weight single unit Ford truck model has been validated through comparisons of the simulations with the crash test results. A full-scale crash test conducted at Texas Transportation Institute was used to evaluate the fidelity of the Numerical Truck model. In the test, the Ford 80 truck was impacted with a rigid single-slope concrete bridge rail to identify the mechanism of impact related to the response of the truck. A comparison between simulation and crash test is shown in Figure 4.8 (at 1.0 second after truck impact). The vehicle is impacted into a single-slope bridge rail at 51.3 mph with an impact angle of 17.9^{o}. Table 4.5 shows a comparative assessment between simulation and crash test results by the TTI. It is observed that the numerical truck model adequately simulated the overall dynamics of the test vehicle.

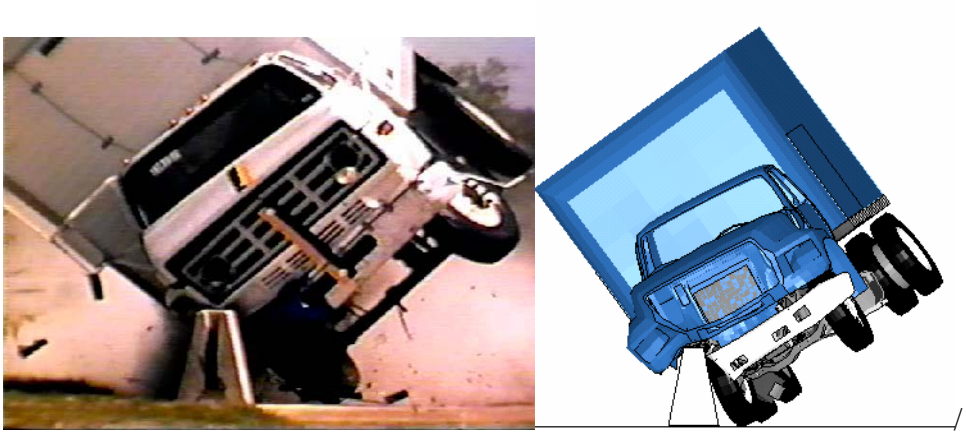

(a) Test (b) Simulation

Figure 4.8 Comparison of Truck Impact for test and Simulation

Table 4.5 Comparison of the Numerical Simulation and the Full-scale Test

	Test	**Simulation**
Impact Conditions		
Speed (km/h)	82.5	82.5
Angle (deg)	17.9	18.0
Impact Velocity (m/s)		
x-direction	2.9	3.2
y-direction	2.8	2.9
Max Ridedown Acceleration (g's)		
x-direction	-2.7	-3.0
y-direction	-10.2	-8.5
Max 50-ms Average Acceleration		
x-direction	-2.0	-2.2
y-direction	-5.6	-5.1

4.3.2 Numerical Model of Highway Bridge with Impacting Vehicle

The medium weight Ford Truck model in Figure 4.7 has been imported into the FEM models of the four example bridges separately in LS-DYNA. The whole bridge-vehicle model for collision simulations is shown in Figure 4.9. Since the ground level is 3 feet above the top surface of the bridge footing, the truck model has been moved up by 3 feet, as shown in Fig 4.10, so that the wheel bottom could contact the ground and move on the ground level.

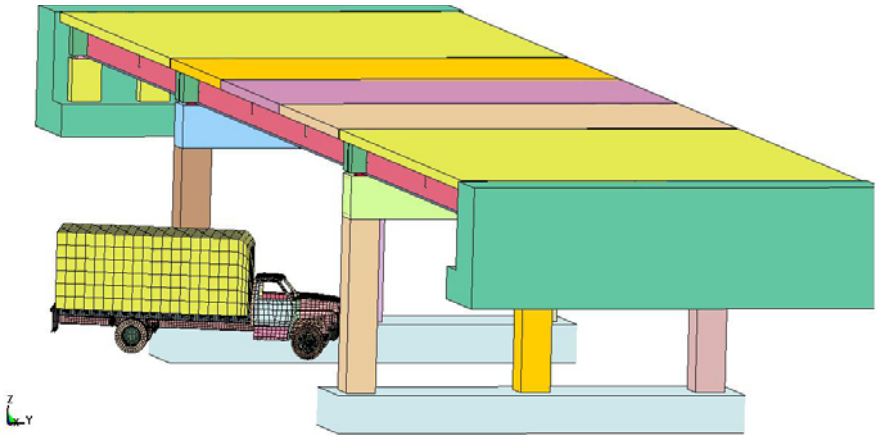

Figure 4.9 Numerical Model Representing the Impact Simulation between Ford Truck and Three-span Bridge

As per AASHTO requirements, an equivalent static force 400 kips should be applied at 4 feet above the ground level in any direction in a horizontal plane in order to assess impact resistance in bridge piers. This truck model has two major mass parts: forehead and carriage. The center of gravity of forehead of the truck is located at 4 feet above the ground level, which satisfies AASHTO provisions. The center of gravity of the carriage is almost 7 feet above ground and is much higher than the 4 feet requirement in AASHTO. However, this height is

based on an actual truck model. Hence, the rationality of using the 4 ft height to apply an equivalent elastic force can be verified through the finite element simulation of the bridge vehicle models in LS-DYNA.

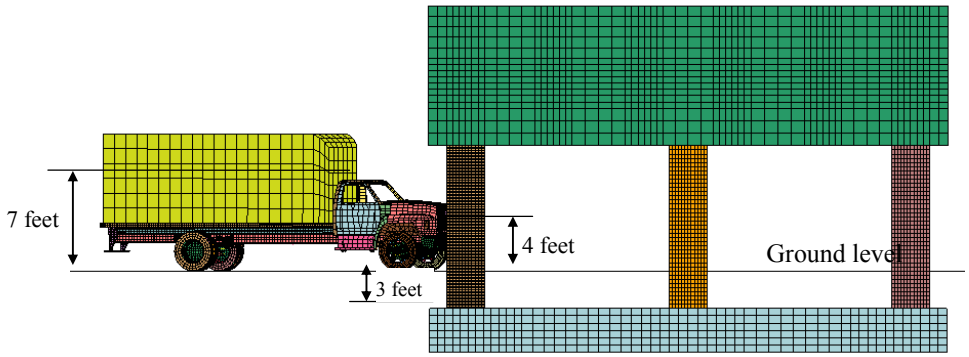

Figure 4.10 Elevation of the Ground Level with Truck Moving

It is reported that the impact angle when the truck hits the bridge across the highway ranges from 0^o to 45^o. However, impact angles of 0^o and 45^o rarely occur [Cota (2007)]. In this dissertation, the average value of 20^o has been chosen as the impact direction as shown in Figure 4.11. The truck model was rotated 20^o about the direction of the highway mid-line such that the mid-point of the truck head could first contact the bridge pier during the collision. In order to investigate the effects of impact angle, a detailed investigation by varying impact angle is carried out later.

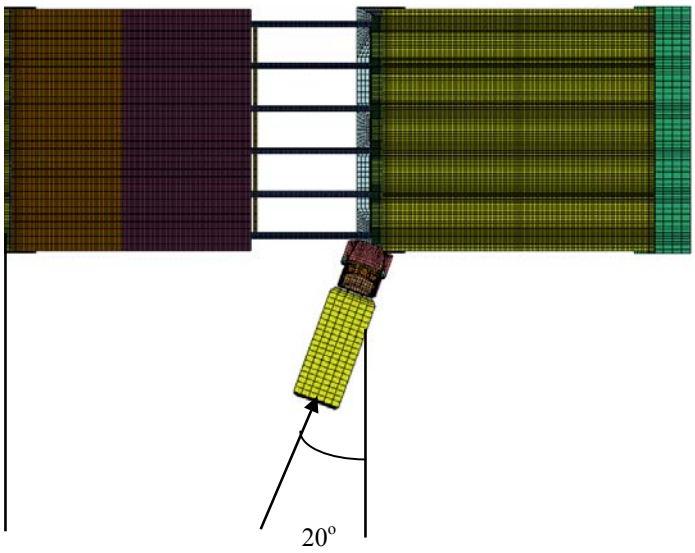

Figure 4.11 Impact Angle of Vehicle-bridge Collision

The range of the truck velocity in the collision is between the 40 and 65 miles/hour based on statistics assembled from collision accidents [Cota (2007)]. In order to carry out a parametric study on various impact velocities, impact velocities of the truck are set as 70 miles/hour, 50 miles/hour and 30 miles/hour in each of the four example bridges. Table 4.6 shows the matrix of bridge-vehicle simulations. There are total twelve bridge-vehicle impact simulations. The simulation time has been set at 300ms based on trial simulation cases to sufficiently capture the behavior of bridge piers during and after collisions.

Table 4.6 Matrix of Vehicle Impact Load Simulations on the Bridges

Load Case	Seismic Capacity	Pier Size(ft)	Impact Velocity(mph)
1	NY Bridge	3	30
2	NY Bridge	3	50
3	NY Bridge	3	70
4	CA Bridge	3.5	30
5	CA Bridge	3.5	50
6	CA Bridge	3.5	70
7	LA Bridge	3.5	30
8	LA Bridge	3.5	50
9	LA Bridge	3.5	70
10	SF Bridge	4	30
11	SF Bridge	4	50
12	SF Bridge	4	70

4.4 Failure Modes of Bridge under Vehicular Impact

Results of twelve numerical simulations of vehicle-bridge collision have been analyzed to (i) identify various failure mechanisms, and (ii) capture time histories of the deformation and impact contact forces during collisions. Verification of the stability of numerical simulations has been carried out through a comparison of various energy quantities for the case of NY-bridge subject to 70 miles/hour vehicular impact, as discussed in Chapter 3.

4.4.1 Failure Mechanism of the Bridge under the Vehicular Impact Loads during the Whole Bridge Simulation

Since both the size of the piers and the reinforcement ratios are smallest for NY bridge case, this bridge is expected to undergo maximum damage at 70 mph vehicular impact. Hence, failure mechanisms of the whole bridge under the vehicular impact load have been captured and identified using this case, as shown in Figure 4.7 at the simulation time of 200ms. The simulation result shows that the NY Bridge piers undergo severe damage when impacted by the truck at 70 MPH velocity.

- Both cover and core concrete in the pier have cracked; concrete and reinforcement debond.
- Both footing and bent experience sudden pull forces towards the impact area on the pier because of a sudden large lateral impact force acting on the longitudinal rebars. The impact force is transmitted to the bent as a sudden downward pull force before longitudinal rebars are ruptured.
- Under the combined gravity load of the superstructure and the pull force caused by impact, the bent acts as a lever beam. Consequently, a plastic hinge is observed to form at the joint of the interior column with the bent as shown in Figure 4.12.

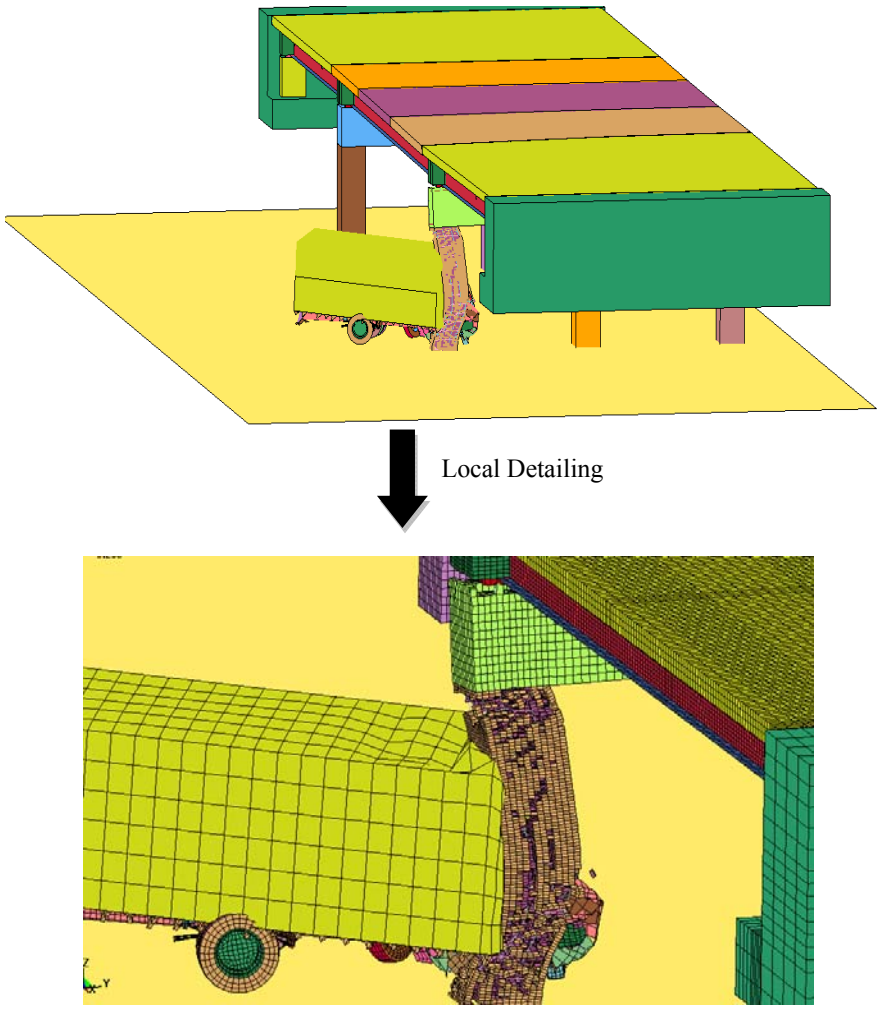

Figure 4.12 Failure Mechanism of the Whole Bridge-Vehicle Collision (NY-70)

As described in the following section, six failure mechanisms have been identified through numerical simulations. These failure mechanisms have been observed to cause minor to severe damage depending on the velocity of impact. For shock loading on structures, Williamson et al (2010) have identified three failure mechanisms in case of blast loads on piers: (i)spalling of cover concrete, (ii) plastic hinge in the column, and (iii)breach of column. In this study, we have identified, in addition to above three mechanisms, other prominent failure mechanisms that maybe present during impact loads: (i) rebar severance, (ii) crushing in the

bent and (iii) flexural failure in the bent. It should be mentioned that Yi (2009) have identified 14 different failure mechanisms in case of bridge piers subjected to blast loads.

The exterior pier in the NY bridge under 70 MPH impact velocity loses its capacity after the rupture of longitudinal rebars. Based on the simulation results, six types of failure mechanisms, labeled as A1 to A6, shown in Figures 4.13 to 4.22, have been identified.

Damage Mechanism A1. Spalling of Concrete Surface: During the impact load on concrete surface of a pier, some of the stress waves are reflected back from the pier surface. This causes a tensile wave effect on the back surface of the pier, resulting in spalling of concrete as shown in Figure 4.13. Hence, spalling of concrete is usually more severe on the back surface of a pier than on the surface impacted by the vehicle. An example of spalling of concrete after an accidental impact on a bridge pier in Texas is shown in Figure 4.14.

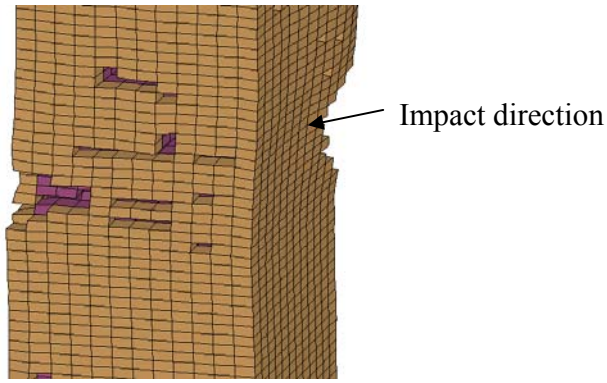

Figure 4.13 Damage Mechanism A1: Spalling of Concrete Surface and Damage of Pier Concrete Core

Figure 4.14 Spalling of Concrete Pier in the Collision Accident of Tyler, Texas (2004).

Damage Mechanism A2. Breakage of Pier: Breakage of piers, as illustrated in Figure 4.15, can occur either because of flexural failure, or shear failure. In case of truck impacts on bridge piers, shear failure is more prominent than flexural failure. This mechanism generally leads to a complete collapse of a bridge. An example of breakage of bridge pier after an accidental impact on a bridge pier is shown in Figure 4.16.

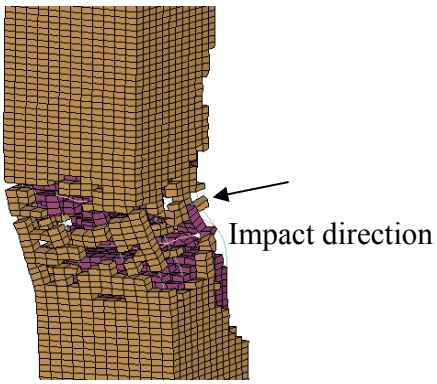

Figure 4.15 Damage Mechanism A2: Breakage of Pier

Figure 4.16 Breakage of Bridge Pier in the Collision Accident of Sealy, Texas (2004).

Damage Mechanism A3. Rebar Severance: If pier is tied well to the bent and the footing, the pier will tend to pull out from the footing and the bent because of stresses induced by the section change between the bent and the pier. This can cause severance of longitudinal rebars, as shown in Figure 4.17. Stirrups fail with the contact of the truck head as the concrete got eroded, as shown in Figure 4.18 for an accidental impact on piers in Texas.

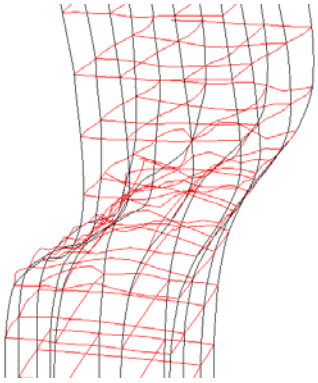

Figure 4.17 Damage Mechanism A3: Severance of Rebars in the Pier Steel Cage

Figure 4.18 Severance of Rebars in the Pier Steel Cage in the Collision Accident of Tyler, Texas (2004).

Damage Mechanism A4: Plastic Hinge Formation in the Pier: concrete core of piers is crushed under the impact of vehicular impact load, resulting in the formation of the plastic hinge in the piers at the location of impact contact and the joint between the bent and the column as shown in Figure 4.19. An example of plastic hinge formation in a pier hit by a truck in Minnesota is shown in Figure 4.20.

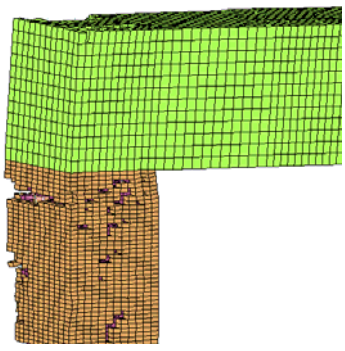

Figure 4.19 Damage Mechanism A4: Plastic Hinge Formation in the Pier

Figure 4.20 Plastic Hinge Formation in the Pier of 2003 Minnesota Collision Accident

Damage Mechanism A5. Concrete Crushing in the Bent: Concrete near the connection between bent and pier may be crushed because of stress concentration as shown in Figure 4.21.

Damage Mechanism A6. Flexural Failure of the Bent: After a bridge pier loses its load carrying capacity because of plastic hinge formation, most of the weight of the superstructure is transferred to the bent. Impact force is also transmitted to the bent as a downward pull force by longitudinal rebars extending into the bent. Because of combined effects of these two loads, the bent acts like a lever beam with large sudden load, resulting in flexural failure at the connection between the bent and the interior pier, as shown in Figure 4.21. An example of damage to a bent of a bridge after a vehicular impact is shown in Figure 4.22

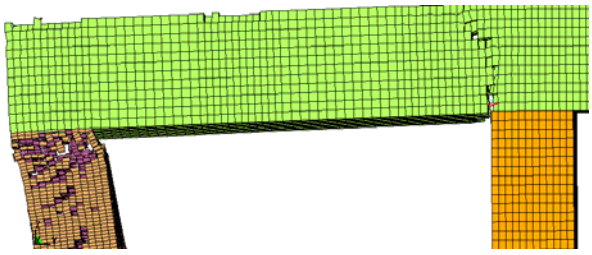

Figure 4.21 Damage Mechanism A5 and A6: Crush in the Bent and Flexural Failure of the Bent Beam.

Figure 4.22 Damage of the Bent in the Collision Accident of Red Oak, Texas (2005)

4.4.2 Failure Mechanisms and Seismic-impact Correlations

The failure mechanisms described above, which were captured during the most damaged case of the NY bridge under 70 mph impact, have been identified from numerous bridge response simulations, even though not all the failure mechanisms may appear during a particular vehicle-bridge collision, depending on the seismic resistance of a bridge pier. In fact, the presence of a particular failure mechanism depends on the bridge geometry, rebar detailing, magnitude of the impact velocity and weight of the truck. In the twelve numerical cases carried out, the failure mechanism during vehicular impact load varies with the seismic capacity of piers. Figure 4.23 to Figure 4.26 show different failure mechanisms observed during different cases of the whole bridge simulation cases in Table 4.6. These damages have been populated in Table 4.7 to investigate multi-hazard seismic-impact correlations. In this multi-hazard table, "X" indicates the presence of a damage mechanism for a particular vehicle impact case.

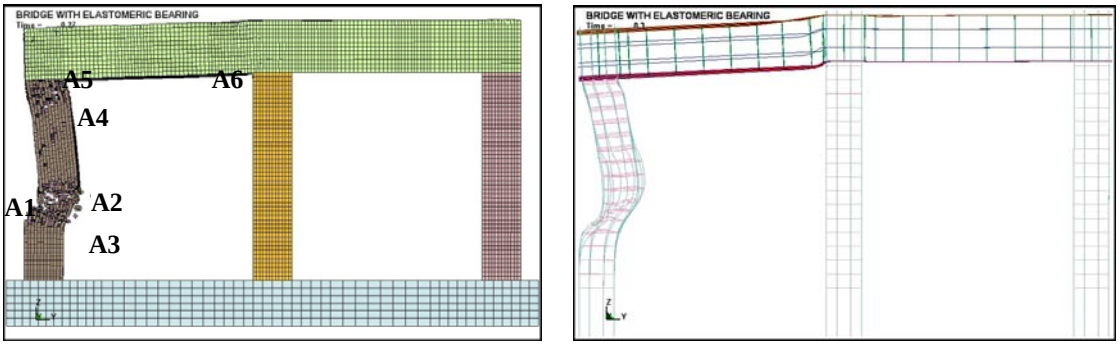

(a) Failure Mechanism with 70 MPH Impact Velocity

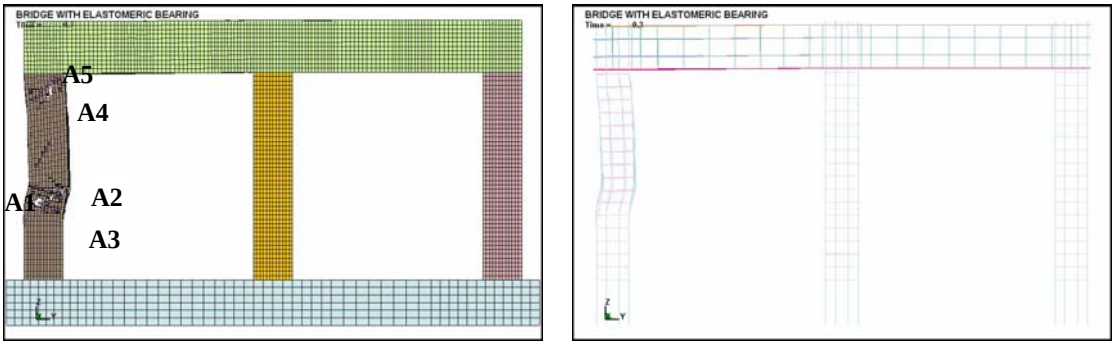

(b) Failure Mechanism with 50 MPH Impact Velocity

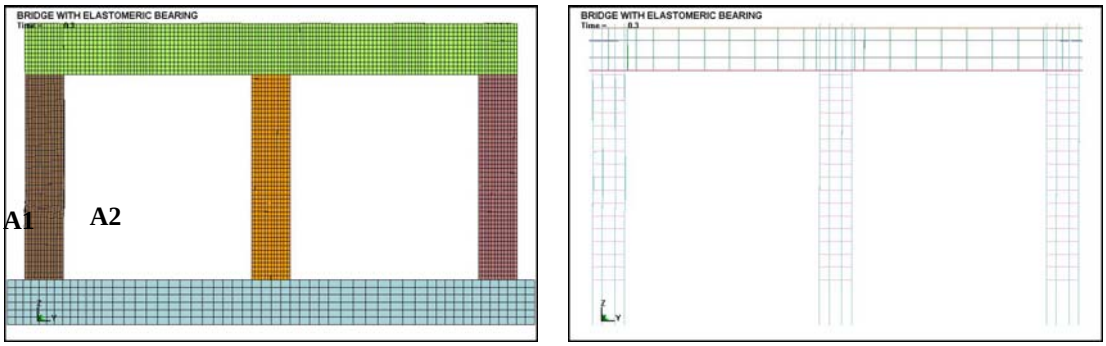

(c) Failure Mechanism with 30 MPH Impact Velocity

Figure 4.23 Failure Mechanisms of NY Bridge under Various Impact Velocities

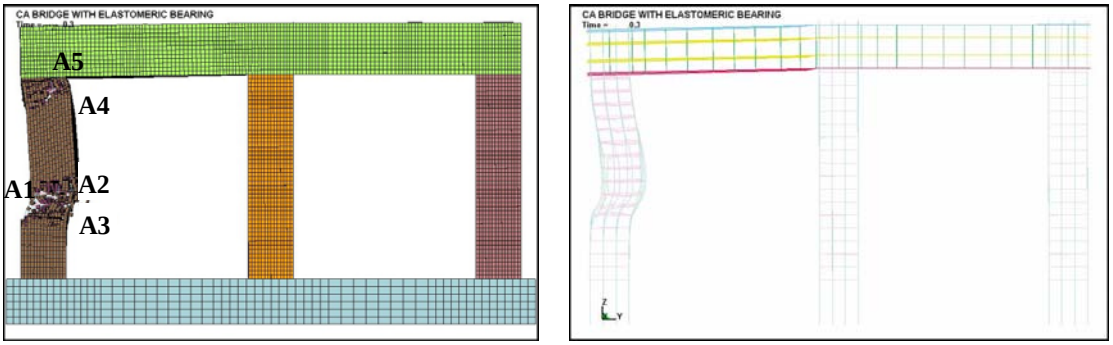

(a) Failure Mechanism with 70 MPH Impact Velocity

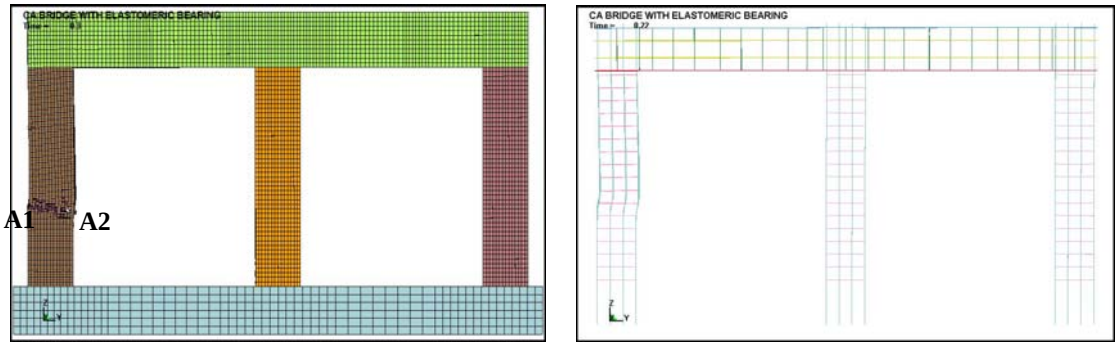

(b) Failure Mechanism with 50 MPH Impact Velocity

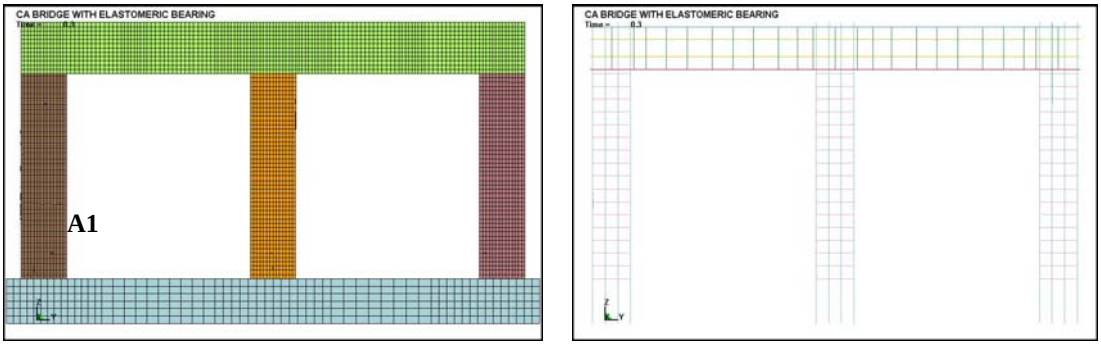

(c) Failure Mechanism with 30 MPH Impact Velocity

Figure 4.24 Failure Mechanisms of CA Bridge under Various Impact Velocity

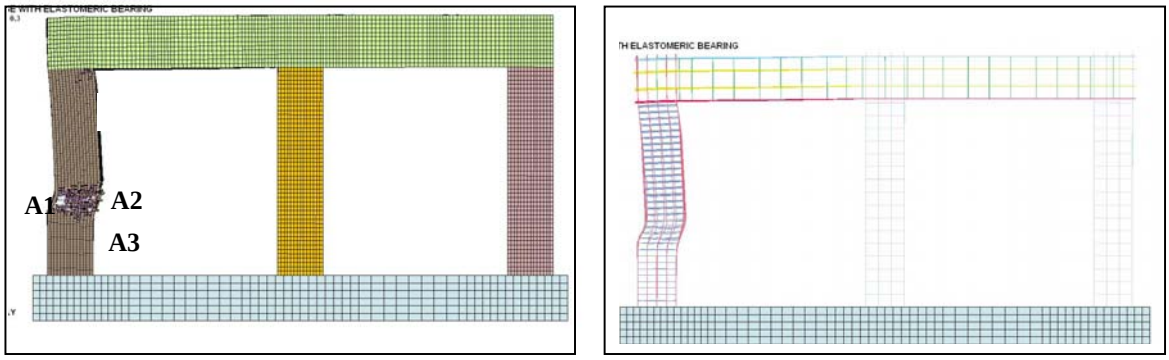

(a) Failure Mechanism with 70 MPH Impact Velocity

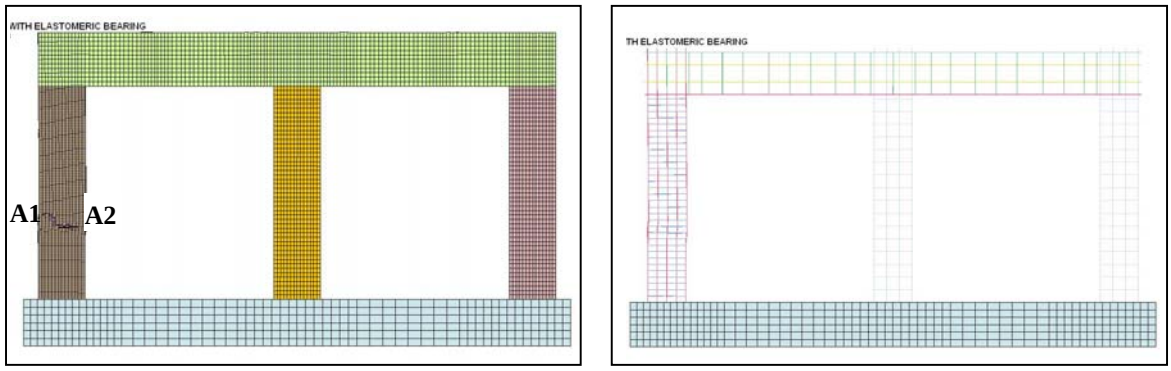

(b) Failure Mechanism with 50 MPH Impact Velocity

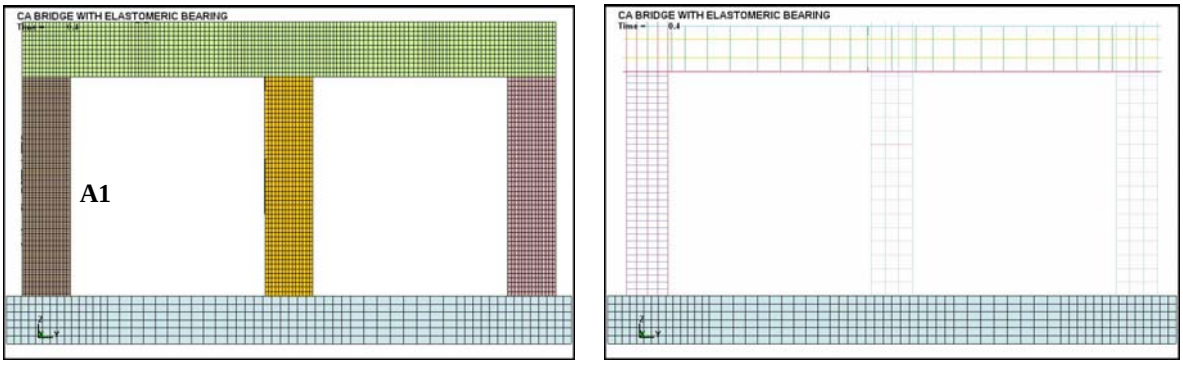

(c) Failure Mechanism with 30 MPH Impact Velocity

Figure 4.25 Failure Mechanisms of LA Bridge under Various Impact Velocity

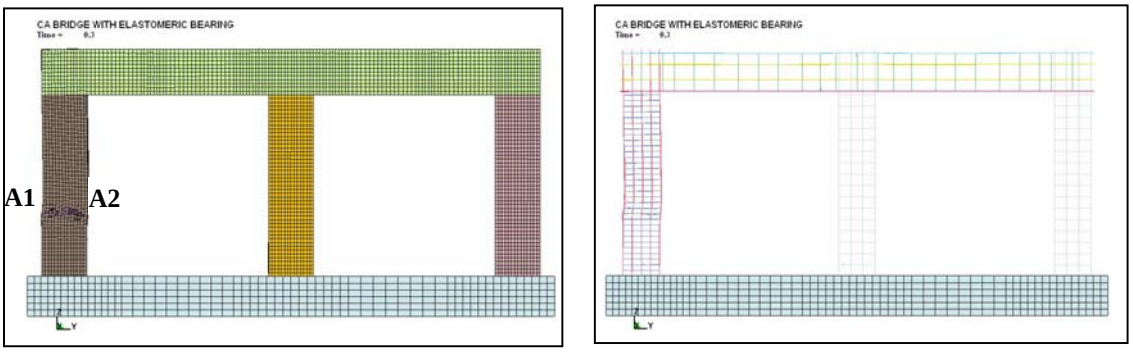

(a) Failure Mechanism with 70 MPH Impact Velocity

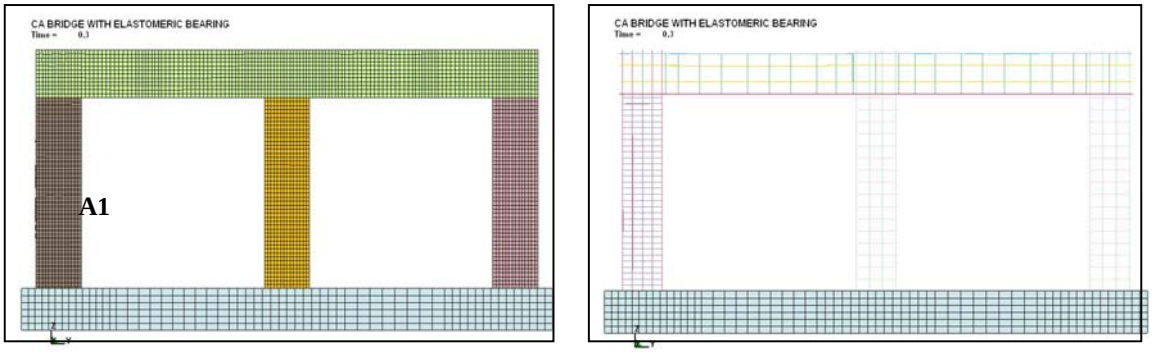

(b) Failure Mechanism with 50 MPH Impact Velocity

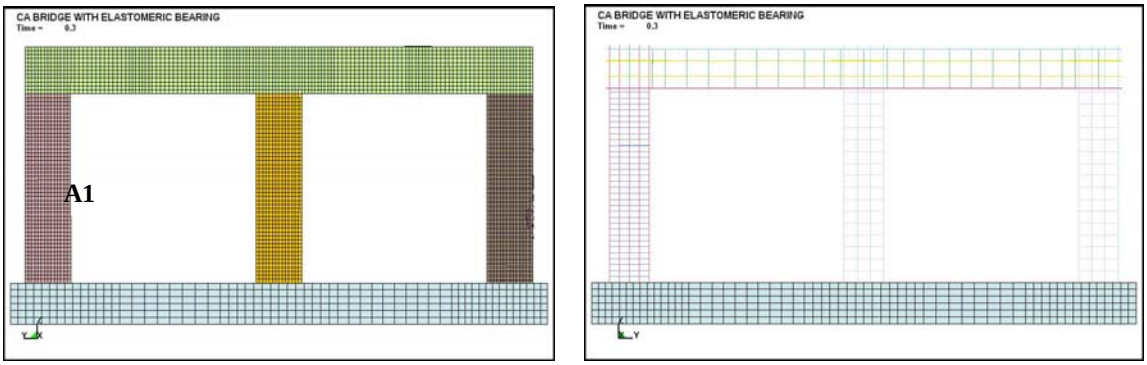

(c) Failure Mechanism with 30 MPH Impact Velocity

Figure 4.26 Failure Mechanisms of SF Bridge under Various Impact Velocity

It has been observed from the finite element simulations of NY and CA bridges under high velocity impacts that (i) the impacted piers in both of these bridges were severely damaged, (ii) concrete in the pier near the impact location is almost crushed and (iii) plastic hinge appeared at the joint of the Pier and the bent after the breakage at the impact point of the pier. Especially in case of NY bridge, plastic hinge was formed at the joint of the bent and the interior pier due to the flexural failure after the pier lost its load carrying capacity. The pier bent of the NY bridge exhibits all the identified failure mechanisms and lost its capacity under the high velocity impact. This bridge is likely to undergo complete collapse. The pier of the CA bridge has been observed to be significantly damaged under high velocity impact. Flexural failure of the bent isn't as severe as the NY bridge. However, damage in the bent could result in a complete collapse of the bridge if the remaining capacity of the bent is not sufficient to carry the superstructure dead load. The LA and SF bridges survive the high velocity impact of the medium weight truck. Only spalling of the cover concrete and fracture of core concrete was observed after the impact. These two minor failure mechanisms won't result in significant loss in the capacity of the pier. Hence, capacities of these piers can be restored through retrofit of damages.

It is observed from the simulation results that the NY bridge exhibits 5 failure mechanisms under the medium (50 mph) velocity impact. Most prominently, the pier is damaged and a plastic hinge is formed at the connection of the pier and the bent. Even though the plastic shear failure in the bent didn't appear, the loss of pier capacity made this bridge vulnerable to

collapse, since the superstructure weight carried by the damaged pier is carried by the bent like a lever beam. Both CA and LA bridges exhibit only 2 mechanisms and may not collapse after the impact since the damage of the pier is local. SF exhibits only one failure mechanism during the impact and is observed to be surviving the impact.

Under the low velocity (30 mph) impact of the medium weight truck, all four bridges have a very low probability of collapse. In particular, CA, LA and SF bridges show very few damage mechanisms and the damage to the concrete piers is local.

It is observed from Table 4.7 that the number of damage mechanisms in any case of vehicle impact velocity decreases with an increase in the seismic resistance capacity of piers. Among the identified damage mechanisms, mechanisms such as severance of longitudinal rebars and stirrups (A3), plastic hinge formation in piers (A4) and shear failure of bent (A6) can cause the failure of the entire bridge system. It has been observed from numerical simulations that the severity and presence of such mechanisms also decrease with increased seismic resistance of bridge piers. These results clearly demonstrate that there is a strong correlation between seismic resistance and impact loads of bridge piers. Bridge piers designed for higher seismic resistance also have better impact resistance.

Tables similar to Table 4.7 have been developed by Yi (2009) for seismic-blast multi-hazard correlations through finite element simulation of bridges similar to those used in this research. However, since blast load originates from one point and spreads to the whole bridge, almost all major components of the bridge, including piers, bents, stringers, deck and

bearings, are affected by blast loads. Local structural members are subjected to high level of blast force during the first few milliseconds and then the force is transferred to other members of the bridge. On the other hand, impact load applied on bridge piers is localized only near the point of impact, although it can affect the integrity of other components indirectly, e.g., longitudinal rebars transferring impact loads on the bent as a downward pull force.

Table 4.7 Seismic-Impact Multi-Hazard Correlation for Continuous-Three-Span Bridges

Failure Mechanism			Failure type for each bridge case											
			NY (New York)			CA (California)			LA (Los Angeles)			SF (San Francisco)		
	Item	Description	Low 30 MPH	Medium 50 MPH	High 70 MPH	Low 30 MPH	Medium 50 MPH	High 70 MPH	Low 30 MPH	Medium 50 MPH	High 70 MPH	Low 30 MPH	Medium 50 MPH	High 70 MPH
Pier	A1	Spalling of Concrete Surface	*X*	*X*	*X*	*X*	*X*	*X*	*X*	*X*	*X*	*X*	*X*	*X*
	A2	Breakage of the Pier	*X*	*X*	*X*		*X*	*X*		*X*	*X*			*X*
	A3	Severance of Longitudinal Rebar and Stirrups		*X*	*X*			*X*			*X*			
	A4	Plastic Hinge Formation in the Pier		*X*	*X*			*X*						
Bent	A5	Crush of Bent		*X*	*X*			*X*						
	A6	Flexural failure of the Bent			*X*									

X : Failure mechanism is observed in the specific bridge impact simulation.

4.4.3 Displacement Profiles and Impact Forces during Vehicular Impact

In order to evaluate the safety of highway bridge piers under vehicular impact loads, it is important to record and compare structural displacements and impact forces during bridge-vehicle impact simulations. It has been noted from observed failure mechanisms of bridges that the maximum deformation in a pier subject to truck impact occurs at mid-height of the pier. Hence, it is reasonable to capture the displacement of this location to characterize the behavior of a pier subject to vehicular impact.

Figures 4.27 to 4.30 show mid-height displacement time histories of the impacted pier of NY, CA, LA and SF bridges respectively. These displacement time histories can be used to study the influence of the impact velocity on bridge pier deformation. For the NY bridge pier subjected to impact by a truck with 70 mph velocity, it is observed from Fig 4.27 that the mid-height displacement of the pier starts to increase suddenly at time instant 0.11 seconds and reaches the maximum value of 500mm at 0.25 seconds. In case of 50 mph impact velocity, mid-height displacement starts increasing at 0.16 seconds (time of impact) and reaches the maximum of 200 mm at 0.20 seconds. The value of mid-height displacement of the pier in the case of 30 mph impact velocity is quite low when compared with those for medium and high impact velocities. It is observed that the maximum displacement decreases more than 50% when the impact velocity is decreased from 70 mph to 50 mph. Similar displacement profiles can be observed in case of CA, LA and SF bridges. However, the ratios of the maximum displacements between 50 mph and 70 mph velocities are approximately 0.2 and 0.1 for CA

and LA bridges respectively. For SF bridge, the maximum displacement in case of 50 MPH impact velocity is quite low as compared with that of 70 MPH impact and the ratio between displacements for 50 and 70 MPH velocities decreases to almost 5%.

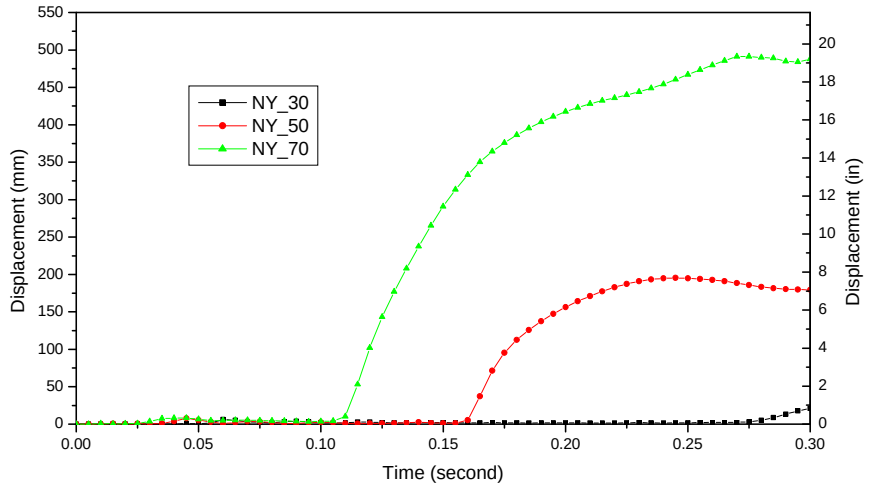

Figure 4.27 Mid-Pier Displacement Time Histories for the NY Bridge under Various Impact Velocities

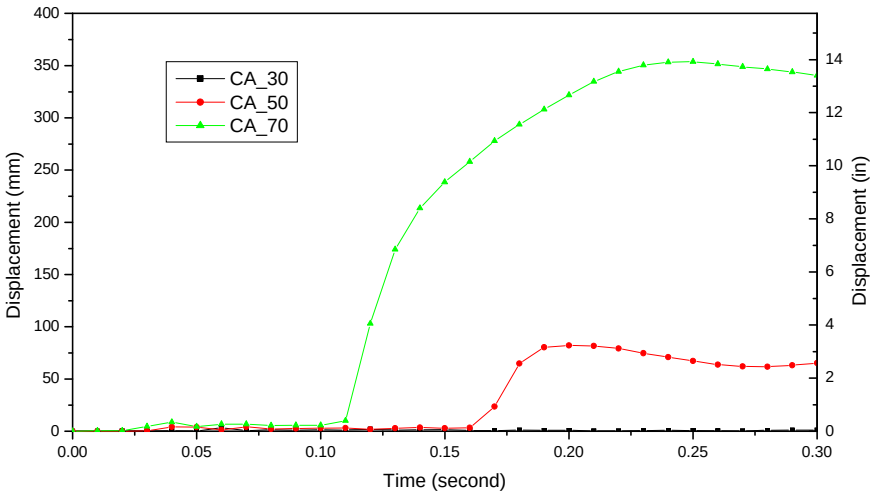

Figure 4.28 Mid-Pier Displacement Time Histories for the CA Bridge under Various Impact Velocities

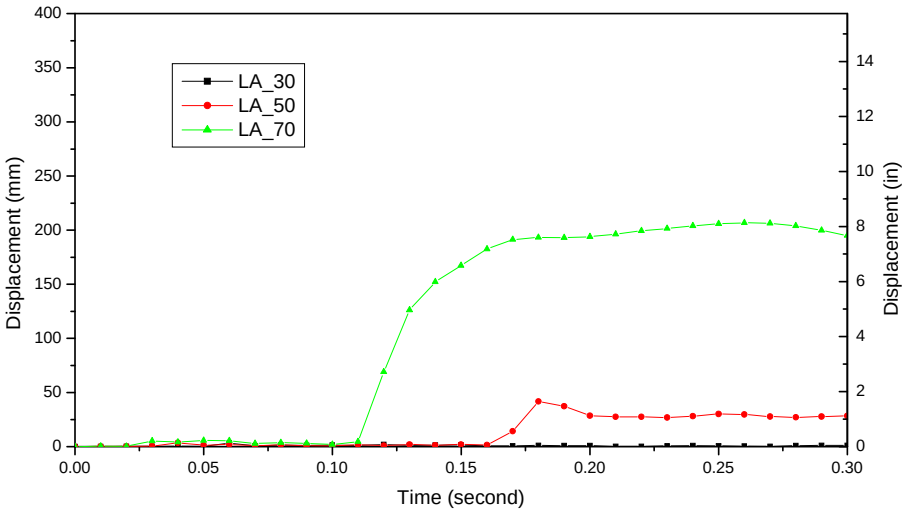

Figure 4.29 Mid-Pier Displacement Time History for the LA Bridge under Various Impact Velocities

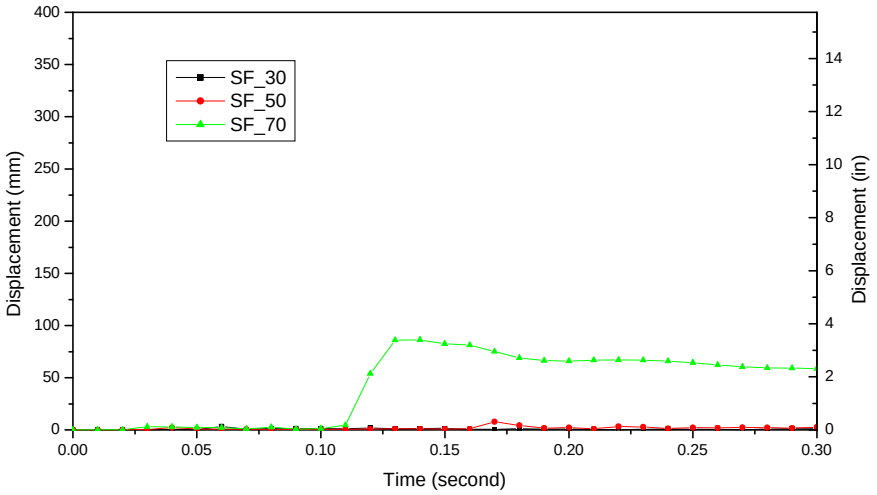

Figure 4.30 Mid-Pier Displacement Time History for the SF Bridge under Various Impact Velocities

Since the displacement time histories under medium and high impact velocities are comparably high, mid-height pier displacements of four bridges are compared for different impact velocities. Figure 4.31 and Figure 4.32 show comparisons between mid-height pier displacement time-histories of four bridges for 70 mph impact and 50 mph impact respectively.

It is observed that the peak mid-height pier displacement decreases with an increase in the seismic resistant of piers.

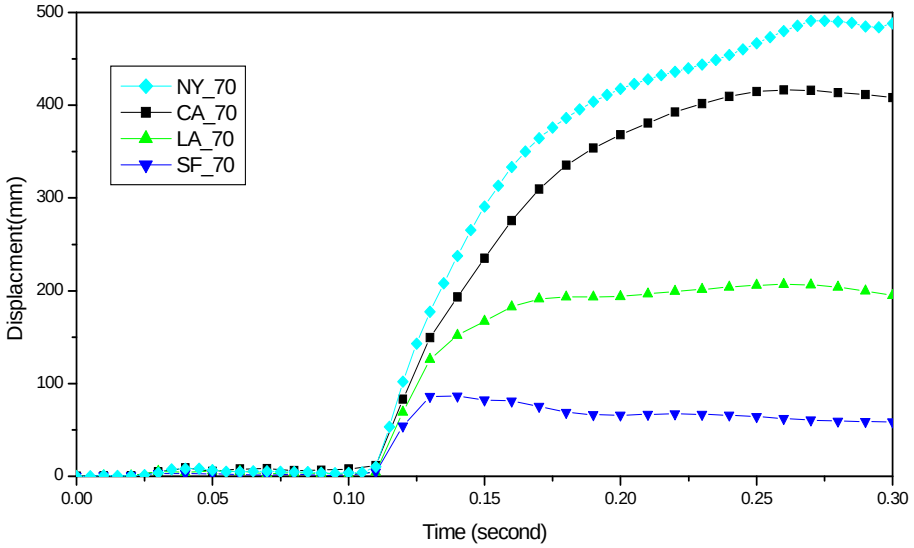

Figure 4.31 Displacement Time Histories of Three Example Bridges under High Velocity Impact (70 MPH)

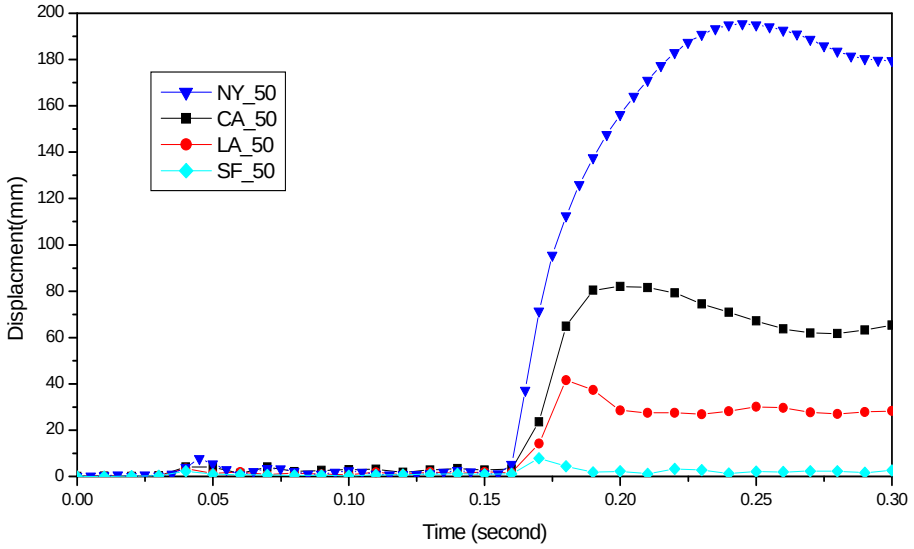

Figure 4.32 Displacement Time Histories of Three Example Bridges under High Velocity Impact (50 MPH)

The impact forces applied by the truck on bridge pier can also be captured in LS-DYNA. Figures 4.33 to 4.35 show impact force time-histories on four bridges for 70, 50 and 30 mph impact velocities respectively. The impact forces have been recorded from 0 to 0.3 second at a sampling interval of 0.001 seconds, i.e., impact forces shown in these figures are averaged by 0.001 second and there are in total 300 data points in each of the force time history plots.

It is observed from Figures 4.33 to 4.35 that impact force time history consists of two peaks, although the second force peak in case of 30 mph seems to be less prominent. The first peak in the impact force time history occurs when the engine block of the truck comes in contact with the pier and applies impact force as it undergoes deformations. The second peak in the impact force time-history corresponds to interaction of the carriage part of the truck with the bridge pier.

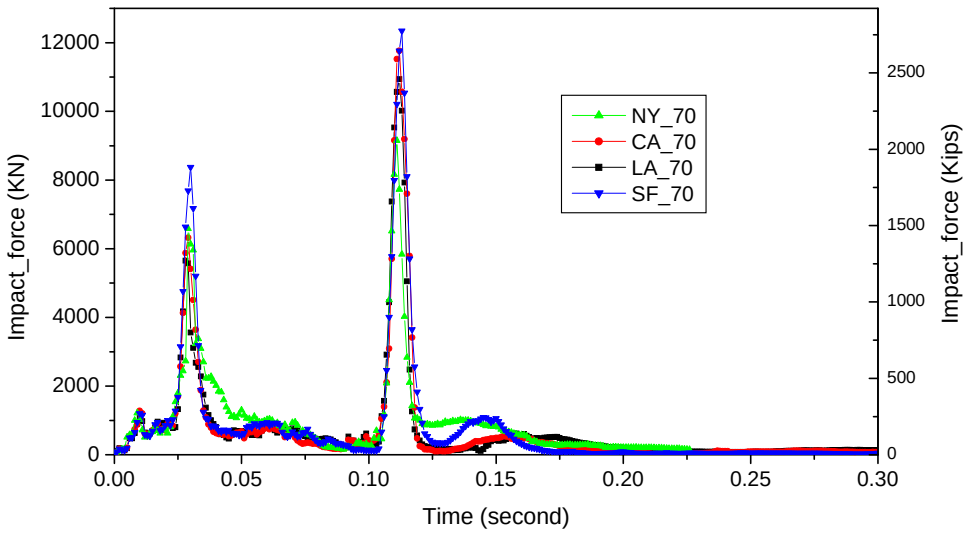

Figure 4.33 Impact Force Time Histories of Medium Weight Truck with High Velocity impact (70 MPH)

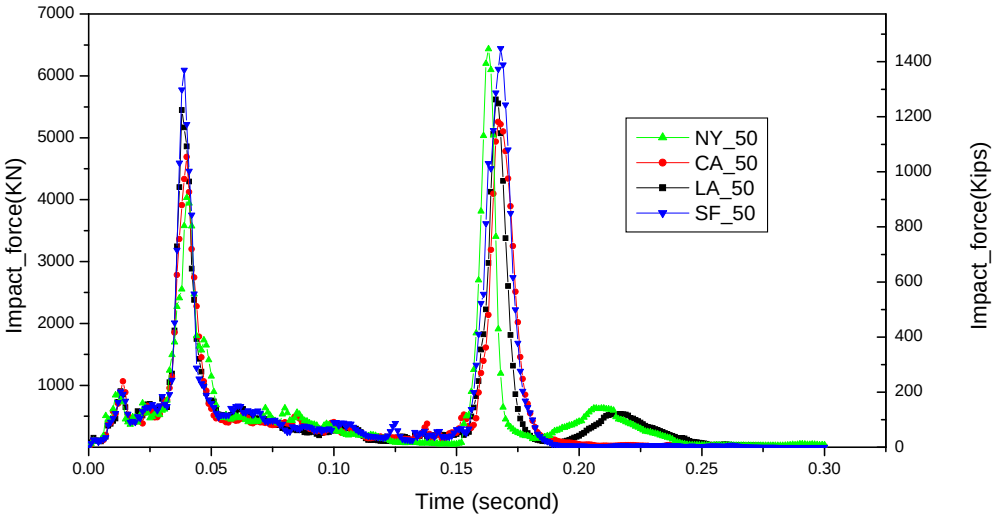

Figure 4.34 Impact Force Time Histories of Medium Weight Truck with Medium Velocity impact (50 MPH)

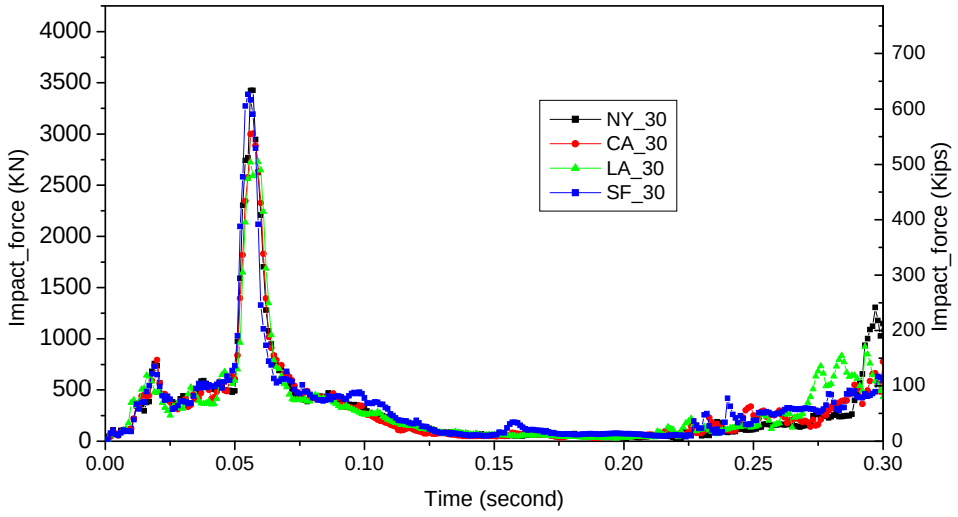

Figure 4.35 Impact Force Time Histories of Medium Weight Truck with Low Velocity impact (30 MPH)

Plots in Figures 4.33 to 4.35 for the four example bridges mostly coincide with each other, implying that the impact forces applied on rectangular bridge piers are largely independent of

the pier size and mainly depend on impact (approach) velocity and weight of the truck. The magnitude of the impact force is determined by the weight and approach velocity of the truck. Specifically, key components affecting the impact force are the characteristics of the engine block and carriage of the truck. Connections of other components of the truck are weak compared with high impact forces. They undergo large deformation and may be separated apart during the impact. Hence, other components of the truck have less influence on the impact force during the collision. The engine block is heavy compared to other components of the truck and is usually made of the cast iron, which has high density and high stiffness. In the truck model used, the mass of the engine block is approximately 15% of the mass of the whole truck. The carriage and the mass carried inside the carriage account for almost 50% of the total mass of the whole truck model. Even though stiffness of the carriage varies and is usually less than the steel, weight of this part makes the most important factor influencing the impact force.

It is observed from Figures. 4.33 to 4.35 that the impact force at second spike in case of 70 mph impact velocity is almost double that of the first spike. Table 4.8 below shows the impact forces at first and second spikes for the three truck impact velocities. It is observed that the maximum impact force during 70 mph is approximately 2500 kips and is significantly higher than the 400 kips recommended in the AASHTO LRFD specifications. In fact, the maximum force during 30 mph is also higher than the 400 kips recommended by AASHTO LRFD to design bridge piers for vehicular impact.

Table 4.8 Peak Impact Forces during Vehicular Impact

Impact Velocity	First Peak (Kips)	Second Peak (Kips)
70 MPH	1450	2357
50 MPH	1201	1381
30 MPH	718	N/A

4.4.4 Impact Response Quantities versus Shear Capacity and Ductility

Peak displacement versus ductility coefficient. The ductility factors of the four example bridges have been calculated as shown in Table 4.3. The peak mid-height displacements versus the ductility factors of the bridge piers are plotted in Figure 4.36. As the seismic capacities increase, the ductility-strength ratio (μ/Ry) decreases from 24.3 to 2.3, implying that the bridge piers become stiffer with an increase in this ratio. For a particular impact velocity, the peak mid-height displacement increases as the ductility of the bridge pier is increased. For the case of the low impact velocity of 30 MPH, the peak mid-height displacement doesn't change much with an increase in ductility since all four example bridges only undergo local damage (spalling of concrete and local cracking of the pier).

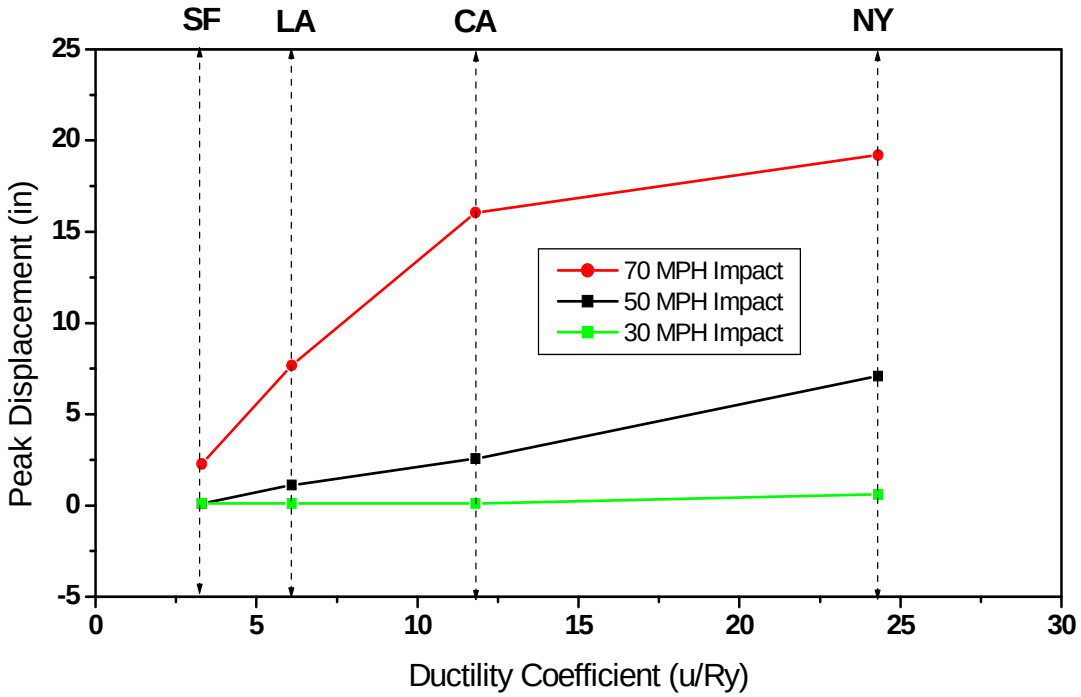

Figure 4.36 Influence of Ductility Factors on the Final Impact Displacements

For the case of medium impact velocity of 50 MPH, the peak displacement increases linearly with an increase in the ductility of bridge piers. Under the medium velocity impact, example bridges with lower ductility factors, such as SF and LA bridges, undergo localized damage. Even though both CA and NY bridges show some of the worse failure mechanisms, these bridges still have a lower possibility to collapse. Furthermore, the peak displacement for high velocity (70 mph) impact increases linearly with ductility till a ductility of 11.8 (CA bridge) and the slope of the peak displacement versus ductility curve decreases drastically as the ductility increases beyond 11.8. In the ductility range of 11.8 to 24.3, both NY and CA bridges are damaged severely because of the high velocity impact. In the context of the design procedure in this dissertation, it can be concluded that the peak mid-height displacement of

bridge piers under vehicular impact increases with an increase in ductility for medium and higher impact velocities. For lower impact velocity of 30 mph, there is significantly smaller increase in peak mid-height displacement with ductility.

Table 4.9 Shear Strength of the Four Example Bridge Piers

	Pier Size (ft)	Longitudinal Bars	Stirrups Bars	Shear Capacity (kips)
NY Bridge	3	Bar 11 4×4	Bar 3 12 in Spacing	274
CA Bridge	3.5	Bar 11 4×4	Bar 4 12 in Spacing	409
LA Bridge	3.5	Bar 11 5×5	Bar 4 6 in Spacing	565
SF Bridge	4	Bar 14 6×6	Bar 5 6 in Spacing	893

Peak displacements versus shear capacities of bridge piers: In the design of the four example highway bridges, the shear capacities of the bridge piers have been checked to satisfy the shear force demand from the seismic induced overturning moments. Actually the shear capacities can also be calculated according to ACI 318R-08. For the bridge members subject to axial load, the shear strength of the concrete can be calculated based on the ACI Equation 11-4 in section 11.2 of ACI 318R-08. The shear strength attributed to shear reinforcement can be calculated using the ACI Equation 11-15 in section 11.4.7 of ACI 318R-08. The shear capacities of the four example bridges are tabulated in the Table 4.9 above. It is noted that the

shear capacities of the bridges piers is changed from 274 kips to 893 kips for the four example bridge piers with increasing bridge pier crossing section byincreasing size of stirrups and decreasing of the stirrups spacing, The peak mid-height displacements versus the shear capacities are plotted in the Figure 4.37. It is observed that the magnitudes of the peak mid-height displacement decreases with the increasing of the bridge pier'an increase in shear capacities under medium and high velocity impacts. For the bridge piers with lower seismic capacity under high velocity impact, longitudinal reinforcement resist major portion of the impact load after the bridge pier is cracked and stirrups loosetheir capacity to confine the core concrete. The shear strength of bridge pier can be taken as one of the key parameters to evaluate the vehicle impact resistance of bridge piers. Peak mid-height displacements are in close range for shear capacity of 893 kips achieved for SF bridge.

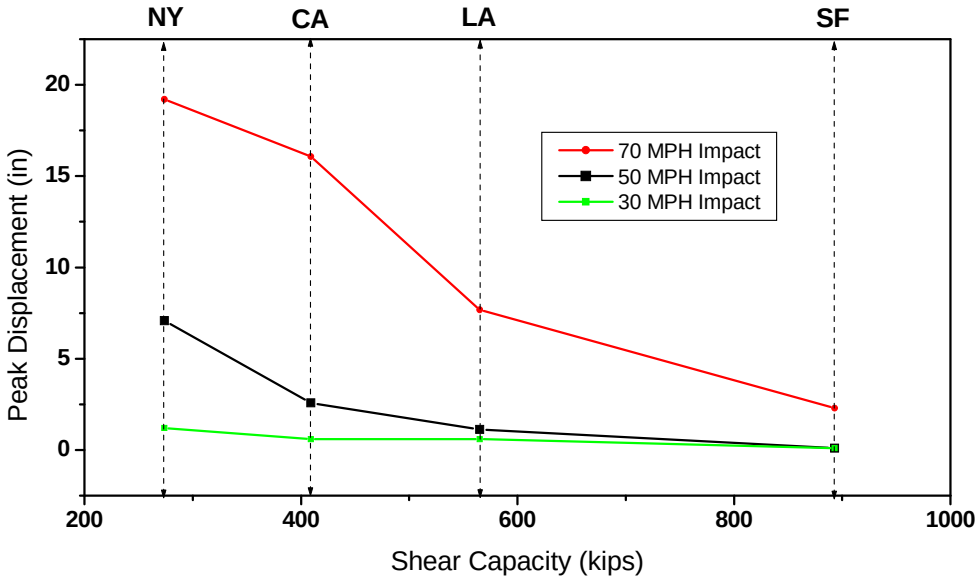

Figure 4.37 Influence of Shear Strength on the Final Impact Displacements

4.4.5 Performance-Based-Design Approach

There are totally 6 failure mechanisms A1 to A6 captured in the numerical simulations of bridges under vehicle impacts, as described in Table 4.5. From mechanism A1 to mechanism A6, the severity of the damage level becomes worse gradually. The design recommendation of ATC-32 describes two performance levels for bridge structures under seismic load: repairable damage and significant damage. Repairable damage indicates that inelastic damage may occur, resulting in concrete cracking, reinforcement yielding and minor spalling of cover concrete. The repairable damage should be sufficiently limited so that the bridge structure can be restored essentially to its pre-earthquake condition without replacement of reinforcement or replacement of structural members. Comparing these damage levels with the definition of failure mechanisms in this dissertation, the failure mechanism A1 can be classified as repairable damage. Significant damage indicates that permanent damage offsets may occur and damage may consist of cracking, reinforcement yielding, and major cracking of concrete. Significant damage may require bridge closure for repair. Partial or complete replacement may be required in some cases of significant damage. Hence, failure mechanisms A2 and A3 can be classified as significant damage.

In the ACT-32 guideline, there is no damage level definition related to the failure mechanisms A4, A5 and A6. The definition of structural performance damage levels in ASCE-41 includes failure mechanisms A4, A5 and A6 in this dissertation, in the context of collapse prevention. The collapse prevention requirement include prevention of extensive

crushing of core concrete, buckling of main reinforcement, rupture of transverse reinforcement and hinge formation in ductile member. Even though failure mechanism A5 causes local minor damage in the bent, this mechanism always occurs after the pier is damaged severely.

Based on fifteen years of bridge seismic research, researchers at the University of California in San Diego developed an inspection and assessment guideline on "Post Earthquake Inspection Manual for RC Bridge Columns" [Hose (2001)]. This inspection and assessment manual provides a step by step approach for post earthquake inspection and assessment procedure. The remaining capacity of the damaged reinforced concrete structures can be determined based on this manual. The procedure of the inspection and assessment procedure consists of three phases: phase I – determine the performance curve that the column is likely to follow; phase II – identify the damage level; phase III – assess bridge system. In phase I, each column needs to be associated with a performance curve that best summarizes the expected seismic response. There are three performance curves to choose from: Ductile; Strength Degrading and Brittle as shown in Figure 4.38.

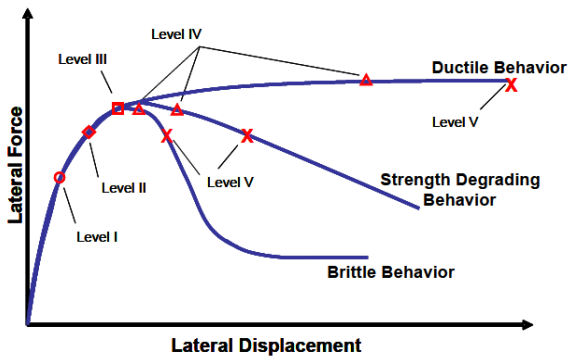

Figure 4.38 Performance Curve for Bridge Piers

An engineer can determine the anticipated performance curve from the decision flow chart in the manual. Phase II provides the step by step procedure to determine where each column is on their respective performance curve (level I- cracking, level II-yielding, level III-initiation of local mechanism, level IV-full development of local mechanism and level V-strength degradation), as shown in Figure 4.38. The quantitative performance definition of each damage level is described inTable 2 of the inspection manual [Hose (2001)]. The damage can be plotted in the performance curve of each column in phase III as shown in Figure 4.38, and this plot can assist the engineer in evaluating the remaining capacity of damaged bridge structures.

According to the above definition of seismic damage level for bridge structures, three damage levels for highway bridge structures under vehicular impact loads can be classified in Table 4.10: Minor damage level includes failure mechanism A1; Moderate damage level includes failure mechanism A2 and A3; severe damage level includes failure mechanism A4, A5 and A6. Bridge structures with minor damage can be restored essentially to their pre-collision condition without replacement of reinforcement or replacement of structural components. If bridge structures suffer moderate damage after vehicular impact, the closure of the bridge may be necessary for repair. A partial or complete replacement may be required in some cases even though the possibility of complete bridge collapse may be low. Bridge structures with severe damage may have a higher probability to collapse. Under the condition of collapse prevention, bridge is required to be closed immediately and major concrete

components need to be replaced. If a repair isn't possible, a severely damaged bridge may have to be demolished and reconstructed.

Table 4.10 Damage Level Definition for Performance Assessment of Vehicle Impact

Damage Level	**Failure Mechanisms**	**Description**
Minor Damage	A1	Spalling of cover concrete, minor inelastic deformation of reinforcements.
Moderate Damage	A2, A3	Shear cracking of core concrete and severance of transverses reinforcements
Severe Damage	A4, A5, A6	Buckling of main reinforcement, crushing of core concrete, plastic hinge formed in the pier and the flexural failure in the bent

The damage levels for four example bridges subject to different impact velocities can be assessed on the basis of Table 4.10. Table 4.11 shows damage levels for bridges with different impact velocities. This table also shows the ratio of impact force and shear capacities (I/S) of each of the piers. These three damage levels (in terms of damage mechanisms present) are plotted in Figure 4.39 as a function of ratio of impact force and shear capacities (I/S) for each of the cases in Table 4.11. The twelve vehicle impact cases can be summarized in Figure 4.39. It is observed that the damage level increases with an increase in I/S ratio for bridge piers. It is noted from Figure 4.39 that bridge piers should be design for a I/S ratio of up to 2 for minor damages and for a I/S ratio of 5 for moderate damage. A bridge

with a I/S ratio of greater than 5 is likely to suffer severe damage leading to collapse or require demolition. This criteria may be more effective than constant force of 600 kips being recommended in recent revisions to the AASHTO provisions on increasing impact resistance of bridges.

Table 4.11 Damage Levels and Impact to Shear Strength Ratio for Four Example Bridges

		Damage Level	Peak Impact Force (Kips)	Shear Strength (Kips)	Impact/Shear Ratio(I_f/S)
NY Bridge	30 MPH	Moderate	718	274	2.6
	50 MPH	Severe	1381	274	5.0
	70 MPH	Severe	2357	274	8.6
CA Bridge	30 MPH	Minor	718	409	1.7
	50 MPH	Moderate	1381	409	3.3
	70 MPH	Severe	2357	409	5.7
LA Bridge	30 MPH	Minor	718	565	1.3
	50 MPH	Moderate	1381	565	2.4
	70 MPH	Moderate	2357	565	4.2
SF Bridge	30 MPH	Moderate	718	893	0.8
	50 MPH	Minor	1381	893	1.5
	70 MPH	Minor	2357	893	2.6

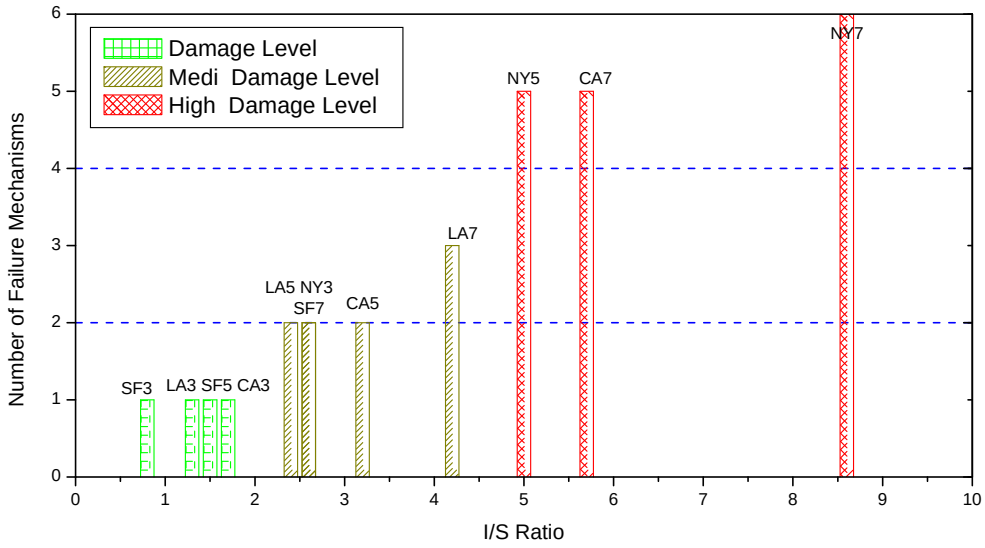

Figure 4.39 Damage Level versus I_f/S Ratio for Bridge Piers

4.4.6 Estimation of Approximate Impact Force

It is observed from Figure 4.39 that the design shear capacity of a bridge pier can be determined for a certain damage level if approximate impact force can be estimated. Since impact force doesn't depend on the size of rectangular piers, it can be determined from numerical simulations by considering truck velocities of 30, 40, 50, 60 and 70MPH for trucks of 15000, 22500 and 30000lb weights. Table 4.12 shows impact force for trucks with different weights and velocities. Figure 4.40 shows plots of impact force versus velocity for different weights.

Table 4.12 Peak Impact Forces for Trucks with Different Weights and Velocities.

	15,000 lb	22,500 lb	30,000 lb
Impact Velocity (MPH)	Peak Impact Force (Kips)	Peak Impact Force (Kips)	Peak Impact Force (Kips)
30	718	929	1345
40	913	1177	1713
50	1381	1794	2166
60	1440	2260	2953
70	2357	2672	3277

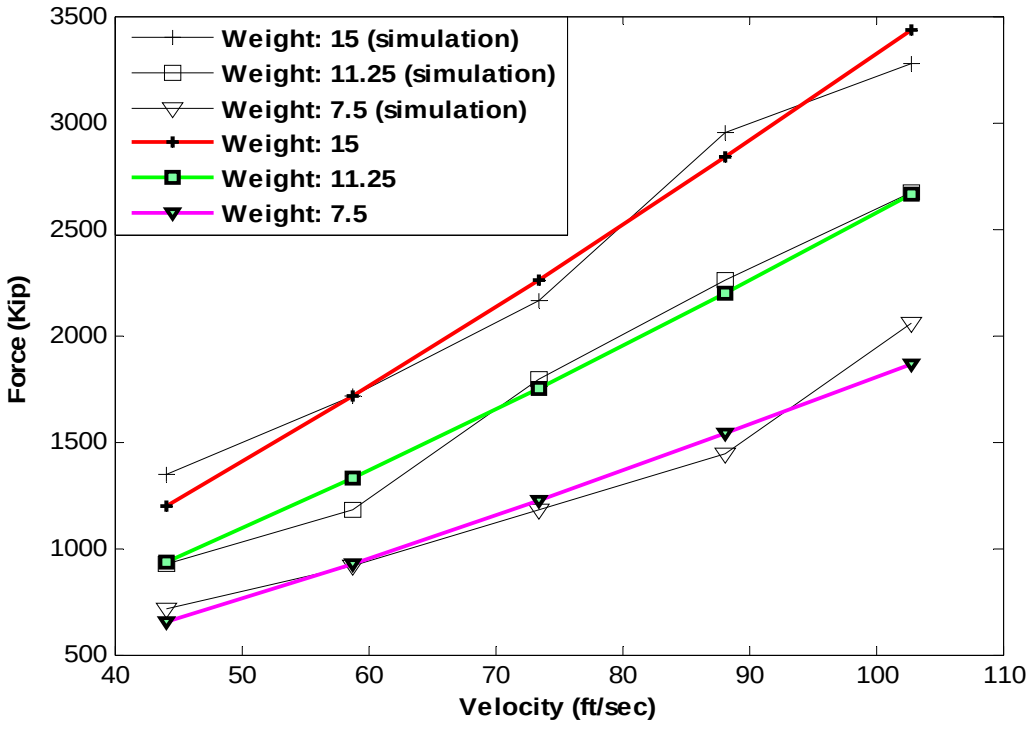

Figure4.40 Peak Impact Forces for Trucks with Different Weights and Velocities

For impact of vessel on bridge piers, AASHTO recommends equation $F = 8.15\sqrt{WV}$ to estimate impact force, where W is the weight in tons and V is the velocity in ft/second. For impact force data in Table 4.12, we propose to use the equation of a form similar to that used by AASHTO for vessel collision,

$$F = aW^b V^c \tag{4.3}$$

Where a, b, c are regression parameter, W is the weight in tons and V is velocity in ft/second.

A nonlinear optimization problem has been formulated where the objective function is the minimization of

$$J = \sqrt{(F_{v,W} - F'_{v,W})^2} \tag{4.4}$$

Where $F_{v,W}$ is the force calculated from equation (4.3) and $F'_{v,W}$ is the impact force in Table 4.12 for a particular weight and velocity. A nonlinear optimization has been carried out by Generic Algorithmic (GA) to determine values of parameters as: a=1, b=0.8824 and c=1.2412. Hence, the empirical equation for estimation of impact force is obtained as

$$F = W^{0.8824} V^{1.2412} \tag{4.5}$$

Figure 4.40 shows a comparison between impact forces from numerical simulation and those calculated from the equation (4.5). It is observed that the equation (4.5) is able to predict impact force from numerical simulation quite accurately. Hence, equation (4.5) can be used to estimate approximate impact force for the design of piers.

Chapter 5 Pier-Bent Model of Highway Bridges under Vehicle Impact loads

5.1 Introduction

Failure mechanisms of highway bridges under different levels of vehicular impact loads have been discussed in the previous chapter. It is been observed that all failure mechanisms during vehicular impacts to bridges occur only in the pier directly impacted and in the bent connecting the impacted pier with other piers. Hence, the pier-bent system containing the impacted pier of the bridge can be considered a key component for the simulation of vehicle-bridge collision. Although a simulation of the whole bridge model can yield detailed information on interaction of different bridge components during the impact, it requires significant level of modeling skills, high-performance computers and long computational time. Given the complexity of bridge-vehicle interaction during impacts, including the nonlinear behavior of the bridge pier and bent, development of traditional design charts and design tables is also not feasible. Hence, in this research, we propose a simplified pier-bent model for the simulation of impact loads on bridge piers. This pier bent model should represent all failure mechanisms observed during full-bridge simulations. Constraints, mass and external forces are used to define the boundary conditions of this simplified pier-bent model.

In the routine bridge design procedure, a pier-bent model with external forces introduced by gravity load is selected for the design of a pier. Therefore, a pier-bent model has been

used by many researchers for investigation of the blast loads on highway bridges. For example, researchers at FHWA and MCEER built a pier-bent model instead of a whole bridge model in blast experiment tests, as shown in Figure 5.1.

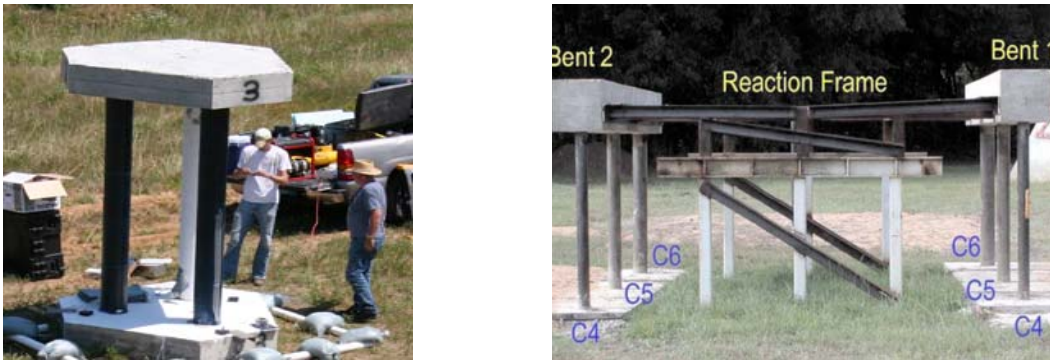

(a) Testing by Univ. of Missouri, Rolla (b) Testing by MCEER, Buffalo Univ.

Figure 5.1 Pier-bent Model Used in the Highway Bridge Blast Experiments

5.2 Description of the Pier-Bent Model

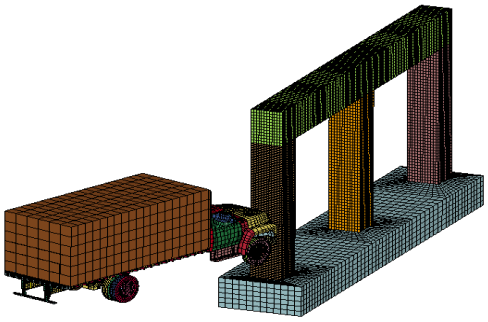

Figure 5.2 Pier-Bent of a Bridge Impacted by the Truck

Figure 5.2 shows the pier-bent of the bridge being impacted by a truck. In order to simulate the effects of superstructure and mass of the deck, a pier-bent model can be built as shown in Figure 5.3

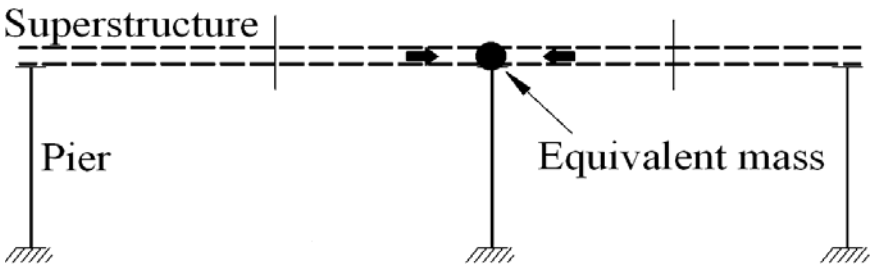

(a) Computation configuration of Pier-mass model

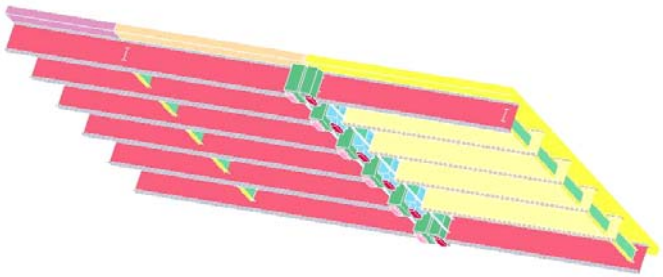

(b) The mass of the half-span Bridge Parts on the Top of Bent

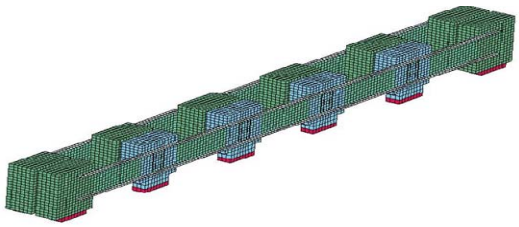

(c) The equivalent Mass on the Top of the Bent

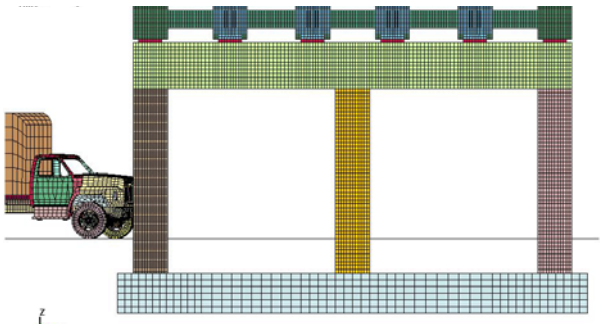

(d) Pier-bent Model with Equivalent Mass on the Top of the Bent

Figure 5.3 The Pier-Bent Model with Mass Load

In this model, an equivalent mass of the deck, calculated as the sum of mass contributions from each of the spans, is applied on top of the bent. The top of the bent is considered to be fixed in the horizontal direction, although it can displace in the vertical direction.

In the pier bent model of Figure 5.3, the weight of the superstructure has to be assigned to the pier-bent model correctly. In seismic analysis, the effect of mass is primarily in the horizontal direction. However, in the case of impact load, the mass plays an important role in both the horizontal and vertical directions. Similar to the case of seismic analysis, half mass of spans on both sides of the pier-bent model is applied to the pier-bent model, as shown in Figure 5.3(a). Figure 5.3(b) shows half-span of the bridge on the top of the bent, including a portion of the deck, portion of the stringers, middle-span diaphragm, end diaphragm, stringer support and bearings. The mass of half span of the bridge is calculated as 400 tons by LS-DYNA. Since the weight of the deck and stringers is transmitted to the pier-bent through stringer supports, it is reasonable to keep stringer support, bearing and end diaphragms in the Pier-bent model. By increasing the density of the stringer support of the pier-bent model, 400 tons mass of the half-span bridge can be condensed on the stringer supports on the top of the bent as shown in Figure 5.3(c). This equivalent mass of the stringer support model is imported into the pier-bent model as shown in Figure 5.3(d). The bearing of equivalent mass model has been moved to have contact with the top of the bent. Horizontal degrees of freedom of nodes on the top of the equivalent mass model are constrained so that the equivalent mass could move freely in the vertical direction without introducing any spurious

lateral turnover force during the impact simulation. This is consistent with our observation of the whole bridge simulation in Chapter 4 that the superstructure wasn't turning over during the impact because of strong constraints from the deck and the girder.

There are several advantages of this pier-bent model with equivalent mass. This model can simulate the interaction between the bearing and the superstructure, and the equivalent mass on the top of the bent can simulate the compressive effects on the pier-bent system without dramatically increasing the number of finite elements. In this sense, this pier-bent mass model is still a simplified numerical model compared with the whole bridge model used in Chapter 4. It has been observed that the required time for the numerical simulations using the pier-bent model is reduced by 70% of that required by the full-bridge model.

5.3 Comparisons between simulations using pier-bent and full-bridge models

The pier-bent has been built using the same geometry and the rebar detailing of the NY bridge described in Chapter 4. The medium weight truck has been input into the pier-bent model. The impact angle of the moving vehicle is set at 20^{o} (the same as the full-bridge model in Chapter 4). Figure 5.4 shows the impact force time-history for the case of 70 mph impact velocity of the truck. It is observed that the impact force time history is the same as that recorded during the whole bridge simulation in Chapter 4. This is expected since impact force is independent of the size of the pier and two models use the same material model.

Figure 5.4 also shows the impulse time-history obtained by the integration of the impact force with respect to time.

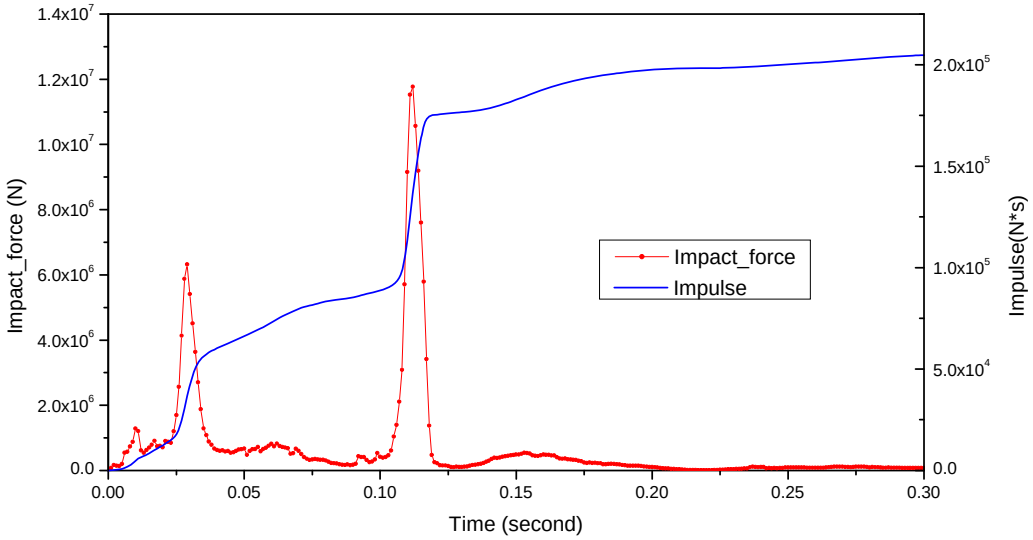

Figure 5.4 Impact force and Impulse Time History for the Case of 70 MPH

Figure 5.5 shows the time-histories of displacement at mid-height of the pier for cases of (i) pier-bent model with the mass of the superstructure assigned, (ii) pier-bent model without the mass of superstructure assigned and (iii) whole bridge simulation indicated by "NY-70". This figure also shows time-history plot of impulse due to impact. It is observed from Figure 5.5 that the pier-bent model without superstructure mass overestimates the deformation of the pier under the vehicle impact, since it doesn't consider axial forces in the piers because of the superstructure weight. Displacement time history using the pier-bent model with mass of the superstructure matches very well with that of the whole bridge model during 0 to 0.2 second. The pier-bent model with mass of the superstructure shows a larger displacement compared to

that of whole bridge model for time t > 0.2 seconds.

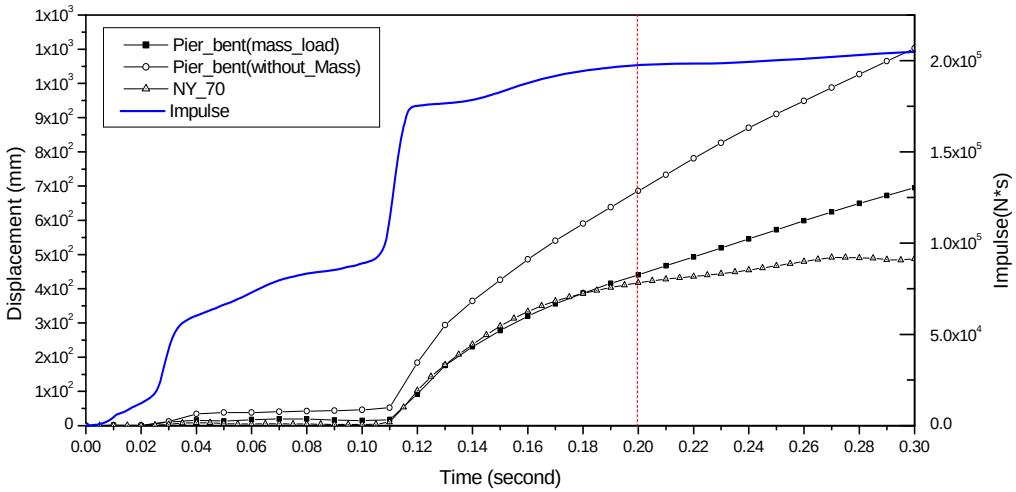

Figure 5.5 Displacement Time Histories of Pier-bent model for the case of 70 MPH

This difference between pier-bent and full bridge models is because of condensed weight of the stringer supports in the pier-bent model. In the simplified pier-bent model, almost 400 tons of weight is assigned to the stringer supports that are combined with end diaphragms. Before the pier was severely damaged, most of the mass load was carried by the bent and the pier. However, after the pier loses its capacity to carry the weight, the bent failed because of imposed cantilever behavior to carry the weight from superstructure components. In the whole bridge model, stringers show some constraints with stringer supports, thereby preventing large deformation of end diaphragms after the impact as shown in Figure 5.6(a). However, entire weight of stringer support is carried by end diaphragms in the pier-bent model after both pier and bent lose their load carrying capacity, as shown in Figure 5.6(b). Redistribution of this large weight creates a plastic hinge in the middle of end

diaphragms, as shown in Figure 5.6(b), resulting in its sudden failure. Following this failure, weight from the superstructure is applied directly on broken pier and bent. This load makes the pier undergo larger deformation as compared to the pier in the whole bridge simulation. This behavior is not observed in case of 50 mph and 30 mph impact velocities because of significantly less severe damage than that in case of 70 mph impact velocity. End diaphragms are intact in these cases.

Hence, a larger displacement than that of the whole bridge model for $t > 0.2$ sec is because of lesser restraint provided by the superstructure part in case of the pier-bent model after the impacted pier loses its gravity load carrying capacity. However, it is observed from impulse time history in Figure 5.5 that the impulse reaches 95% of the maximum impulse during $t \leq 0.2$ seconds. Most of the energy exchange has already been completed during this period. Hence, maximum displacement around the time when impulse reach 95% of its peak value can be considered as the peak displacement before the pier looses its vertical load carrying capacity in this case. Results presented in Figure 5.5 clearly demonstrate that the pier bent model successfully models the behavior of the impacted pier before the pier loses its vertical load carrying capacity.

Figure 5.7 shows the mid-pier displacement time-histories for the case of 50 mph impact. In this case, it is observed that the pier displacement predicted by the pier-bent model matches with that by the full-bride model during the entire duration, since the pier doesn't lose its vertical load carrying capacity. In case of 30 mph impact velocity shown in Figure 5.8, peak

displacements match very well. There is some disagreement between displacements by the two models after the peak displacement. This may be caused by different levels of restraints applied by the full-bridge and pier-bent models. However, this occurs during displacement less than 1 mm during high-frequency vibration caused by bridge-vehicle impact dynamics. Hence, overall, the pier-bent model can be used to predict mid-pier displacement quite accurately in comparison to the full-bridge model.

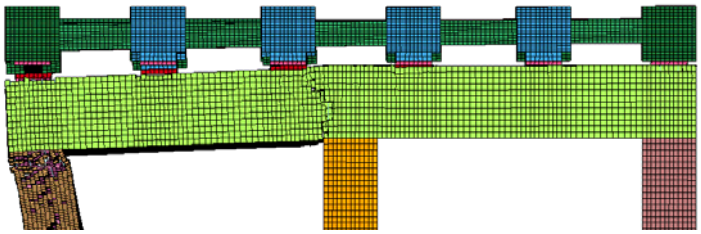

(a) Bent-pier Damage Mechanisms in Whole Bridge Simulation

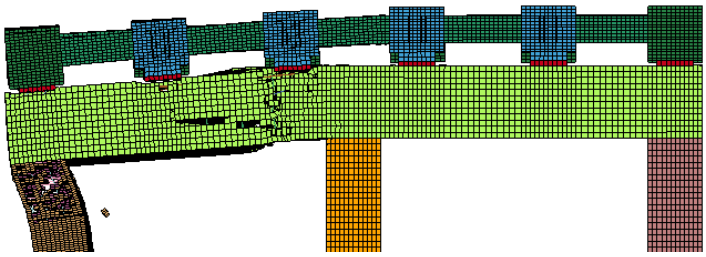

(b) Bent-pier Damage Mechanisms in Pier-Bent Simulation

Figure 5.6 Pier-Bent Damage Mechanisms during 70 MPH impact velocity

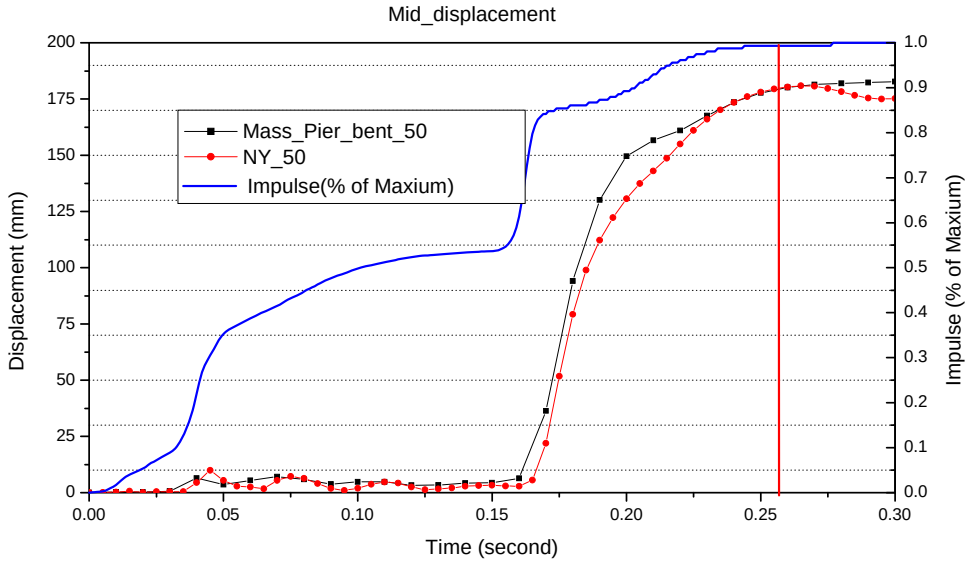

Figure 5.7 Mid-pier Displacement Time Histories during 50 MPH Impact Velocity

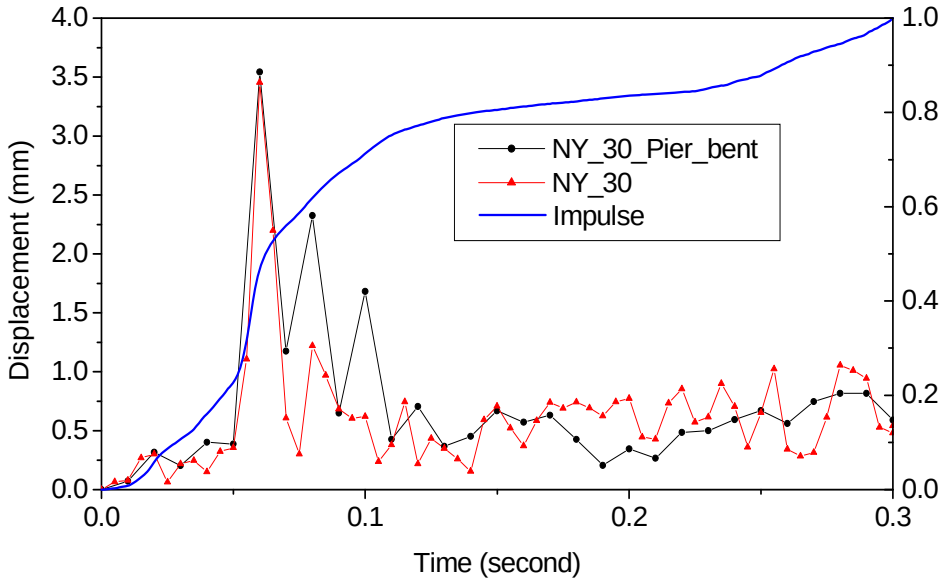

Figure 5.8 Mid-pier Displacement Time Histories during 30 MPH Impact Velocity

5.4 Conclusions

In this chapter, a simplified pier-bent model has been proposed to investigate vehicle impacts on a bridge pier. The Pier-bent model without mass load from the superstructure

overestimates vehicle impact load effects. However, the pier-bent model with tributary weight from the superstructure has been found to give results similar to that of the full-bridge model. The superstructure equivalent mass affects the pier behavior both in horizontal and vertical directions. Simulation results show that the failure mechanisms and displacement time-histories of the pier-bent model match with that of the whole bridge model, although mid-pier displacement in case of 70 mph velocity for the whole bridge model is smaller than that of the pier-bent model after the pier loses its load carrying capacity. This difference is attributed to restraints provided by the superstructure after piers loose gravity load carrying capacity. However, this displacement only occurs after 95 % of the impulse because of impact has been applied. The proposed pier-bent model has significant advantages in terms of lesser simulation time.

Chapter 6 Effects of Retrofits on Vehicular Impact Resistance

6.1 Introduction

Results presented in previous chapters indicate that there in an intrinsic relationship between impact and seismic resistance capacities of bridge piers. Generally bridge piers with higher seismic capacity can sustain higher impact loads. Seismic guidelines after the 1971 San Fernando earthquakes have undergone significant improvements. Hence, recently built bridges in California are likely to have sufficient capacities to sustain vehicular impact loads.

However, many bridges constructed before new design standard are still in service. These bridges have insufficient amount of transverse reinforcement in piers. Typically, transverse reinforcements are No.3 or No.4 rebar spaced at 12 in. For an instance, the transverse reinforcement in example NY bridge is No.3 bars at the spacing of 12 inches as shown in Figure 3.19. The shear capacity of these piers are approximately 274 kips as calculated in Table 4.11. The shear capacity of 274 kips is even below the 400 kips which is defined as the equivalent vehicular impact load in the current AASHTO design guidelines. Hence, this bridge is vulnerable damages by vehicular impact loads, as observed from numerical simulations in Chapter 4. Insufficient transverse reinforcement indicates that many older bridges are susceptible to shear failures. Moreover, insufficient confinement can lead to buckling of longitudinal reinforcement under seismic load or vehicular impact loads.

In order to retrofit older bridges to satisfy current safety requirements, various retrofit efforts of bridges are being carried out. In current AASHTO LRFD Guide Specifications on Bridge Seismic Design, detailing is prescribed to ensure that inelastic deformations occur at locations in piers (top or bottom or both) that can be readily inspected and repaired. Most common seismic retrofit approaches focus on increasing moment and shear Capacities of bridge piers. This chapter discusses seismic retrofit approaches for piers and evaluation of these approaches in sustaining vehicular impact loads.

6.2 Seismic Retrofit of Bridge Piers

California Department of Transportation (Caltrans) initiated seismic retrofit program before the 1994 Northbridge earthquake. Seismic retrofits of bridge piers using steel and composite jacketing of columns are highly recommended approaches. Old Concrete piers have insufficient flexural strength, flexural ductility and shear strength. Chai and Priestley (1991) have investigated retrofit of circular bridge columns with circular steel jackets and rectangular bridge columns with elliptical steel jackets. A high-strength FRP fabric was post-tensioned around the plastic hinging region of a column in the test by Priestley et al (1998). It was found that the retrofit using FRP jacket can enhance the flexural ductility without bond failures. This has also been observed through tests on bridge piers retrofitted by steel jackets also. Shinozuka and Kim (2002) have generated analytical fragility curves of concrete bridges retrofitted by column jacketing. These fragility curves for bridge piers

retrofitted by steel jackets demonstrate the effectiveness of steel jackets in reducing seismic fragility of bridge piers. Xiao and Wu (2003) have studied the effectiveness of partially stiffened steel jackets to retrofit reinforced concrete columns. Their test results show that partially stiffened steel jackets can not only prevent brittle shear failure of columns but also improve the ductility of the columns with an ultimate drift ratio of more than 8%. More recently, Agrawal et al. (2011) have investigated seismic fragility of bridge piers retrofitted by FRP wrapping. Their work shows that the fragility (or risk of failure) of bridge piers is reduced significantly because of FRP wrapping.

Generally, concrete pier can be retrofitted by three types of jacketing systems: (i) steel jacketing, (ii) active confinement by prestressing composite material jackets (e.g., wrapping by FRP) and (iii) jacketing with reinforced concrete. Since example NY bridge has been found to be vulnerable to damages by vehicular impacts, we will investigate the effectiveness of various jacketing approaches in improving impact resistance of this to a level similar to that of LA bridge investigated in Chapter 4.

The cross section of NY bridge pier is 36-in wide. The longitudinal rebar in piers of this bridge are number 11 with a yielding strength of 60 ksi. The transverse reinforcement is provided by number 4 bars at a spacing of 12 inches. From the moment-curvature of the NY bridge in Figure 4.4, effective sectional property for seismic analysis can be calculated as

$$E_C \times I_{eff} = \frac{M_y}{\phi_y} \tag{6.1}$$

Hence, the effective stiffness of the pier-bent can be calculated as

$$K_{bent} = 3 \times \frac{3 \times E_c I_{eff}}{l^3} = 190.8 kips/in \tag{6.2}$$

The spectral acceleration for LA bridge is 1.25g as shown in table 4.1. Considering the equivalent mass at the top of pier-bent is 800kips, displacement demand on the NY bridge during 1.25g seismic load is calculated as

$$\Delta d = \frac{1.25g \times 800}{K_{bent}} = 5.56in \tag{6.3}$$

The displacement capacity of unretrofitted NY bridge is 4.01 in as shown in Table 4.3. The retrofit with steel or composite jacket is applied to ensure the concrete column of NY bridge can survive with a plastic deformation of 5.56 in.

Priestley and Seible (1996) have provided a straightforward procedure for the design of steel and composite (FRP) jackets to increase ductility capacity of vulnerable bridge piers. In this chapter, we follow this procedure by Priestley and Seible (1996) to design retrofit jackets for the NY bridge so that it can satisfy displacement requirement of LA bridge. The formulas in the following calculation are from Chapter 8 of Priestley and Seible (1996).

The plastic rotation θ_p of the bridge column can be calculated as

$$\theta_p = \frac{\Delta}{L} = \frac{5.56}{12 \times 16} = 0.029 \tag{6.4}$$

The plastic hinge length of the bridge column is given by

$$L_p = g + 0.3 f_y d_{bl} = 2 + 0.3 \times 60 \times 1.41 = 27.4in \tag{6.5}$$

Hence the plastic curvature in the plastic hinge zone can be found by

$$\phi_p = \frac{\theta_p}{L_p} = \frac{0.029}{27.4} = 0.0011 \tag{6.6}$$

Then, the maximum require curvature is given by

$$\phi_m = \phi_y + \phi_p = 0.0012 \tag{6.7}$$

Where ϕ_y is yield curvature based on the moment-curvature analysis. The maximum required compressive strain in the pier is given by

$$\varepsilon_{cm} = \phi_m c = 15 \times 0.0012 = 0.019 \tag{6.8}$$

Where $c = 15in$ is the neutral-axis depth based on moment-curvature analysis.

Steel Jacket Retrofit: Steel jackets have been used widely in California as the most effective retrofit technique for bridge piers. The yield stress of steel jacket is usually taken as $f_{yi} = 40ksi$, and the strain at maximum stress for the jacket steel is $\varepsilon_{sm} = 0.15$. The steel jacket thickness can be calculated by the following equation [Priestley (1996)].

$$t_j = \frac{0.18(\varepsilon_{cm} - 0.004) D f_{cc}^{'}}{f_{yj} \varepsilon_{sm}} \tag{6.9}$$

Where $f_{cc}^{'}$ is the compressive strength of the confined concrete and D is the steel jacket diameter. For rectangular columns, the recommended practice for seismic retrofit is to use an elliptical jacket that provides a continuous confining action similar to that by circular piers, since enhanced flexural ductility will not be provided by the rectangular steel jacket except at the corners.

Even though using rectangular jacket for the retrofit of rectangular columns is not very effective for seismic loads, the jacket can still be fully effective for shear strength enhancement. The design of circular pier retrofit can be applied to rectangular piers with elliptical jackets using an appropriate definition of equivalent diameter (D=2R). In this research, circular steel jacket for the rectangular pier is assumed only to calculate the equivalent diameter. Then, equation (6.9) is used to calculate the thickness of the steel jacket. This jacket is applied to the piers of the NY bridge. The numerical simulation is conducted to evaluate the effectiveness of the rectangular steel jacket under the vehicular impact load. Based on Eq.(6.9), the thickness of the jacket is calculated as 0.21 in. However, since the minimum thickness of steel plates in USA is 5/16 in, the thickness of steel jacket in the retrofit of the NY bridge is set as 5/16in.

Composite Jacket Retrofit: Composite materials such as fiberglass, carbon fiber and Kevlar can be bonded to column with epoxy. For structures under seismic load, as shown in Figure 6.1, extensive research and testing has demonstrated that FRP wrapping of existing reinforced-concrete bridge columns is very effective in increasing a bridge pier's seismic resistance. Tests on circular piers retrofitted with composite-materials jackets to improve ductility show that the composite jacketing is more efficient than steel jacketing. Although FRP wrapping of bridge pies has been used extensively for improving seismic resistance of bridge piers there has been no study on the effectiveness of FRP wrapping in improving impact resistance of bridge piers.

Figure 6.1 Testing of the FRP Wrapped Bridge Piers

The required thickness of FRP wrapping around rectangular piers can be calculated from the following equation [Priestley and Seible (1996)].

$$t_j = \frac{0.1(\varepsilon_{cu} - 0.004)Df'_{cc}}{f_{uj}\varepsilon_{uj}} \tag{6.10}$$

where f_{uj} and ε_{uj} are the ultimate stress and ultimate strain of the FRP material, respectively. In this research, the carbon fiber-epoxy composite jacket is selected as an example of composite with an ultimate stress of $f_{uj} = 150ksi$ and ultimate strain of $\varepsilon_{uj} = 0.0125$. The thickness of composite jacket for NY bridge is calculated as $t_j = 0.52in$ by equation (6.10).

6.3 Effectiveness of Steel Jacketing

As discussed previously, the thickness of retrofit steel jacket is 5/16 in. The steel jacket is grouted with the cover concrete of bridge column. For seismic retrofit of the bridge pier, steel jacketing is required only near top and bottom of the pier, which are locations of maximum moment and shear loads. On the other hand, most of the damage is localized at the contact region between the vehicle and the bridge pier. In order to investigate the effectiveness of

steel jacketing, we consider three cases of steel jacketing: (i) Local jacketing, (ii) Half-pier jacketing and (iii) Full pier jacketing. In local jacketing, the region of impact damage is jacketed, as shown in Figure 6.2(a). In case of half jacketing, bottom portion of the pier, including the region of impact damage is jacketed, as shown in Figure 6.2(b). In case of full jacketing, entire pier is jacketed; see Fig. 6.2(c). The height of the local jacketing is approximately 67 in, based on the height of damage region measured from the simulation of NY bridge under 70 MPH impact in Chapter 4. Fully integrated shell elements are used to model steel jacket. Both the jacket and the column are bonded together by coinciding nodes of solid and shell elements. The impact velocities of the truck are set as 50 MPH and 70 MPH, since the case of 30 MPH shows minor damage for the NY bridge. Figure 6.3 to 6.5 shows simulation results of retrofitted bridge pier impacted by the truck moving at 50 and 70 mph. It is observed from Figure 6.3 that the bridge pier still undergoes severe damage under 70 MPH impact because of the transmission of the impact force to the top and bottom of the pier, as shown in Fig. 6.3(b). Hence, local jacketing of the pier cannot adequately protect the bridge pier from vehicular impacts.

The local steel jacket can be extended to the bottom of the column as shown in Figure 6.2(b). Figure 6.4 shows simulation results of the half jacketed bridge pier subjected to impact by the truck moving at 50 and 70 mph velocities. It is observed that the pier still undergoes severe damages during 70 mph impact, although the severity of the impact is lesser than that

for locally jacketed pier.

Figure 6.5 shows the simulation results for bridge pier retrofitted by full jacketing. It is observed that the fully jacketed pier sustains only minor damages even during impact by a truck moving at 70 mph. Hence, unlike the cases of local and half jacketing, full jacketing is effective in protecting bridge piers during high impact forces from trucks.

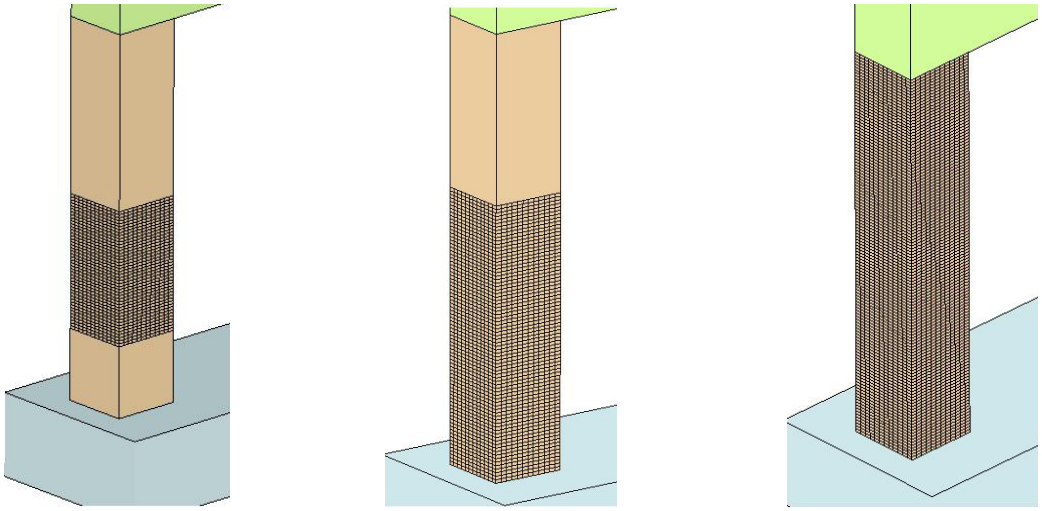

(a) Local Jacketing (b) Half Pier Jacketing (c) Full-Pier Jacketing.

Figure 6.2 Three Cases of Steel Jacketing of Bridge Piers

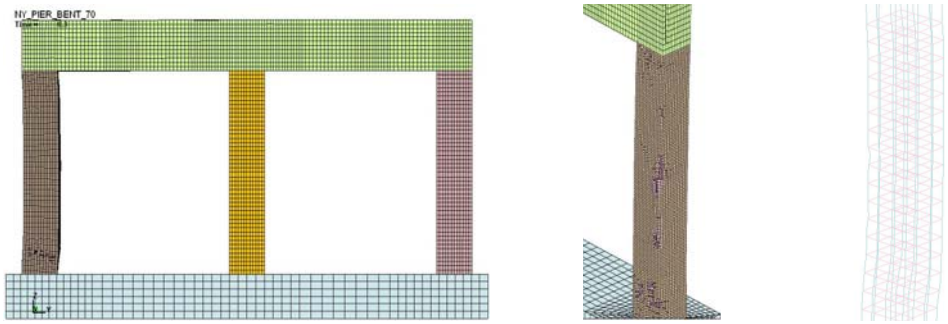

(a) 50 MPH Impact

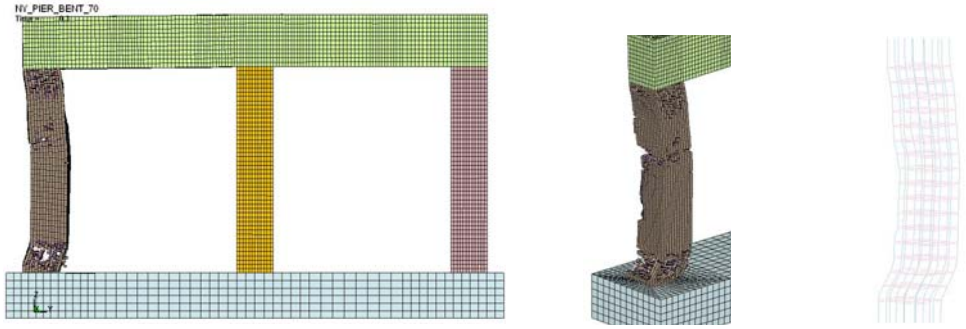

(b) 70 MPH Impact

Figure 6.3 Vehicular Impact on the Bridge Pier Retrofitted with Local Steel Jacketing

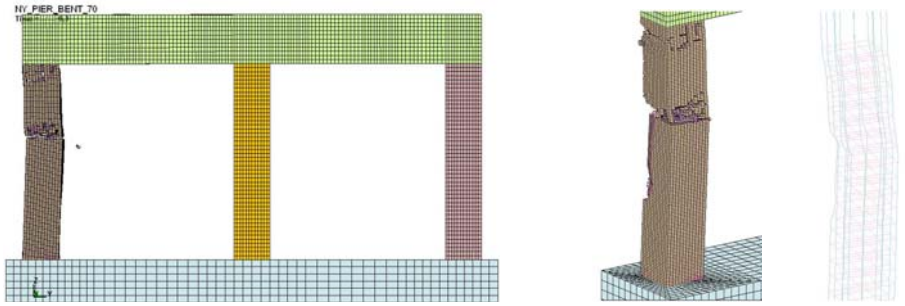

(a) 50 MPH Impact

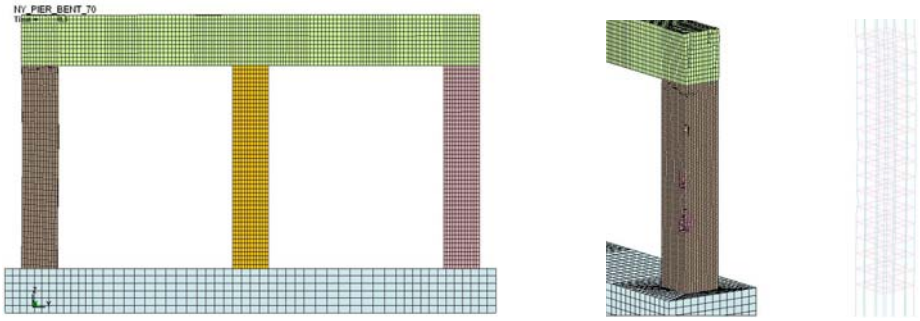

(b) 70 MPH Impact

Figure 6.4 Vehicular Impact on the Bridge Pier Retrofitted with Bottom Half Steel Jacketing

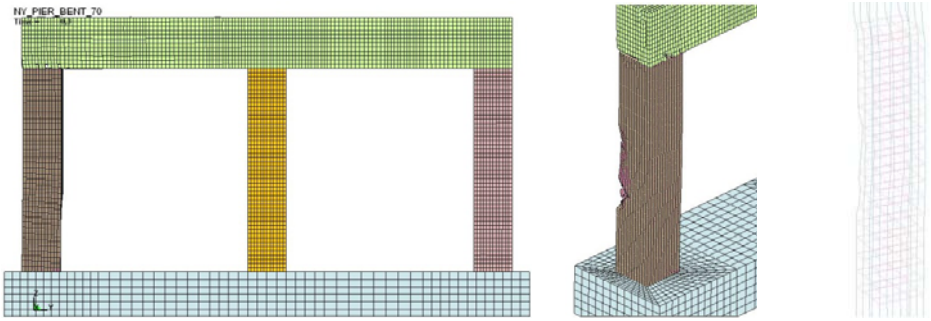

(a) 50 MPH Impact

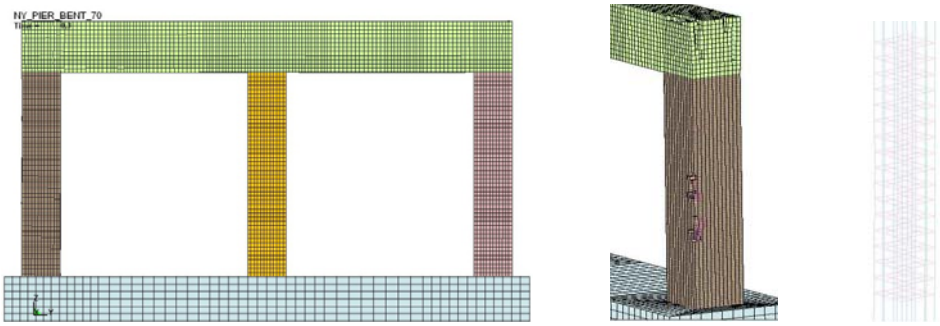

(b) 70 MPH Impact

Figure 6.5 Vehicular Impact on the Bridge Pier Retrofitted with Full Steel Jacketing

The impact forces in case of three types of jacketing are plotted in Figure 6.6. It is observed that three impact force profiles almost coincide each other in case of a particular impact velocity, since impact forces depend only on the characteristic of the vehicle and the approach speed.

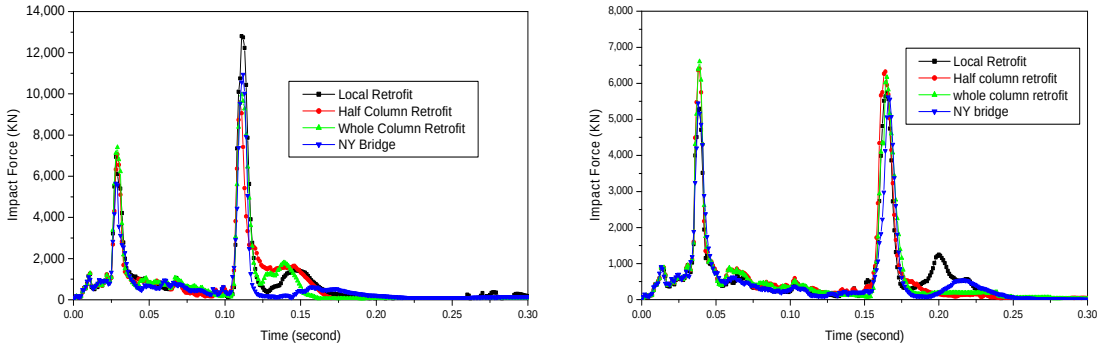

(a) 70MPH Impact (b) 50 MPH Impact

Figure 6.6 Impact Force Time-histories for the Pier Retrofitted by Steel Jackets

Figure 6.7 and Figure 6.8 show comparisons between pier mid-height displacement time histories for three cases of steel jacketing for truck velocities of 50 and 70 mph, respectively. For purpose of comparison, mid-pier displacement time history of NY bridge pier without retrofit is also plotted in these figures. For the case of 50 MPH velocity impact, the ultimate displacement of the bridge pier without retrofit is approximately 7 in. This value is reduced to 2.8 in, 1 in and 0.3 in for cases of local jacketing, half pier jacketing and full-pier jacketing, respectively. Hence, peak mid-height displacement of the bridge pier is reduced approximately 95% in case of 70 MPH impact velocity by fully jacketing the pier.

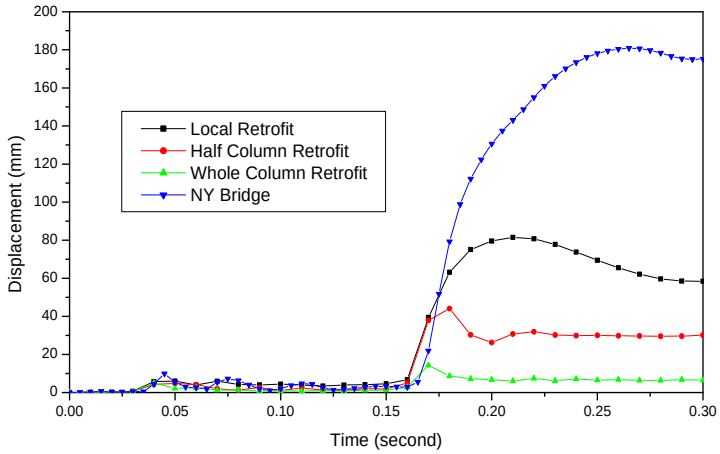

Figure 6.7 Peak Mid-height Displacement Time-histories of the Pier Retrofitted by Steel Jackets during 50 MPH Impact Velocity

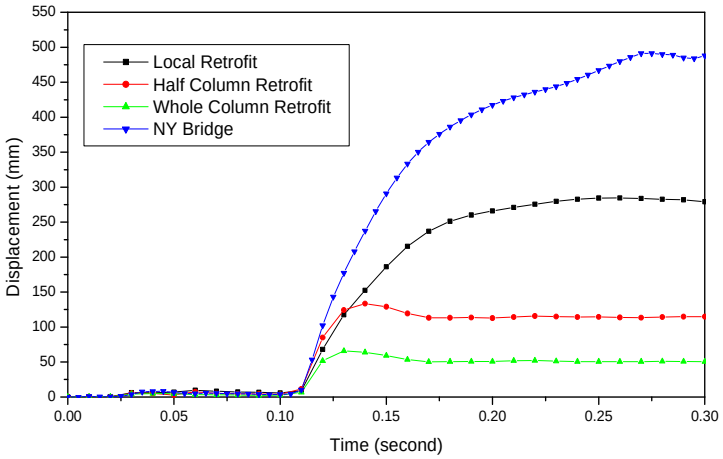

Figure 6.8 Peak Mid-height Displacement Time-histories of the Pier Retrofitted by Steel Jackets during 70 MPH Impact Velocity

6.4 Effectiveness of Composite Jacketing

As described previously, a 0.52-in thick carbon fiber epoxy composite material with modulus $E_j = 12 \times 10^6 \, psi$, ultimate stress $f_{uj} = 150 ksi$ and ultimate strain $\varepsilon_j = 0.0125$ is selected for the retrofit of bridge piers. Four nodes integrated shell element is used to model

the composite material jacket. This element has compatible degrees of freedom with the solid element of concrete. The wrap layer of composite material jacket is assumed as plies with $0^0/90^0/0^0/90^0$. The zero degree ply is expected to strengthen the shear capacity of the bridge pier in the transverse direction, whereas the ninety degree ply is expected to strengthen the bending capacity of the bridge pier in the longitudinal direction. Material model 55 (enhanced composite with damage material) is used to model the composite retrofit jacket. When failure occurs in all composite layers (through-thickness integration points), the shell element is deleted.

Similar to the case of steel jacketing, three cases of retrofits, i.e., local jacketing, bottom half jacketing and full pier jacketing, are considered in this study. Figures 6.9 to 6.11 show simulation results for these three cases, respectively, for impact velocities of 50 and 70 MPH. Similar to the case of steel jacketing, it is observed that the locally jacketed pier still sustains significant damages. Half jacketing is effective in providing higher level of protection than that by local jacketing. On the other hand, fully jacketed pier suffers only minor damages during 70 MPH impact velocity. The minor damage in case of full jacketing is localized only in the contact region between the vehicle and pier, and the bridge pier does not undergo global failure after the high speed impact.

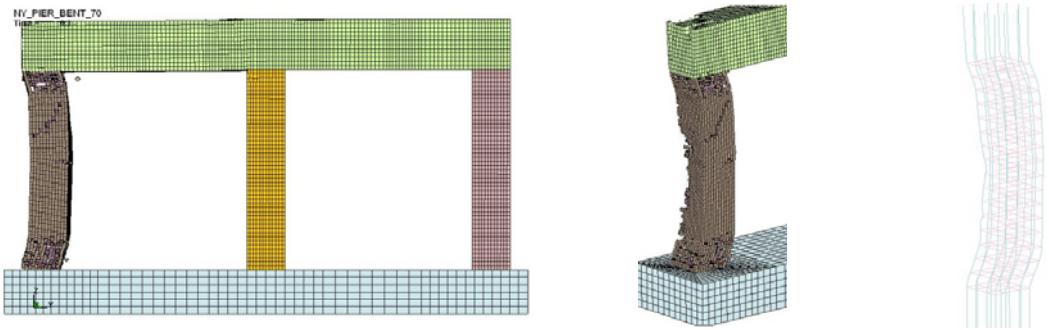

(a) 70 MPH Impact

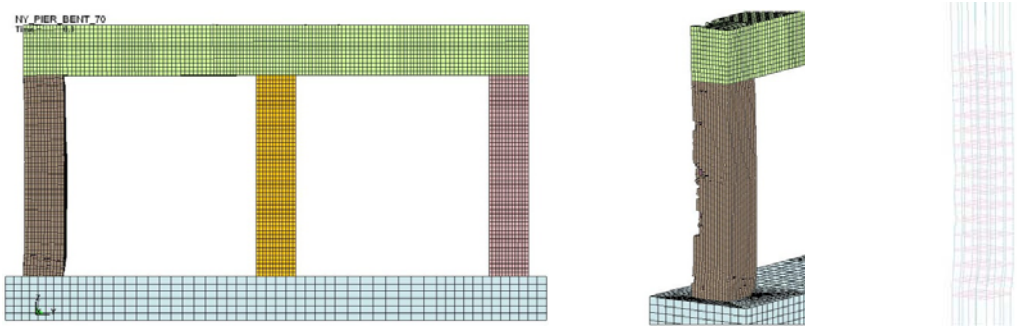

(b) 50 MPH Impact

Figure 6.9 Vehicular Impact on the Bridge Pier Retrofitted with Local Composite Jacketing

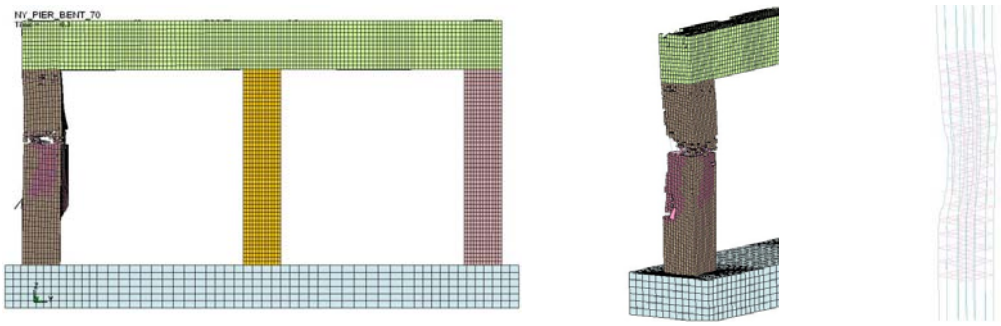

(a) 70 MPH Impact

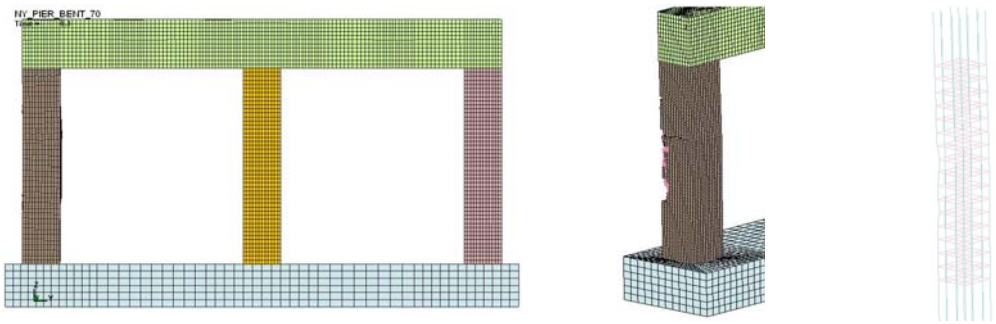

(a) 50 MPH Impact

Figure 6.10 Vehicular Impact on the Bridge Pier Retrofitted with Half Composite Jacketing

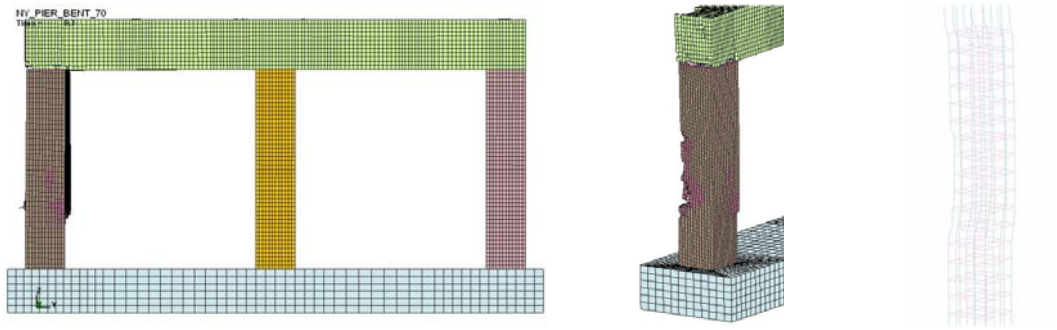

(a) 70 MPH Impact

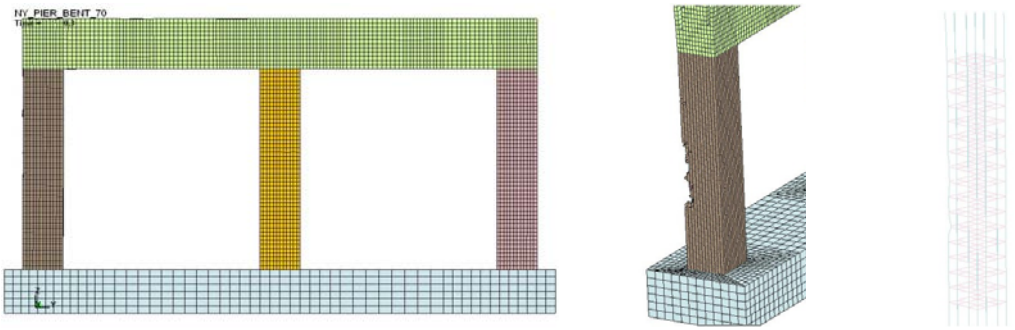

(a) 50 MPH Impact

Figure 6.11 Vehicular Impact on the Bridge Pier Retrofitted with Full Composite Jacketing.

Figure 6.12 and Figure 6.13 show the peak mid-pier displacement time histories of the bridge piers retrofitted with composite jackets under medium and high speed impacts, respectively. For the case of medium speed impact, composite jacketing can effectively reduce the ultimate displacement of the bridge pier. It is noted that the peak displacement in case of full jacketed pier is reduced by approximately 90% of the pier without retrofit under 50 MPH impact velocity. This reduction by full pier jacketing is approximately 85% in case of 70 MPH impact velocity and the pier doesn't undergo global failure mode that was observed in case of the pier without retrofit. This shows that the wrapping of piers by composite is an effective approach to reduce vehicular impact damage.

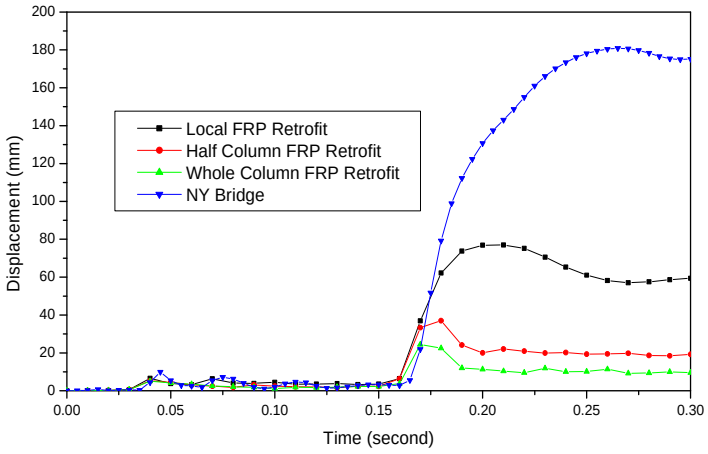

Figure 6.12 Peak Mid-height Displacement Time-histories of the Pier Retrofitted by Composite Jackets during 50 MPH Impact Velocity

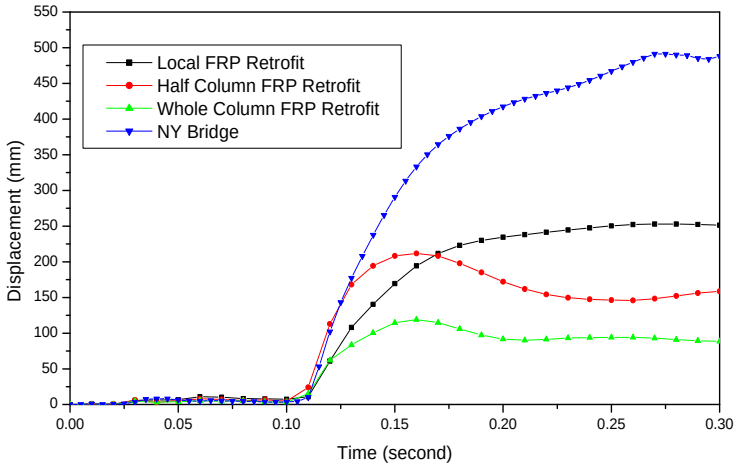

Figure 6.13 Peak Mid-height Displacement Time-histories of the Pier Retrofitted by Composite Jackets during 70 MPH Impact Velocity

6.5 Comparison and Discussion

A comparison between performances of retrofit by steel and composite is carried out to identify advantages of each of these methods. Figure 6.14 and 6.15 show comparisons of between peak mid-height pier displacement time histories for piers retrofitted by steel and composite jackets for 50 and 70- MPH impact velocities, respectively. It is observed from Figure 6.14 for 50 MPH impact velocity that the time-history plots of displacements for two types of retrofit coincide with each other for all three cases of retrofit schemes, e.g., local jacketing, half pier jacketing and full pier jacketing. Table 6.1 shows peak displacements before and after jacketing and percentage reductions for each of the cases in Figure 6.14. It is observed that percentage reductions in displacements are almost the same for the two methods of jacketing. Hence, effectiveness of the two retrofit approaches in increasing the impact resistance of bridge piers is almost the same.

For the bridge pier subject to high speed (70 MPH) impact velocity, it is observed from Figure 6.15 that the percentage reduction in the peak displacement by the steel jacketing method is higher than that by the composite retrofitting, although the difference isn't very significant. For rectangular columns, retrofitting by steel retrofit jackets isn't recommended for seismic protection since steel jackets cannot provide required enhanced flexural ductility to bridge piers except at corners. The costs and efforts (labor) required in installing steel jacketing are also likely to be significantly higher because of bending of steel plates to fit the shape of bridge piers. Welding of plates and pure cement grouting also add significantly to costs required for steel jackets. The procedure for the installation of composite jacketing is significantly less expensive and requires much lesser effort. The composite fiber sheets are wrapped around the column using appropriate epoxy to ensure bonding between concrete and composite material. Composite wrapping can also be placed on any shaped piers without much significant efforts required. Hence, installation of composite jacketing around highway bridge piers is much more cost effective and sufficient in protecting bridge piers from vehicular impacts.

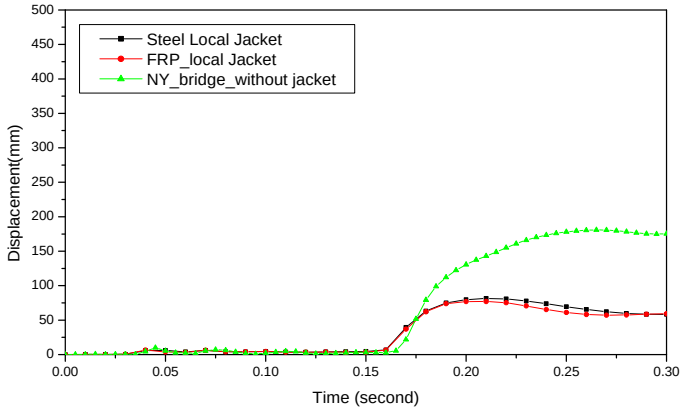

(a) Local Jacket

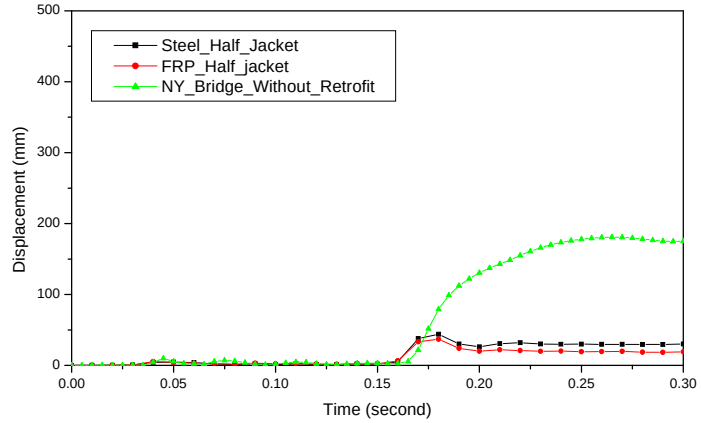

(b) Half Jacket

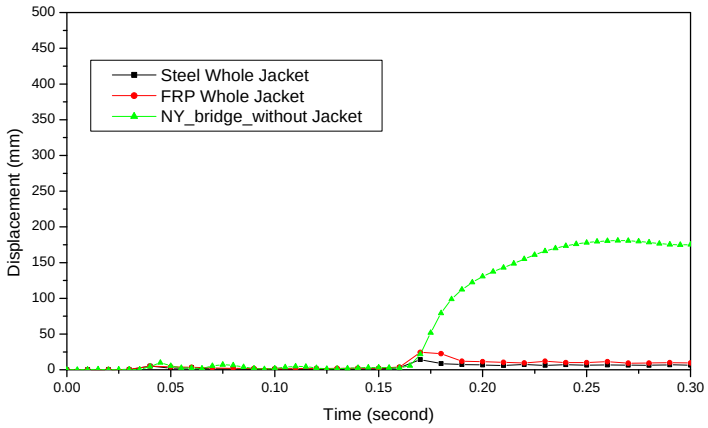

(c) Whole Jacket

Figure 6.14 Comparisons between Peak Mid-height Displacement Time-histories of the Pier Retrofitted by Steel and Composite Jackets during 50 MPH Impact

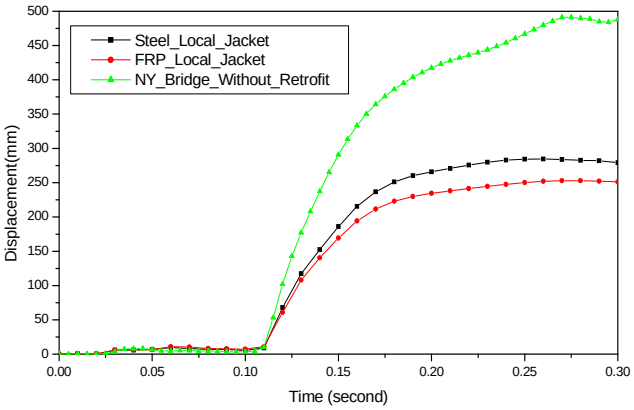

(a) Local Jacket

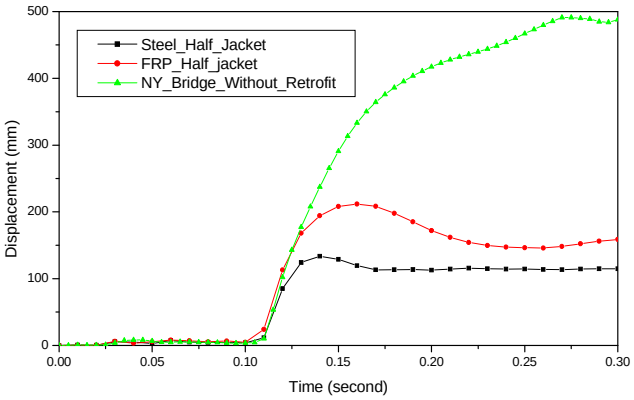

(a) Half Column Jacket

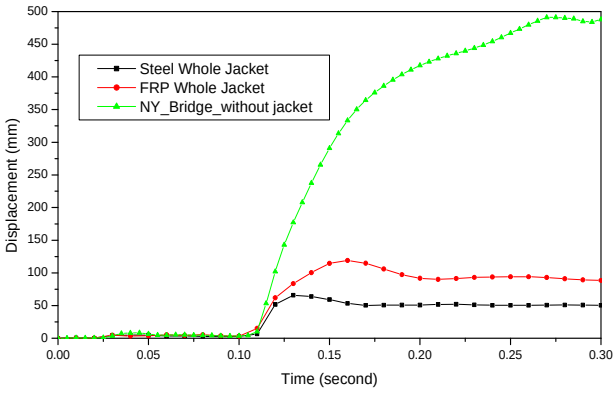

(b) Whole Column Jacket

Figure 6.15 Comparisons between Peak Mid-height Displacement Time-histories of the Pier Retrofitted by Steel and Composite Jackets during 70 MPH Impact

Table 6.1 Percentage Reduction in Peak Displacements by Steel and Composite Jackets around Bridge Piers Subject to 50 MPH Impact Velocity.

50 MPH Impact	Local Jacket Retrofit		Half-Column Jacket Retrofit		Whole-Column jacket Retrofit	
	Steel Plate	FRP Jacket	Steel Plate	FRP Jacket	Steel Plate	FRP Jacket
Displacement After Retrofit	58.4 mm	59.1 mm	30.1 mm	19.3 mm	6.5 mm	9.5 mm
Displacement Before Retrofit	175 mm	175 mm	175 mm	175 mm	175 mm	175 mm
Decreasing Percentage	66.7%	66.2%	82.8%	88.9%	96.3%	94.5%

Table 6.2 Percentage Reduction in Peak Displacements by Steel and Composite Jackets around Bridge Piers Subject to 70 MPH Impact Velocity.

70 MPH Impact	Local Jacket Retrofit		Half-Column Jacket Retrofit		Whole-Column Jacket Retrofit	
	Steel Jacket	FRP Jacket	Steel Jacket	FRP Jacket	Steel Jacket	FRP Jacket
Displacement After Retrofit	279mm	251mm	144mm	158mm	50.4mm	88.6mm
Displacement Before Retrofit	488mm	488mm	488mm	488mm	488mm	488mm
Decreasing Percentage	43%	48.6%	70.5%	67.6%	89.6%	81.8%

Chapter 7 Conclusions and Future Research

In addition to natural hazards such as earthquake, flood and scour, highway bridge structures are also expected to withstand the human induced extreme events (such as blast, fires, vehicular impacts etc.) during their life time. After September 11, 2011 incident, safety of infrastructure systems has received heightened public concerns. Transportation infrastructures are considered to be attractive target because of their accessibility and their potential impact local economy and environment. A bridge engineer should prepare for the new generation of bridges and tunnels that are redundant and resilient to withstand unforeseen extreme events [Duwadi and Lwin (2006)]. This dissertation focuses on the behavior and safety of highway bridge structures subject to vehicular impacts, which is considered to be the third leading cause of bridge failures in this country. This objective had been achieved by the numerical simulation of vehicular impact on a high fidelity finite element model of a highway bridge in LS-DYNA. Based on a comprehensive investigation presented in this dissertation, following conclusions are made on vehicular impacts on highway bridges:

1. A reliable and high fidelity numerical model of highway bridges depends on the validated concrete material model. LS-DYNA provides several material models to simulate the behavior of concrete structures. Each material model is generated based on different physical assumption and mathematical description. For impact simulation, Johnson-cook material model and CSCM material model are appropriate for concrete structures. The

simulations of plain concrete cylinder under various strain rates visually indicates that Johnson-cook model is not appropriate for the simulation of vehicular impacts on concrete components since it can't describe typical brittle shear failure concrete structures. CSCM model has been found to be more appropriate for this purpose.

2. A typical three span simply supported bridge in New York State has been selected as an example bridge to investigate the behavior of highway bridge piers under vehicular impacts. Three dimensional high fidelity finite element model of the bridge has been developed based on the construction drawings. The concrete components are modeled with solid brick elements and rebars are modeled by beam elements. Both brick and beam elements are combined together through coinciding nodes shared by the two types of finite elements. The characteristic mesh size of reinforced concrete in the impact area is set as 1 in based on verification of experimental results on impact testing of a beam in LS-DYNA.
3. Bridge models in LS-DYNA have been combined with a medium weight single unit truck model with approach velocities of 70 MPH, 50 MPH and 30 MPH. Simulation of 70 MPH impact velocity on the typical NY bridge has been carried out to identify all possible failure mechanisms, since this bridge is damaged severely when impacted by the truck moving at 70 MPH. Failure mechanisms captured are: spalling of concrete surface; breakage of the pier; severance of the longitudinal rebar and stirrups; plastic hinge formation in the pier; crush of the bent; and flexural failure of the bent. First two failure mechanism can be classified as repairable (minor) damage. Other failure mechanisms are

classified as moderate to severe damage. After a vehicular impact, a bridge pier with minor damage can be repaired without replacement of the concrete component. A bridge pier with moderate damage may have to be repaired with structural rehabilitation. A severely damaged bridge pier may pose high risk of collapse of the bridge. Hence, the bridge may have to be demolished and reconstructed.

4. In order to investigate correlations between the seismic detailing and vehicular impact effect, numerical models of four three span bridges with various levels of seismic resistance have been developed. These four example bridges have been designed as per 2007 AASHTO Guide Specifications for Seismic Design of Highway Bridges for different seismic categories. Each bridge model has been simulated with three approaching impact speeds of 70 MPH, 50 MPH and 30 MPH. The impact forces and mid-height displacements of four piers have been captured during the simulations. It has been found that the impact forces depend only on the impact velocities of the medium weight truck and are independent of bridge pier's geometry. Numerical results indicate that seismic capacities and vehicle impact loads on bridge piers are strongly correlated. A bridge pier with higher seismic capacity will undergo lower level of damage under the same impact velocity. Better seismic capacity directly implies better vehicular impact resistance.
5. Four example bridges have been designed on the basis of deformation ductility induced by earthquake loads. A higher seismic demand results in higher overturning moment applied on the bridge piers, which is resisted by larger size longitudinal rebars. Because of

stronger overturning moment, shear forces in the pier are also increased. Hence, the transverse reinforcement must be designed with lager size of rebars and the spacing should be decreased to increase shear capacity of the pier. Shear capacities of four example bridges increase with an increase in the design seismic load. Since bridge piers undergo obvious shear failure during a vehicular impact, a bridge pier with higher shear capacity suffers lower level of damage during vehicular impact. It has been found that the ratio of impact force to shear capacity can be taken as the key parameter determining the capability of a pier resist vehicular impact load. A pier with peak impact force to shear capacity ratio less than 2 suffers only minor damages, that with a ratio between 2 and 5 suffers moderate damage and that with the ratio greater than 5 suffers damage severe enough to cause collapse or demolition for replacement.

6. The impact simulation of whole 3-D model of the bridge requires specialized modeling skill and high-performance computer. The simulation of whole bridge-vehicle impact demonstrates that all failure mechanisms of the bridge after the vehicular impact are localized in the impacted pier–bent system. Hence, a simplified pier-bent system containing the impacted pier of the bridge with equivalent mass load has been found to correctly predict mid-height pier displacement of the whole bridge model reasonably well. The proposed pier-bent model in this dissertation has significant advantage in terms of computational time and numerical modeling complexity.
7. AASHTO LRFD guidelines recommend applying an equivalent static force of 400 kips on

vulnerable piers at a height of 4 ft. This load has been found to be under-representing actual impact force that may act on a bridge pier. Texas Transportation Institute has proposed to change the point load of 400 kips to 600 kips based on a peak impact force of 900 kips from their tests on rigid steel pier. The peak impact forces recorded in the simulations of this dissertation shows that the actual magnitude of the impact force may be much higher than this value. For vehicular speed of 70 MPH, this force may be around 2500 kips. It has been found that a pier designed for higher seismic resistance can sustain higher vehicular impact. Hence, an alternative approach for improving vehicular impact resistance of bridge piers is to design it for higher seismic loads. It has been observed that a bridge designed as per seismic requirements in Los Angeles is able to sustain 70 mph impact velocity without significant damage.

8. Steel and composite (FRP) jacketing is used frequently for improving seismic resistance of bridge piers. It has been observed that jacketing of whole length of a vulnerable bridge pier by steel or composite is very effective in improving vehicular impact resistance of a bridge under high velocity impact. Such bridge pier without any jacketing would have collapsed during high velocity vehicular impact. Hence, a properly designed jacketing can have direct multi-hazard benefit through better performance during both seismic and vehicular impact.

A Simplified Design Approach

Based on results presented in this research, a simplified design approach for bridge pier

against vehicular impacts can be formulated as:

a) Determine design speed of impacting truck based on local traffic conditions and agency requirements.

b) Determine design truck weight based on local traffic conditions and agency requirements.

c) Calculate peak impact force as $I_F = W^{0.8824} V^{1.2412}$.

d) Choose the damage level (D).

   Minor damage: $D = 2$

   Moderate Damage: $D = 5$

e) Based on Figure 4.39, determine shear capacity of bridge pier as $S = \frac{I_F}{D}$ in kips. Here S is the designed static shear capacity.

f) Design the rebar detailing or if necessary, change pier size to achieve the design shear capacity S.

Example: Consider a bridge pier of dimension $3' \times 3'$ vulnerable to impact by a 15,000lb truck moving at 60 MPH velocity.

$v = 60\ MPH = 88.02\ ft/Sec$

$W = 15000lb = 7.5\ tons$

$I_F = 7.5^{0.8824} \times 88.02^{1.2418} = 1533\ kips$

For minor damage $D = 2$, shear capacity: $S = I_F / 2 = 766.5\ kips$.

For moderate damage $D = 5$, shear capacity: $S = I_F / 5 = 306\ kips$.

Recommendations for Further Work

High speed impact on concrete structures is highly nonlinear because of high strain, high strain rate and failure of damage elements. Although a detailed study on vehicular impact on highway bridges has been conducted in this dissertation, the research presented in this dissertation lays the framework of further investigation of vehicular impact effects and multi-hazard seismic-impact correlations for highway bridges. More extensive work described in the following can be performed in the future to extend the methodology of the research in this dissertation.

1. In this dissertation, only one type of typical bridge has been selected to investigate the vehicular impact effects on bridge piers. The investigated typical three-span simply supported bridge has rectangular concrete piers. However, in order to fully understand the impacted behaviors of bridge piers and develop a comprehensive guideline, it is necessary to investigate different variations of bridge piers, e.g., circular piers. Due to computational limitations, only one type of vehicle model in LS-DYNA, which is medium-weight single-unit truck, could be considered. In order to fully understand and develop adequate guidelines. Models of vehicles with different weight and stiffness, such as heavy tractor-semitrailer, should be developed for the simulation of vehicular impact loads on highway bridge piers.
2. Numerical simulation plays key role in this research. The reliability of numerical model for concrete structures should be validated by an experimental test. The capacity of concrete

structure under impact load is far different than the traditional static capacity. It is crucial to conduct comprehensive experimental tests to determine scaling parameters between equivalent static strength and impact resistant strength of the concrete structures. There is no data available of full-scale tests because of high costs and logistics. The only test case available is the impact test on rigid steel column conducted by TTI. However, this test doesn't represent concrete structures. Hence, it is necessary to carry out large scale test of vehicle impact on concrete bridge pier.

3. Materials (steel, concrete) used in highway bridge components have inherent uncertainties. Especially for concrete, variations in fracture mode and final strength are very difficult to quantify. Impact loads on bridge piers also have uncertainties because of impact velocity, impact angle and weight of the truck. Both weights of the truck and impact velocities can be parameterized as a single quantity referred to as "impact parameter" (similar to conversion factor during blast). Then, numerical simulations can be carried out to categorize damages into four different categories, e.g., small damage, medium damage, high damage and near collapse. Fragility curves for the 4 damage states can be developed as a function of impact parameter. These fragility curves can serve as hands on tool for highway bridge engineers when designing bridge piers susceptible to impact loads.

4. Simplified Pier-Bent model has been developed in Chapter 5. Compared with the whole 3-D bridge model, complexity of the modeling and computation has been reduced dramatically. However, the Pier-Bent model still consists of 3-D solid elements. The

modeling of 3-D FEM analysis is still complicated for the design purposes. In order to find a simpler and feasible approach to design bridge piers vulnerable under vehicular impact loads, further research is needed to (i) simplify the pier-bent model into a frame model; (ii) represent impact loads from the moving vehicle as an equivalent static load. Pushover analysis in seismic design can be considered as the basis of future research in developing a simplified frame model since pushover analysis is basically an equivalent static method to determine the dynamic capacity of the bridge pier under the seismic load. To carry out plastic analysis of an equivalent frame with a load P applied at the point of impact can determine P and displacement when the frame develops a plastic hinge mechanism. Equivalent frame will be carrying the superstructure weight in the form of applied compressive load in the pier. The approach described above is preliminary and has not been verified. Extensive simulations required to carry out this task. However, successful completion of this research will help designers incorporate impact resistance into their design using a relatively simple analysis.

References

American Association of State Highway and Transportation Officials Load and Resistance Factor Design.(1998). *AASHTO-LRFD Bridge Design Specifications -fourth edition, AASHTO*, Washington, D.C.

American Association of State Highway and Transportation Officials Load and Resistance Factor Design.(2007). *AASHTO-LRFD Bridge Design Specifications -fourth edition , AASHTO*, Washington, D.C.

American Association of State Highway and Transportation Officials Load and Resistance Factor Design.(2007). *AASHTO Guide Specification for LRFD Seismic Bridge Design, AASHTO*, Washington, D.C.

Antonio Nanni.(2003). "North American design guidelines for concrete reinforcement and strengthening using FRP: rinciples, applications and unresolved issues," *Construction and Building Materials*, V17 (2003), pp: 439–446.

Akram Abu-Odeh, Brackin M. S. (2008). *Guidelines for Designing Bridge Piers and Abutments for Vehicle Collisions-Phase I-Simulation Analysis*. College Station, Texas.

Anil K. Agrawal.(2008). *Multi-hazard Seismic-blast-impact Load Effects on Highway Bridges for Performance Based Design*. NJDOT Technology Transfer Seminar, Ewing, NJ.

Anil K. Agrawal.(2010). *Bridge Vehicle Impact Assessment.* University Transportation Research Center and New York State Department of Transportation(UTRC/NYSDOT).

Agrawal, A.K., Ghosn, M. And Alampalli, S. And Pan, Y. "Seismic Fragility of Retrofitted Multi-Span Continuous Steel Bridges in New York ", Accepted for publication in ASCE *Journal of Bridge Engineering*, 2011.

APTEK, Inc. (2007). *Evaluation of LS-DYNA Concrete Material Model 159*. Spring, Colorado .

Blejwas, T. E., Feng, C. C., Ayre, R. S.(1979). " Dynamic interaction of moving vehicles and structures," *Journal of Sound and Vibration*, Vol(67), 513-521.

Bazant, Z. P. (2002). *Scaling of Structural Strength*, Hermes Penton Science, London.

Belytschko, T., Liu, W. K., and Moran, B. (2000). *Nonlinear Finite Elements for Continua and Structures*, John Wiley & Sons Ltd., West Sussex.

Benson,D. J.,(2009) .*The History of LS-DYNA.* Dept. of Mech. & Aero. Eng, University Of California, San Diego.

Buckle, I.G., Mayes, R.L.,and Button, M.R. (1987). *Seismic Design and Retrofit Manual for Highway Bridges*, Prepared for Federal Highway Administration, FHWA-IP-87-6.

Chai YH and Priestley MJN (1991). "Seismic Retrofit of Circular Bridge Columns for Enhanced Flexural Performance," *ACI Structural Journal*, V8(5):572-584.

Chen, G., and Baker, G. (2003). "Influence of bond slip on crack spacing in numerical modeling of reinforced concrete." *Journal of Structural Engineering*,129(11), 1514.

Chen, G. (2007). "Wood Pier Bridge Blast Experiments of UMR." Rolla, MO.

Chopra, A. K. (2001). *Dynamics of Structures: theory and applications to earthquake*

engineering, Prentice Hall, Upper Saddle River

Consolazio, G. (2005). "Barge Impact Testing at the St. George Island Bridge: Test Results & Design Implications". 2006 FICE/FDOT Design Conference, Orlando, Florida.

Consolazio, G. R. and Cowan, D. R. (2003). "Nonlinear analysis of barge crush behavior and its relationship to impact resistant bridge design," *Computers and Structures*, V(81):547-557.

CSI.(2004). CSI *Analysis Reference manual for SAP 2000*. Computers and Structures, Inc. Berkeley, California.

Crawford, J.E, Malvar, L.J., Morrill, K.B., Ferritto, J. M.(2001). "Composite Retrofits to Increase the Blast Resistance of Reinforced Concrete Bulidings". Presented at the Tenth International Symposium on Interaction of the Effects of Munitions with Structures. Burbank, CA.

Duwadi S. R. and Lwin M. "Securing the highway infrastructure-An R and D problem." St. Louis, MO, United States, 177.

Fujikura, S., Bruneau, M., Lopez-Garcia, D.(2008). "Experimental Investigation of Multihazard Resistant Bridge Piers Having Concrete-Filled Steel Tube under Blast Loading," *Journal of Bridge Engineering*, Vol(13), No.6.

Fujikake K., Li B. (2009). "Impact Response of Reinforced Concrete Beam and Its Analytical Evaluation". *Journal of Structural Engineering*, Vol.135(2009), No. 8.

Garden, H.N., Quantrill, R.J., HollawayU, L.C.(1998). "An experimental study of the

anchorage length of carbon fiber composite plates used to strengthen reinforced concrete beams," *Construction and Building Materials*, V(12)1998. pp:203-219.

Gebbekin, N. and Ruppert M. (1999). "On the safety and Reliability of High Dynamic Hydrocode Simulations," *International Journal for Numerical Methods in Engineering*, Vol(46): 839-851.

Hanchak, S. J., Forrestal M. J. and Young, E. R.(1992). "Perforation of concrete slabs with 48 MPa and 140 MPa unconfined compressive strengths," *International Journal of Impact Engineering*, Vol(12), No.1-7.

Hallquist, J. O.,(1987). DYNA3D Course Notes, University of California, Lawrence Livermore National Laboratory, Rept. UCID-19899, Rev. 2, 1987.

Habibullah, A. and Pyle, S. (1998). "Practical Three Dimensional Nonlinear Static Pushover Analysis". *Structure Magazine*, Winter, 1998.

Hargrave, M. W., Munley, E. and Pasko, T. J. (1997). "Federal Highway Administration's (FHWA's) applied highway infrastructure research program on composite materials," *Public Road Magzine*(TFHRC),Spring 1997, Vol(60): No. 4.

Holmquist, T., J., Johnson, G. R. and Cook W. H. (1993). "A Computational constitutive model for concrete subjected to large strains, high strains rates and high pressure." Presented at Fourth International Symposium on Ballistics. Quebec City, Canada, September 1993.

Hose Y.D. [2001] "Seismic Performance and Flexural Behavior of Plastic Hinge Regions in Flexural Bridge Columns", *PhD Dissertation*, University of California at San Diego, La

Jolla, CA.

Johnson, G. R. and Cook, W. H. (1985). "Fracture Characteristics of Three Metals Subjected to Various Strains, Strain Rates, Temperatures and Pressures," *Journal of Engineering Fracture Mechanics*, Vol(21), No.1, pp.31-45.

Kwasniewskia, L., Li Hongyi and Wekezerb, J. (2006). "Finite element analysis of vehicle-bridge interaction," *Finite Elements in Analysis and Design*, Vol(42): 950-959.

Krauthammer, T. & Otani, R. K.(1997). "Mesh, gravity and load effects on finite element simulations of blast loads reinforced concrete structures", *Computers and Structures*, V63(6), 1113.

Kishi N., Nakano O. (2001)."Experimental Study on Ultimate Strength of Flextural-Railure-Type RC Beams under Impact Loading", *Transactions, SMiRT16*, Washington DC.

Keith A. Cota.(2007)."Summary Changes For NCHRP REPORT 350 Guidelines" [NCHRP 22-14 (02)], Technical Committee on Roadside Safety, May 4, 2007

LS-DYNA. (2007). *Theory manual for version 971* (2007). Livermore Software Technology Corporation, Livermore.

LS-DYNA.(2007). *LS-DYNA key word user's manual*, Livermore Software Technology Corporation, Livermore.

LSTC. (2007). "http://www.lstc.com/applications.htm", LS-DYNA applications to Aerospace industry. LSTC, Livermore.

Minnesota Department of Transportation, 2007. *Bridge Office Substructure Protection Policy*. Saint Paul, Minnesota.

Miele, C.R., Plaxico, C. A., and Kennedy, J.C.(2005). *Heavy Vehicle-infrastructure asset interaction and Collision*. Heavy Vehicle Research Center, Oak Ridge National Laboratory.

Murray, Y. D.(2004). "Theory and Evaluation of Concrete Material Model 159". 8th International LS-DYNA Users Conference for Material Technology. Dearborn, MI.

Murray, Y. D. (2007). *User manual for LS-DYNA Concrete Material Model 159*. Federal Highway administration Turner-Fair bankhighway research center, Mclean, VA.

Magnusson, J., and Hallgren, M.(2004)."Reinforced high strength concrete beams subjected to air blast loading, " *Structures under Shock and Impact,* VIII, Crete, Greece, 53-62.

New York Sate Department of Transportation. (1996). *Bridge safety assurance, Collision Vulnerability Manual,* Albany, New York.

National Transportation Safety Board. (1994). *Safety Recommendation (In Reply Refer to H-94-5 & -6)*, Washington, D. C., 20594.

NBI, N. B. I.(2003), *Recording and Coding Guide for the Structure Iventory and Appraisal of Nation's Bridge. FHWA-PD-96-001*, U.S. Department of Transportation, Federal Highway Administration, Washington, D.C.

National Transportation Research Center & Heave Vehicle Research Center. (2005). *Heavy Vehicle Infrastructure Asset Interaction and Collision*. University of Tennessee Knoxville

Nam, J. W., Kim, J. J. and Kim S. B. (2008). “A study on Mesh Size Dependency of Finite Element Blast Structural Analysis Induced by Non-uniform Pressure Distribution from High Explosive Wave,” *KSCE Journal of Civil Engineering*, (2008) 12(4):259-265.

Park, R., Priestley, M.J.N.,Grill. W.D.(1982). “Ductility of Square Confined Concrete Columns”, *Journal of the Structural Division*, ASCE, VOl.108, No. ST4, pp912-950.

Popovics, J. S. and Song, W. (1998). “One-sided Stress Wave Velocity Measurement in Concrete,” *Journal of Engineering Mechanics*, Vol(124), No.12.

Priestley M. and Seible F. (1996), *Seismic Design and Retrofit of Bridges,* John Wiley &Sons, Inc.

Ron Ko.(2004). *Vehicle Collision Loading Criteia for bridge Piers.(Henderson Colloquium 2004).* Highways Agency, United Kingdom.

Sherif EI-Tawil and Edward S. (2005). “Vehicle Collision with Bridge Piers,” *Journal of Structure Engineering,* Vol(10), pp 345-353.

Shinozuka M. and Kim S.H. (2002). “Fragility Curves of Concrete Bridges Retrofitted by Column Jacketing”. *Earthquake Engineering and Engineering Vibration*. Vol(1)No2. PP 195-205

Tan, G. H., Brameld G. H. and Thambiratnam, G. H. (1998). “Development of an analytical model for treating bridge-vehicle interaction,” *Engineering Structures*, Vol(20), NO.1, pp 54-61.

Teng, M.H., Sotelino, E. D. and Chen, W. F. (2003). “Performance Evaluation of

Reinforced Concrete Bridge Columns Wrapped with Fiber Reinforced Polymers," *Journal of Composites for Construction*, Vol(7), No.2.

TIMOSHENKO, S., Young, D. H., and Weaver, W. (1974). *Vibration Problems in Engineering*. New York: Wiley, fourth edition.

Texas Transportation Institute. (2008). *Guidelines for Designing Bridge Piers and Abutments for Vehicle Collisions*, College Station, Texas.

Wallace, J. W. (1992). "BIAX, A Computer Program for the Analysis of Reinforced Concrete and Reinforced Masonry Sections." Report No.CU/CEE-92/4, Department of Civil Engineering, Clarkson University, Potsdam, New York.

Wardhana, K. and Hadipriono F.C.(2003). "Analysis of Recent Bridge Failures in the United States," *Journal of Performance of Constructed Facilities*, Vol.17, No.3.

Wallace, J. W., and Ibrahim, Y. A. (1996). *User's manual for BIAX*, "Strength analysis of reinforced concrete sections program."

Williamson Eric B. and Bayrak O.(2010). "Blast-Resistant Highway Bridges: Design and Detailing Guidelines", NCHRO Report 645, Transportation Research Board, Washington D.C., 2010.

Woisin G.(1976). "The collision tests of the GKSS," *Jahrbuch Schiffbautech Gesellsch*, 1976,V70:465-487.

Xiao Y. and Wu H. (2003). "Retrofit of reinforced Concrete Columns Using Partially Stiffened Steel Jackets", Journal of Structural Engineering, Vol.129, No. 6, pp725-732.

Xiao Y., Liu C.L.(2010), “Study of Anti-Ram Bollards Based on Truck Collision Testing. “, *Proceeding of International Symposium on life-Cycle Performance of Bridges and Structures*, Science Press, Hunan.

Yang,Y.B., Liao, S.S., Lin, B.H. (1995). “Impact formulas for vehicles moving over simple and continuous beams,” *Journal of Structural Engineering*, 121 (11):1644-1650.

Yang,Y.B. , Lin, B.H. (1995). “Vehicle–bridge interaction analysis by dynamic condensation method,” *Journal of Structural Engineering*, 121 (11)1636–1643.

Yi, Z. H. (2008). *Blast Load Effects on Highway Bridges*. City University of New York, New York.

Yvonne D. M.& Roger Bligh,(2007). *Evaluation of LS-DYNA Concrete Material Model 159*. Texas Transportation Institute, College Station, TX.

Zaouk, A. K. & Marzoughi, D.(1996). “Validation of a non-linear finite element vehicle model using multiple impact data,” *Crashworthiness and occupant protection in transportation systems*, AMD,Vol(218): PP: 91–106. ASME, New York.

Zukas, J. A. (1990). *High Velocity Impact Dynamics*, Wiley Interscience, New York.